

**Academic Year 2018-2019**

Faculty Pharmaceutical, Biomedical  
and Veterinary Sciences

Biomedical Sciences



**The *in vivo* quantification of iron deposition in the brain and its relation to pathological hallmarks of Alzheimer's disease**

By:

**Wachtelaer, Eva**

*Master Thesis in partial fulfillment of the requirements for the degree  
Master in Biomedical Sciences*

Promoter: Prof. Dr. Pedro Rosa-Neto

Co-promoter: Prof. Dr. Sebastiaan Engelborghs

**Douglas Mental Health University Institute**  
6875 LaSalle Boulevard  
Montreal, Quebec H4H 1R3  
Canada



# Table of contents

<b>Table of contents</b> .....	<b>2</b>
<b>Abstract</b> .....	<b>4</b>
<b>Samenvatting</b> .....	<b>6</b>
<b>Introduction</b> .....	<b>8</b>
1. General overview .....	8
2. Properties of iron in humans .....	9
a) <i>The iron element</i> .....	9
b) <i>Iron metabolism</i> .....	9
c) <i>Iron in the brain</i> .....	10
d) <i>Brain iron regulation</i> .....	12
e) <i>Role of iron in neurological function in humans</i> .....	13
f) <i>Iron related to pathology: neurodegeneration with brain iron accumulation</i> .....	13
g) <i>Magnetic properties of iron and its effects on magnetic resonance imaging</i> .....	14
h) <i>The contribution of different iron forms to the MRI signal</i> .....	16
3. Current knowledge of the involvement of iron in healthy aging .....	18
4. Current knowledge of the involvement of iron in Alzheimer's disease .....	18
a) <i>Relation between iron and oxidative stress</i> .....	18
b) <i>Gender differences in susceptibility to Alzheimer's disease</i> .....	22
c) <i><math>\beta</math>-Amyloid neuropathology</i> .....	22
d) <i>Tau neuropathology</i> .....	24
e) <i>Genetic findings</i> .....	24
f) <i>Knowledge from drugs</i> .....	25
g) <i>Knowledge from diet</i> .....	25
5. Conclusion .....	26
<b>Materials and method</b> .....	<b>28</b>
1. Study design .....	28
2. Magnetic resonance acquisition and processing protocols .....	28
3. Positron emission tomography acquisition and processing protocols .....	29
4. Mini-mental state examination .....	29
5. Genetic analysis .....	30
6. Statistical analysis .....	30
<b>Results</b> .....	<b>32</b>
1. The site of acquisition affects brain iron quantification .....	32
2. The brain does not show sex differences in iron values .....	33
3. Iron tends to accumulate in the healthy aging brain .....	33
4. Alzheimer's disease patients show differences in iron load compared to controls .....	35
5. Iron load is not related to $\beta$ -amyloid deposition .....	38
6. Iron load relates to global tau load .....	38
7. Iron values relate to MMSE scores .....	39
8. Iron values differ for varying <i>APOE</i> $\epsilon$ 4 variants .....	39
<b>Discussion</b> .....	<b>44</b>
1. Strengths and limitations .....	47
2. Future perspectives .....	50
<b>Conclusion</b> .....	<b>54</b>
<b>Acknowledgements</b> .....	<b>56</b>
<b>References</b> .....	<b>58</b>
<b>Supplementary material</b> .....	<b>68</b>



## Abstract

**Background:** Alzheimer's disease (AD), the most common cause of dementia, affects millions of people worldwide. Its increasing incidence and the lack of disease-modifying drugs is of major concern to our society. An improved understanding of the pathophysiology of the disease and the discovery of novel therapeutic targets are strongly desired. Iron dyshomeostasis has been found to damage the brain by inducing oxidative stress and has been associated with the pathological hallmarks of AD. Investigating the role of iron can contribute to an improvement of the understanding of the disease and might provide insight into new therapeutic options. We hypothesize that brain iron dyshomeostasis is related to the development and progression of AD. In addition, we hypothesize a relation between abnormal brain iron levels and the pathological hallmarks characterizing AD.

**Objective:** This study investigates the role of brain iron dyshomeostasis in healthy aging and the pathophysiology of AD.

**Material and methods:** A cross-sectional study was performed to analyse brain iron load across clinical populations. In total, 180 subjects participated in this study, including 127 controls (22 young and 105 elder) and 53 patients (21 diagnosed with mild cognitive impairment (MCI) and 32 with AD). MRI  $T_2^*$  relaxometry was performed to assess iron load in the brain grey matter.  $R_2^*$  ( $1/T_2^*$ ) values were calculated by applying a voxel-wise mono-exponential fit. PET imaging provided estimates of  $\beta$ -amyloid and tau deposition using the [ $^{18}\text{F}$ ]AZD4694 and [ $^{18}\text{F}$ ]MK6240 standardized uptake value ratio (SUVR), respectively. Cognitive function was evaluated by MMSE. *APOE* genotyping was carried out using the polymerase chain reaction. Multiple least squared linear regression models were applied for the statistical modeling with the MATLAB analysis software.

**Results:** No sex differences in brain iron levels were observed. Healthy elderly subjects showed higher iron load compared to young controls, as expected. Late onset AD patients showed lower iron levels compared to controls, whereas early onset AD patients showed higher iron load. No significant differences were found for MCI patients, either compared to age-matched controls or AD patients. Furthermore, no relation between iron and  $\beta$ -amyloid deposition was observed in our cohort. For higher brain tau levels, lower iron concentrations were observed. Higher MMSE scores were related to higher brain iron deposition. Finally, carriers of one  $\epsilon 4$  *APOE* allele demonstrated lower iron values compared to non-carriers and homozygotes of the  $\epsilon 4$  allele showed increased brain iron load compared to heterozygotes.

**Conclusion:** This study provides additional support for the involvement of iron dyshomeostasis in the healthy aging process and AD pathophysiology. In healthy aged individuals we found profound subcortical iron deposition. By contrast, AD patients demonstrated changes in iron load particularly in the cortical regions. The specific role of brain iron load in the amyloid cascade hypothesis in AD remains a topic of further research.

Therefore, we acknowledge the need for the establishment of a golden standard technique to assess brain iron load *in vivo*. This will allow for the achievement of an unquestionable understanding of the role of iron in AD pathophysiology.



## Samenvatting

**Achtergrond:** De ziekte van Alzheimer is de meest voorkomende oorzaak van dementie en treft wereldwijd miljoenen mensen. Toenemende incidentie en een gebrek aan ziektemodificerende geneesmiddelen is van grote zorg voor onze samenleving. Er is een grote vraag naar een verbeterd begrip van de pathofysiologie van deze ziekte en de ontdekking van nieuwe therapeutische doelen is erg begeerd. Onderzoek heeft aangetoond dat ijzer dyshomeostase de hersenen kan beschadigen door het induceren van oxidatieve stress en geassocieerd is met de pathologische ‘hallmarks’ van de ziekte van Alzheimer. Onderzoek naar de rol van ijzer kan bijdragen aan een verbeterd begrip van de ziekte en kan inzicht geven in nieuwe therapeutische opties. We stellen de hypothese dat ijzer dyshomeostase in de hersenen gerelateerd is aan de ontwikkeling en progressie van de ziekte van Alzheimer. Verder veronderstellen we een relatie tussen abnormale niveaus van ijzer in de hersenen en de pathologische ‘hallmarks’ die de ziekte van Alzheimer kenmerken.

**Doel:** Dit project onderzoekt de rol van ijzer dyshomeostase in de hersenen in het gezond verouderingsproces en in de pathofysiologie van de ziekte van Alzheimer.

**Materiaal en methode:** Een cross-sectioneel onderzoek is uitgevoerd om de hoeveelheid ijzer in de hersenen te analyseren over klinische populaties. In totaal namen 180 individuen deel aan deze studie, inclusief 127 controles (22 jong en 105 oud) en 53 patiënten (21 met ‘mild cognitive impairment’ (MCI) en 32 met de ziekte van Alzheimer). MRI  $T_2^*$  relaxometrie werd uitgevoerd om de hoeveelheid ijzer in de grijze massa van de hersenen te testen.  $R_2^*$  ( $1/T_2^*$ ) waarden werden berekend door het toepassen van een mono-exponentiële fit per voxel. PET beeldvorming leverde schattingen van  $\beta$ -amyloid en tau neerslag door het gebruik van de  $[^{18}\text{F}]\text{AZD4694}$  en  $[^{18}\text{F}]\text{MK6240}$  ‘standardized uptake value ratio’ (SUVR), respectievelijk. Cognitieve functie werd geëvalueerd door middel van MMSE. *APOE* genotypering werd verkregen door het gebruik van de polymerasekettingreactie. Meervoudige kleinste-kwadraten lineaire regressie modellen werden toegepast voor de statistische modelering met MATLAB analyse software.

**Resultaten:** Er werden geen geslachtsverschillen in de niveaus van ijzer in de hersenen geobserveerd. Gezonde ouderen toonden hogere niveaus in vergelijking met jongeren. ‘Late onset AD’ patiënten vertoonden lagere ijzer hoeveelheden in vergelijking met controles, terwijl bij ‘early onset AD’ patiënten hogere hoeveelheden gevonden werden. Geen significante verschillen werden aangetoond voor MCI patiënten, vergeleken met leeftijd-overeenkomstige controles of patiënten met de ziekte van Alzheimer. Bovendien werd geen relatie vastgesteld tussen ijzer en  $\beta$ -amyloid neerslag in onze cohorte. Voor hogere hersenwaarden van tau, werden lagere ijzerwaarden geobserveerd. Hogere MMSE scores werden gerelateerd aan hogere ijzer depositie in de hersenen. Ten laatste vertoonden dragers van één  $\epsilon 4$  *APOE* allel lagere ijzerwaarden in vergelijking met niet-dragers en in homozygoten voor het  $\epsilon 4$  *APOE* allel werden hogere ijzerwaarden in de hersenen vastgesteld vergeleken met heterozygoten.

**Conclusie:** Dit project voorziet aanvullende ondersteuning voor de betrekking van ijzer dyshomeostase in het gezonde verouderingsproces en de pathofysiologie van de ziekte van Alzheimer. In gezonde oudere individuen werd uitgesproken subcorticale ijzer depositie teruggevonden. In tegenstelling vertoonden patiënten met de ziekte van Alzheimer vooral veranderingen in ijzerwaarden in de corticale regio’s. De specifieke rol van ijzer in de ‘amyloid cascade’ hypothese blijft een onderwerp dat verder onderzoek vraagt.

Als gevolg erkennen we de nood voor de ontwikkeling van een gouden standaard techniek om ijzerwaarden in de hersenen te onderzoeken. Dit geeft de mogelijkheid om onbetwistbare kennis omtrent de rol van ijzer in de pathofysiologie van de ziekte van Alzheimer te behalen.



## Glossary

•OH = hydroxyl radical; A $\beta$  =  $\beta$ -amyloid; AD = Alzheimer's disease; APOE = apolipoprotein E; APP = amyloid precursor protein; ATP = adenosine triphosphate; BBB = blood-brain barrier; CIC = Cerebral Imaging Centre; CN = control; CSF = cerebrospinal fluid; DcytB = duodenal cytochrome B; DKT = Desikan-Killiany-Tourville; DMT-1 = divalent metal transporter 1; EOAD = early onset Alzheimer's disease; FDR = false discovery rate; Fe<sup>2+</sup> = ferrous iron; Fe<sup>3+</sup> = ferric iron; H<sub>2</sub>O<sub>2</sub> = hydrogen peroxide; HCPI = heme carrier protein 1; HFE = human hemochromatosis (High iron Fe); HRRT = High Resolution Research Tomograph; IRE = iron-responsive element; LOAD = late onset Alzheimer's disease; LTD = long-term depression; LTP = long-term potentiation; MCI = mild cognitive impairment; MCSA = McGill University Research Centre for Studies in Aging; MMSE = mini-mental state examination; MNI = Montreal Neurological Institute; MP-RAGE = magnetization-preparation radio-frequency pulses and rapid gradient; MRI = magnetic resonance imaging; NBIA = neurodegeneration with brain iron accumulation; NIA-AA = National Institute on Aging and Alzheimer's Association; NINCDS-ADRDA = National Institute of Neurological and Communicative Disorders and Stroke and the Alzheimer's Disease and Related Disorders Association; NO = nitric oxide; O<sub>2</sub>• = superoxide; PCA = posterior cortical atrophy; PCR = polymerase chain reaction; PET = positron emission tomography; PPA = primary progressive aphasia; QSM = quantitative susceptibility mapping; RF = radio frequency; ROI = region of interest; ROS = reactive oxygen species; SCD = subjective cognitive decline; SD = standard deviation; SUVR = standardized uptake value ratio; SWI = susceptibility-weighted imaging; TE = echo time; Tf = transferrin; TI = inversion time; Tim = Total imaging matrix; TR = repetition time

---

## Introduction

### 1. General overview

Alzheimer's disease (AD) is the most prominent cause of dementia (60-80% of the cases) [1]. About 5.7 million people in the United States and 40 million people worldwide are currently suffering from this disease [1, 2]. Brookmeyer et al. predicted the worldwide prevalence of AD to be 106 million in the year 2050. This can particularly be explained by the increasing lifespan of humans, as age is the major risk factor for developing AD [3].

AD dementia is characterised by progressive cognitive decline, behavioural disturbances and the inability to perform daily tasks [4, 5]. This slowly progressing disease can be divided into different stages, according to characteristic physiological and anatomical features, as well as typical symptoms. The first stage is called subjective cognitive decline (SCD) in which the patient experiences memory complaints. However, these cannot be objectified by neuropsychological examinations [6]. SCD individuals can progress to a subsequent stage, called mild cognitive impairment (MCI). The SCD stage differentiates from MCI by the fact that the symptoms of the MCI patient can be objectively confirmed. The cognitive decline of these patients is more prominent than expected for a cognitive healthy person of similar age. If only the patient is unable to perform daily activities, the diagnosis of AD dementia is established [7].

Despite the extensive research and improved understanding of AD, diagnosing patients remains challenging [8]. The initially proposed diagnostic criteria, known as the 'National Institute of Neurological and Communicative Disorders and Stroke and the Alzheimer's Disease and Related Disorders Association' or 'NINCDS-ADRDA Alzheimer's criteria', focussed on a clinical diagnosis [9].

With an increasing understanding of the pathophysiology of AD, the realisation of the importance of biomarkers emerged. More recent diagnostic criteria, like those introduced by the 'National Institute on Aging and Alzheimer's Association' or 'NIA-AA', acknowledged the considerable contribution of biomarkers to the diagnostic framework of AD [10]. Their most recent proposal of criteria includes the 'A/T/N system' [10, 11]. This system emphasizes the importance of biomarkers in AD and comprises a descriptive classification scheme that divides

the most relevant biomarkers into three categories. ‘A’ refers to  $A\beta$ , ‘T’ to tau and ‘N’ to neurodegeneration. In this classification system, every subject is assigned a positive or negative sign for each category. It is important to note that this system is independent of clinically defined diagnostic criteria, which bypasses the current issue of the lack of consensus on defining the different stages across the AD spectrum among AD specialists [11].

To date, no successful treatment has been developed to cure or prevent the disease [1]. To find an effective treatment, an improved understanding of the pathogenesis and risk factors is likely necessary. AD is considered as a neurodegenerative disease characterised by three pathological hallmarks; amyloid plaques, neurofibrillary tangles and neurodegeneration. The respective roles of these features in AD pathogenesis and their medical relevance is still not clear.  $\beta$ -amyloid ( $A\beta$ ) has been a major target of medical intervention. However, to date, therapies targeting  $A\beta$  have shown limited results [12]. As a consequence, there is a need for novel therapeutic targets.

A growing body of evidence suggests the implication of iron dyshomeostasis in the development and progression of AD. Iron is the most abundant transition metal on Earth and is essential for life. It is involved in multiple functions, including erythropoiesis, DNA replication, oxygen transport, neurotransmitter and adenosine triphosphate (ATP) synthesis, and myelination processes. In addition, several enzymes utilize iron to catalyse chemical reactions in the body [13-15]. As a consequence, strictly regulated homeostatic mechanisms have been developed in the body to maintain appropriate levels of iron [14, 15]. In the case of iron dyshomeostasis, essential biological systems are disrupted, leading to failure of important bodily functions. Elevated iron levels have been found to be toxic and potentially result in pathological processes [2].

## **2. Properties of iron in humans**

### **a) The iron element**

Iron is represented in chemistry by the symbol ‘Fe’ and is the 26<sup>th</sup> element in the periodic table. Although it exists in many oxidation states (-2 to +7), ferrous iron ( $Fe^{2+}$ ) and ferric iron ( $Fe^{3+}$ ) are the most common forms. Next to its occurrence in meteoroids, the inner core and crust of the Earth, it is also abundantly present in the human body. In addition, four stable isotopes of iron naturally occur, namely  $^{54}Fe$  (5.9%),  $^{56}Fe$  (91.6%),  $^{57}Fe$  (2.2%) and  $^{58}Fe$  (0.33%).

As previously mentioned, iron belongs to the group of transition metals. The elements constituting this group are situated in the centre of the periodic table and are characterized by the presence of electrons in their d sub-shell. Iron can be described by the electron configuration of  $Ar3d^64s^2$ . An important feature of iron is its ability to readily exchange electrons by redox cycling. Under acidic circumstances or in the presence of oxygen,  $Fe^{2+}$  acts as a reducing agent by easily donating an electron, rendering  $Fe^{3+}$ . In alkaline solutions, the latter acts as an oxidizing agent and reduces itself to  $Fe^{2+}$  by accepting an electron [16, 17].

### **b) Iron metabolism**

Iron is absorbed in humans by gut enterocytes, which are the key modulators of the concentrations of iron throughout the body. On average, healthy adult individuals have a total of 3.5 to 5.0 grams of iron in their body, of which the majority is present in the liver and red blood cells. Only minor amounts are present in the brain (about 60 mg in healthy adults) and kidneys [18-20]. In the human body, iron uptake consists of three stages. First,  $Fe^{2+}$  iron is transported into the enterocyte. Then, it is transported to the basolateral membrane or stored in ferritin. Finally, iron is released into the blood circulation [14, 21]. A detailed description of intestinal iron uptake can be consulted in the supplementary material.

### **c) Iron in the brain**

In the human body, iron exists in one of two forms, heme or non-heme iron. The former is contained by haemoglobin and certain enzymes. In brain tissue, non-heme iron can be subdivided into different types [22]. It can be found in the ionic form, storage proteins like ferritin, metalloproteins like transferrin and low-molecular-weight complexes [23, 24].

Iron distribution in the brain is heterogeneous and highly dependent on age. At birth, brain iron load is very low and it progressively increases with age during the first four decades of life [22]. During neurodevelopment, iron co-localizes with myelinogenic foci as it is an important player in myelination processes. Moreover, oligodendrocytes, cells essential for creating myelin sheaths surrounding axons, contain the highest levels of iron among all brain cells. Although, as previously mentioned, iron levels are low in the brain, certain cerebral structures do contain high iron amounts. In particular, the iron load in the basal ganglia is comparable to that in the liver [19, 20, 24-27].

#### Iron transport into the brain

To access the brain, iron must cross the blood-brain barrier (BBB). This barrier, separating the blood and brain parenchyma, is characterized by highly regulated transport mechanisms and is composed of endothelial cells sealed by tight junctions [14, 28]. Three pathways of iron transport into the brain have been proposed (Figure 1). Method number 1 as shown in Figure 1, is currently the most widely accepted mechanism [14]. It involves the iron transport protein transferrin, which is a glycoprotein produced by oligodendrocytes and choroid plexus cells [2]. Transferrin carrying iron binds to transferrin receptors (Tf receptor in Figure 1). Subsequently, the formed complex of transferrin and its receptor is subjected to endocytosis, after which the acquired endocytic vesicle traverses the endothelial cell. Finally, the complex is released into the brain parenchyma. However, to date, there is no conformity on this ‘transcytosis mechanism’ and therefore, other iron uptake pathways have been proposed [14].

Duck et al., suggested another endocytic pathway as an alternative brain iron uptake mechanism, presented as number 2 in Figure 1. Similar to the previous pathway, the complex of transferrin bound to its receptor is transferred into the endothelial cell by endocytosis. By contrast, in this model the pH of the endosome is lowered, resulting in the release of  $\text{Fe}^{3+}$  from the established complex. After the reduction by a  $\text{H}^+$ -ATPase,  $\text{Fe}^{2+}$  is transported via divalent metal transporter 1 (DMT-1) to the cytoplasm of endothelial cells. Equivalent to the intestinal transport of iron (Supplementary Figure 1) endothelial cells can utilize  $\text{Fe}^{2+}$ , store it in ferritin or transfer it to the brain parenchyma via ferroportin. The latter enables uptake by apo-transferrin and subsequent circulation in the brain [14, 29, 30].

Evidence for this mechanism arises from results indicating that endothelial cells are capable of storing iron. This cannot be explained by the ‘transcytosis mechanism’, as it only includes a passive transfer of iron through endothelial cells [14, 31]. However, there is no agreement on the presence of DMT-1 in the BBB [14, 32]. Thus, more research should be performed to increase the understanding of this potential pathway.

Finally, as discussed in the supplementary material for enterocytes, ferritin carrying iron might have the ability to traverse the endothelial cells directly (number 3 in Figure 1).

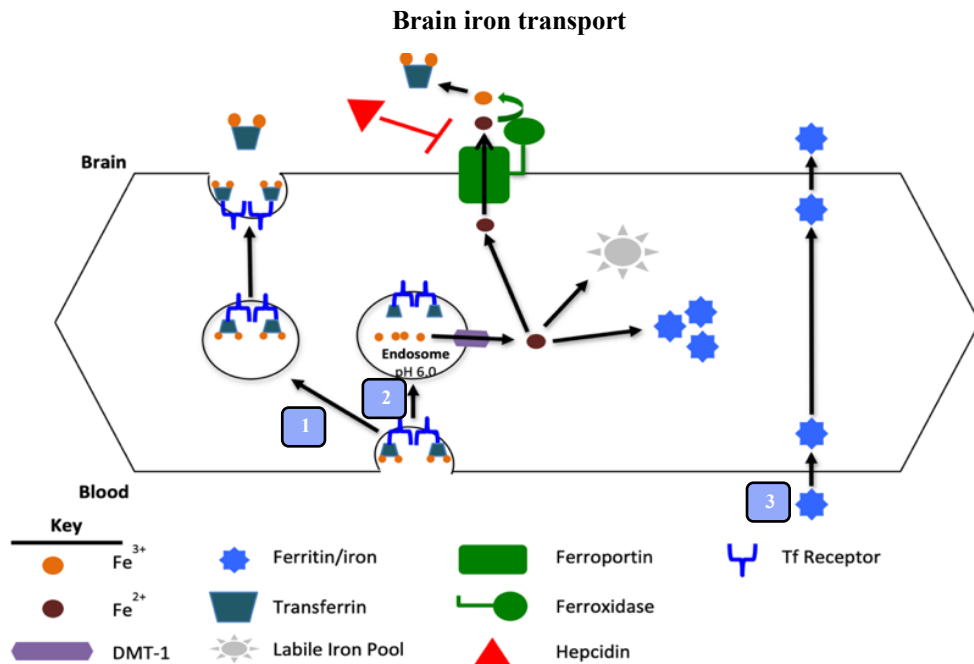


Figure 1 Schematic presentation of three potential transport mechanisms of iron into the brain parenchyma through the BBB. Number 1 demonstrates the transcytosis mechanism by which transferrin carrying iron binds to the transferrin receptor (Tf receptor) to form a complex. The complex then undergoes endocytosis, after which the endocytic vesicle traverses the cell and the complex is released in the brain parenchyma. Number 2 shows an alternate endocytic pathway involving the release of  $Fe^{3+}$  out of the transferrin complex, which is thereafter reduced to  $Fe^{2+}$ . The latter can be used by the cell, stored in ferritin or transferred to the brain parenchyma by ferroportin. Finally, number 3 indicates a direct transport of ferritin-bound iron through the endothelial cell [14].

### Effects of diet on cerebral iron levels

Although the relationship between systemic and brain iron is not completely elucidated, several studies indicate dietary intake and systemic iron levels affect the amount of iron in the brain [13, 33-36]. An example of a diet low in iron is the Mediterranean diet (Figure 2) [37]. This diet is considered to include many of the healthiest food consumption habits known globally [37-39].

The Mediterranean diet is characterized by a high intake of vegetables, fruits, water, whole grain products, olive oil and nuts. In addition, moderate amounts of fish, white meat, dairy products and wine are included. It is important to note that the Mediterranean diet does not only include specific food products, but it pertains to a lifestyle including physical activity, conviviality and adequate rest [38, 40-42]. As a result, this lifestyle pattern has been linked to a decreased risk of developing type 2 diabetes, cardiovascular incidents, certain types of cancer, neurodegenerative diseases and overall mortality [43-48].

### Mediterranean diet pyramid

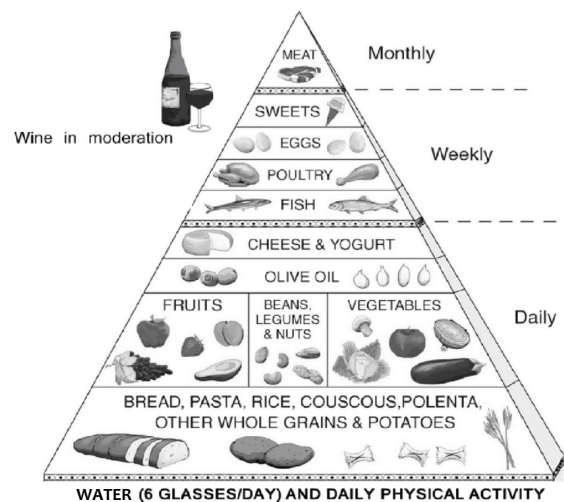


Figure 2 The composition of the Mediterranean diet and associated life style. Characteristic high intake of water, whole grain products, fruits, vegetables, beans, nuts, olive oil and dairy is visualized, together with lower intake of fish, eggs, sweets, meat and wine. Daily physical activity is also included [32].

Significant relations between the Mediterranean diet and lower incidence of AD have been found. These findings highlight the relevance of dietary factors in the origin and development of the disease. The beneficial effects of the Mediterranean diet can be related to several factors

and, additionally, their interactions. More research is required to understand the established relation. Nevertheless, as this diet contains low iron content, research groups investigating effects of iron load on AD pathophysiology refer to this diet to support their suggestions of the influence of dietary iron on the development of AD. They also speculate that dietary iron levels influence their respective brain concentrations [37, 38, 40, 49].

Other indications for the influence of dietary iron levels on brain iron load are provided by *in vivo* studies in rats performed by Pinero et al. They evaluated the effect of dietary iron excess and shortage on brain iron levels in rats at different stages in development. Irrespective of the age of the rats (10 to 35 days of age), they found changes in brain iron levels when providing the animals with different diets. Iron enriched meals were consistently related to increased levels of iron in the brain, whereas iron deprived animals showed lowered cerebral iron levels [34, 50]. Several other researchers who performed animal studies drew similar conclusions [49, 51, 52].

Hagemeier et al. investigated this proposed dietary relation in humans by applying susceptibility-weighted magnetic resonance imaging. They focussed on the deep grey matter structures of the brain and found significant relations between diet and the magnetic resonance imaging (MRI) values obtained in these regions. They claim that the intake of iron supplements and iron-rich foods increase brain iron values, similar to the conclusions drawn from animal studies. However, to date, the effect of dietary iron levels on brain iron load is still fairly poorly characterized and requires further investigation [34].

#### Gender affecting brain iron values

Undoubtedly important to consider are gender differences in body iron values. As discussed in the supplementary material, iron excretion is limited. However, women of reproductive age do lose significant amounts of iron due to menstruation, during pregnancy and during delivery. As a result, women show lower total body iron levels compared to men. However, due to this periodic loss of iron, women are more often advised to take iron supplements by their general practitioner, equalizing their body iron values to men's [34].

Hagemeier et al. found lower brain iron values in females. The same research group also suggested that the equalization in body iron load by the intake of supplements is reflected in the brain [34, 53].

#### **d) Brain iron regulation**

As the brain has a high rate of oxygen consumption, it requires large amounts of iron to transport sufficient amounts of oxygen to the brain [14, 54]. However, excessive quantities can induce oxidative stress and brain damage. As a result, iron transport over the BBB is highly regulated by several mechanisms.

First, similar to the regulation demonstrated in the intestinal tissue (see supplementary material), the ferroxidases hephaestin and ceruloplasmin control the transport of iron into the brain. McCarthy and Kosman found that blocking the activity of these ferroxidases evokes the internalization of ferroportin. As a result, iron transport into the brain is decreased [14, 29]. Second, in accordance with the findings in enterocytes, hepcidin can reduce iron transport into the brain as confirmed by Du et al [14, 55]. Third, astrocytes, located at the interface of the endothelium and brain parenchyma, are proposed as key modulators of iron entry. They are believed to exert a sensor function for iron circulating in the brain and could affect iron transport via signalling peptides. However, these peptides still need to be identified [14, 31].

### e) Role of iron in neurological function in humans

Several studies have indicated the relevance of iron for multiple body functions, including cognitive performance. Iron levels are critical, particularly in the neonatal period, and can cause irreversible damage. Unfortunately, iron deficiency is the most common form of nutrient deficiency. Most often children of age zero to five are affected, although it occurs in all age groups [56, 57].

Perinatal iron deficiency is related to impairment of cognitive development. Functions involving attention, intelligence, learning, memory, sensory perception, emotions and behaviour can be altered [19, 57, 58]. In addition, iron supplementation in adults suffering from iron deficiency (e.g. iron deficiency anaemia) has been shown to improve their cognitive functions, like attention and IQ, and behaviour [58, 59].

### f) Iron related to pathology: neurodegeneration with brain iron accumulation

As iron exerts multiple important functions in the body, dysregulation of its homeostasis is suggested to be related to pathology. Moreover, the association of iron accumulation in the brain with pathology is not a completely new finding. A group of inheritable neurological disorders, named neurodegeneration with brain iron accumulation (NBIA), is characterized by progressive iron deposition in the brain and subsequent neurodegeneration. The iron accumulation is particularly prominent in the basal ganglia and is related to multiple symptoms, including dystonia (sustained or repetitive muscle contractions), muscle rigidity, parkinsonism (tremor, bradykinesia, instability), dysarthria (speech difficulties), ataxia (impaired coordination of movements), confusion, disorientation, optic atrophy, seizures and dementia. Although cognitive symptoms have been associated with specific types of NBIA, the majority of patients are spared from cognitive deterioration [60].

Ten types of NBIA can be distinguished and are associated with different genes (Table 1). Mutations in these genes affect either the iron, phospholipid or ceramide metabolism. Lysosomal impairment has also been implicated, whereas other demonstrated mutations occur in genes with unknown functions [60-68]. Due to the genetic origin of the disease, an early onset is often established (ranging from infancy to adulthood). The progression of the disease can either be fast or slow and can include periods of stability [60].

**Table 1. Ten types of NBIA**

<b>Disease</b>	<b>Abbreviation disease</b>	<b>Associated gene</b>
Pantothenate Kinase-Associated Neurodegeneration	PKAN	<i>PANK2</i>
PLA2G6-Associated Neurodegeneration	PLAN	<i>PLA2G6</i>
Mitochondrial Membrane Protein-Associated Neurodegeneration	MPAN	<i>C19orf12</i>
Beta-Propeller Protein-Associated Neurodegeneration	BPAN	<i>WDR45</i>
Fatty Acid Hydroxylase-Associated Neurodegeneration	FAHN	<i>FA2H</i>
Kufor-Rakeb syndrome	KRS	<i>ATP13A2</i>
Neuroferritinopathy	NF	<i>FTL</i>
Aceruloplasminemia	/	<i>CP</i>
Woodhouse-Sakati syndrome	WSS	<i>DCAF17</i>
COASY Protein-Associated Neurodegeneration	CoPAN	<i>COASY</i>

The name and abbreviation of the diseases are shown as well as their associated genes.

### g) Magnetic properties of iron and its effects on magnetic resonance imaging

To facilitate an understanding of the magnetic properties of iron, a short introduction to magnetism is provided. Magnetic properties detected by MRI are mediated by protons present in the nucleus of atoms. These small, positively charged particles are continuously spinning around an axis, resulting in the generation of an electrical current. According to laws of physics, every electrical current induces a magnetic field. As a consequence, the protons behave similar to small magnets.

When a patient is placed into an MRI scanner, he or she is exposed to an external magnetic field. Hydrogen protons present in the patient's body align with the main static magnetic field. During this alignment, the protons move around like a spinning top, a movement called precession (Figure 3). The speed at which the protons precess is called the precession frequency. This frequency depends on the strength of the external magnetic field and can be calculated using the Larmor equation (equation 1). In the Larmor equation,  $\omega_0$  presents the precession frequency,  $\gamma$  the material-dependent gyromagnetic ratio and  $B_0$  the applied external magnetic field [69].

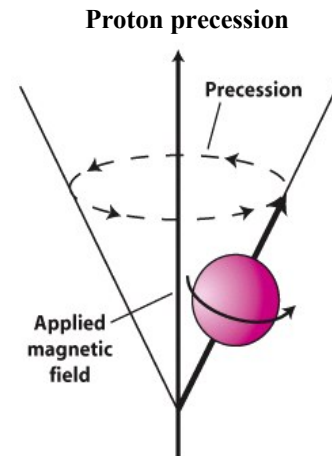


Figure 3 Protons precess with a specific frequency in an applied external magnetic field [66].

$$\omega_0 = \gamma * B_0 \quad (\text{equation 1})$$

Parallel alignment is associated with a lower energy state and the majority of protons align in the direction of the applied magnetic field. As a result, the net magnetic vector is in this direction, called the longitudinal magnetization (Figure 4A). As this vector is in the same direction as the external magnetic field, it cannot be used to measure the magnetization of the patient. To accomplish excitation, a radio frequency (RF) pulse is applied during the execution of the MRI protocol. Only if the frequency of this RF pulse equals the precession frequency of the protons, can energy be transferred to the protons for signal generation in MRI. As a result, the longitudinal magnetization decreases, and a new vector arises, called the transversal magnetization (Figure 4B and 4C). The latter process is generated by a synchronization process that forces the protons to be 'in phase'. As a consequence, after this disturbance of the alignment of the protons, the net magnetization is not aligned to the direction of the applied magnetic field any longer. This allows for the ability to measure the MRI signal of the patient [69].

From the moment the RF pulse is switched off, the transversal magnetization decreases, and the longitudinal magnetization increases. This is called transversal or  $T_2$  relaxation and longitudinal or  $T_1$  relaxation, respectively (Figure 4).  $T_1$  relaxation or spin-lattice relaxation takes place when protons transfer the energy received by the RF pulse, to their surroundings (lattice). As a result, the majority of protons re-establish their parallel alignment with the external magnetic field. In addition to this phenomenon, the protons lose their synchronized phase, causing the disappearance of the transversal magnetization. This is the result of the protons being exposed to a not entirely homogenous applied magnetic field and to small magnetic fields of neighbouring nuclei, causing them to precess at different speeds [69].

### Longitudinal and transversal magnetization

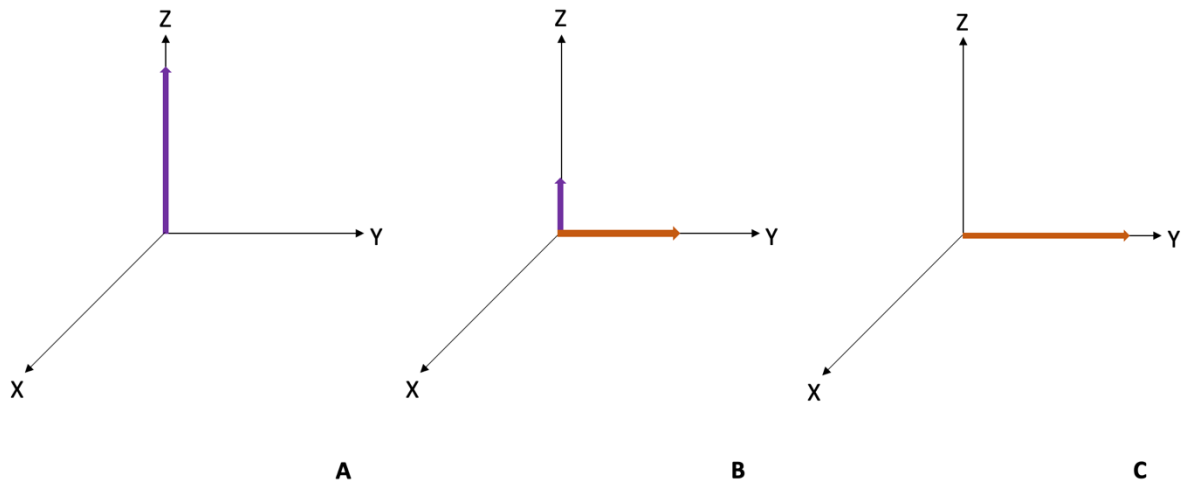


Figure 4 When introducing a patient to an external magnetic field, the protons align with this field and the longitudinal magnetization vector emerges (A). After sending in an RF pulse, the longitudinal vector starts to decrease due to energy transfer to the protons and a new vector arises, the transversal magnetization vector (B). Depending on the RF pulse, the longitudinal vector can disappear completely (C). After switching off the RF pulse, the reverse (from C to A) takes place until the transversal vector disappears completely ( $T_2$  relaxation) and the longitudinal magnetization is completely recovered ( $T_1$  relaxation).

Various magnetic properties of tissue can affect the MRI signal. These can be divided into three categories, namely diamagnetism, paramagnetism and ferromagnetism.

Diamagnetism is established when all electrons of an atom are paired-up in their orbitals (the area surrounding the nucleus in which the odds to encounter an electron constitute 90%). As a result, the electrons, either spinning up or down, cancel each other out which renders a total spin of zero. When exposing diamagnetic materials to an external magnetic field, changes in the orbital motion of the electrons occur. As a result, a magnetic field in the opposite direction is induced, yielding a negative susceptibility effect.

Paramagnetic atoms contain unpaired electrons in their orbitals. In this case, the spin of the electrons is not cancelled out, which renders the regarding orbitals a net spin (either up or down). When applying an external magnetic field to paramagnetic materials, a magnetic field in the same direction is induced. Thus, the concerning material has a positive susceptibility. Ferromagnetism regards strong magnetic properties which allow the materials to become permanently magnetized. When ferromagnetic materials are introduced into an external magnetic field, positive susceptibility occurs [17, 20, 69, 70].

Iron is a ferromagnetic material. Its magnetic properties are created by electrons in the unfilled d sub-shell. However, the majority of iron in the body is incapsulated in molecules, affecting its magnetization. Two major phenomena can be distinguished, namely the inner and outer sphere mechanism. Iron ions not associated with other molecules are in direct contact with the surrounding protons. This allows for the acceptance of energy, which, as mentioned before, shortens the  $T_1$  relaxation time. This phenomenon is called the inner sphere mechanism. By contrast, iron ions incorporated in molecules are shielded by a protein shell, which prevents them from exchanging energy with the surrounding protons. Nonetheless, they have the ability to dephase the spins of the protons, which accelerates  $T_2$  relaxation, called the outer sphere mechanism [69].

In fact, there are additional factors affecting the magnetic properties of iron-containing molecules [71]. For instance, iron associated with transferrin and deoxyhaemoglobin have paramagnetic properties, whereas oxyhaemoglobin-binding results in diamagnetism [17, 70]. The iron-transport protein, transferrin, by contrast, demonstrates superparamagnetic features when bound to iron. Superparamagnetic materials behave similar to paramagnetic ones but have a larger magnetic susceptibility [17, 70, 72]. The differing magnetic properties of oxyhaemoglobin and deoxyhaemoglobin can be explained by a change in the number of unpaired electrons. Iron present in deoxyhaemoglobin possesses four unpaired electrons, rendering paramagnetic properties. However, after binding oxygen, iron retains none of the unpaired electrons and becomes diamagnetic [73].

The MRI technique is very sensitive to iron present in tissues of the body. It is important to note that MRI scanners do not directly measure the magnetic fields created by the electrons of the iron atoms. The associated decay occurs in nanoseconds, which is too fast to detect for conventional MRI scanners. The presence of iron rather affects the relaxation rates of surrounding protons, especially the  $T_2$  relaxation rate. As mentioned before, transversal magnetization disappears due to the protons getting out of phase. This process is accelerated in conditions of proton exposure to varying surrounding magnetic fields. As iron has significant magnetic properties, it generates microscopic magnetic field inhomogeneities that accelerate the de-phasing process. As a result, the  $T_2$  relaxation rate is higher and  $T_2$  relaxation time shorter. In a  $T_2$ -weighted image, this would be visualized as darker regions, as less signal will be provided by the surrounding protons [20, 69].

In addition, a discrimination can be made between  $T_2$  and  $T_2^*$ .  $T_2^*$  depends, similarly to  $T_2$ , on spin-spin interactions. However, it differentiates from  $T_2$  relaxation in its sensitivity to static magnetic field inhomogeneities. The latter are caused by imperfections in the magnetic field generated by the MRI scanner and by magnetic susceptibility effects in the patient [24, 74, 75]. Iron constitutes one of the elements that can affect this additional component of  $T_2^*$ . As a consequence,  $T_2^*$  relaxation has been found to be more sensitive to changes in iron concentration than  $T_2$  relaxation [76].

#### **h) The contribution of different iron forms to the MRI signal**

As iron exists in many different biochemical forms and complexed to different molecules, varying effects on the MRI signal can be exerted. Although the effect of each form of iron hasn't been elucidated yet, some propositions have been made by researchers.

First of all, the ability to contribute to the MRI signal depends on the extent to which iron can affect the proton relaxation times, which is in turn determined by the concentration and relaxivity of the iron ions [71, 77]. The latter is defined as the increase in the relaxation rate when increasing the iron content with 1 mg/g and depends on the molecule iron is associated with. In general, it is accepted that only a concentration of at least 0.1 mM of magnetic ions will have the ability to contribute to the MRI signal [20, 71].

In the body, the free iron aqua ion content is very low ( $Fe^{2+} < 10^{-7} M$  and  $Fe^{3+} < 10^{-17} M$ ) and not considered to influence the MRI signal [71]. The majority of occurring iron is incorporated in molecules involved in transport and storage. The association of iron with different molecules can, as previously mentioned, affect its contribution to the MRI signal.

Therefore, the two major forms of iron, heme and non-heme iron, have different contributions to the MRI signal. The majority of heme iron is associated with haemoglobin. As mentioned before, the presence of oxygen in this molecule changes its magnetic properties. Oxygenated haemoglobin is classified as diamagnetic. As diamagnetism only shows weak magnetic properties, no significant effects on the MRI signal can be exerted. By contrast, deoxyhaemoglobin possesses paramagnetic properties and has the potential to significantly affect the MRI signal. However, under normoxic conditions its contributions to the MRI signal are very limited [20, 78].

Furthermore, the effects of varying forms of non-heme iron also need to be considered. As explained in the supplementary material, the cytosol of cells contains a labile iron pool. The composition of this pool is, however, poorly characterized. It is hypothesized to include iron-containing enzymes and proteins, as well as iron chelated with citrate, ATP, amino acids and probably other molecules. However, as the total amount of iron in the labile iron pool is low ( $\sim 1.5\mu\text{M}$ ), it is not expected to have any influence on the MRI signal [20, 22, 71].

The major iron-transporting molecule, transferrin, has a concentration of  $20\text{-}50\mu\text{M}$  in the serum. In the cerebrospinal fluid transferrin levels only reach  $0.2\mu\text{M}$  and in the brain grey matter its levels are approximately 10-50 times lower than ferritin. As a result, the effects of transferrin on the MRI signal are very limited [20, 79].

Nevertheless, ferritin and hemosiderin reach sufficiently high concentrations in the brain to influence the MRI signal. These storage proteins together contain 33-88% of non-heme iron in the brain. Ferritin has the capacity to store up to 4500 iron atoms in the form of ferrihydrite, a mineralized form of iron. The latter is the most abundant form of iron in the body and is associated with ferritin and hemosiderin [71, 80].

Particularly ferritin's effects on the MRI signal have been examined. *In vitro* studies showed a faster transversal relaxation in the presence of ferritin. Moreover, the relaxation time decreased proportionally with the concentration of ferritin [20, 81]. Vymazal et al. even found a relation between the amount of iron atoms contained in the ferritin molecule and the relaxational decay [20, 82]. Finally, it is also important to consider the effect of the applied field strength. The effect of ferritin on the MRI signal increases linearly with the strength of the applied magnetic field [20, 83].

Although iron constituting the labile iron pool cannot be detected by MRI, it draws the most attention of researchers. It is hypothesized that redox-active forms of iron are mostly contained in this pool and iron incorporated in ferritin and hemosiderin is expected to be harmless to the cell. Under pathological conditions, iron might build up in the labile iron pool, leading to cytotoxicity [84]. Fortunately, both hemosiderin and ferritin concentrations are related to the amount of iron in the pool of the cytosol. A dynamic equilibrium between them exists, which allows for iron load in the labile iron pool to be derived from the MRI signal intensity [84]. Moreover, as storage proteins like ferritin exert a protective function by incorporating iron, its concentration may increase due to higher iron levels in the iron pool. As a result, the storage proteins can reach such abundant amounts, causing physical blockage of essential cellular functions. Thus, leading to cell death by mechanisms unrelated to redox activity. This additionally indicates the importance of measuring its concentration [71].

### **3. Current knowledge of the involvement of iron in healthy aging**

Both human post-mortem analysis and *in vivo* imaging have provided indications for the involvement of iron in aging [13]. With age, iron tends to accumulate in the brain [2, 14, 85-87]. At the age of 30-40 years, a plateau is reached and at 60 years iron concentrations are more variable within the population [2, 88]. Although the cause of this accumulation remains elusive, different mechanisms have been proposed.

First, excessive iron can be caused by the occurrence of an imbalance in iron storage and transport proteins. Next, mitochondrial dysfunction and neurovascular mechanisms can play a role. Finally, iron release and accumulation due to myelin breakdown and repair malfunctions has been suggested [2, 89-91].

As mentioned before, in young healthy individuals, iron is mainly present in oligodendrocytes, necessary for myelination processes of neuronal axons [2, 92]. However, when people age, a redistribution can be observed. In elderly, iron tends to accumulate mainly in astrocytes [13, 93]. In the aged population, the majority of iron is located in the basal ganglia, including the putamen, globus pallidus and caudate nucleus [13, 87, 88]. In addition, Hebbrecht et al. found age-related iron increases in the cerebral cortex and white matter [13, 94, 95].

Furthermore, Ashraf et al. claims that healthy aging is characterized by iron dysregulation and that it is related to progressive cognitive decline [2, 92, 96].

The research group of C. Ghadery, investigated the relation between iron accumulation and cognition in healthy, aged individuals. They found that higher iron accumulation is related to more severe cognitive decline, supporting the hypothesis of Ashraf et al. Moreover, they identified a nearly linear association between iron accumulation in the globus pallidus and putamen, and cognitive performance. However, no causal relationship could be concluded from their data. More research should be performed to elicit the potential causality of iron on cognitive decline [87].

### **4. Current knowledge of the involvement of iron in Alzheimer's disease**

Next to normal aging, abnormally elevated iron levels have been found in areas typically affected by AD. Including the hippocampus, an important cerebral region for memory and orientation [13, 95]. An interesting observation is the coincidence of the age of expression of late onset AD (after age 65) and the elevation of iron brain levels in individuals susceptible to iron overload [2, 97]. Next, early onset AD (EOAD) can be found in individuals of age 40, which is the age at which iron levels reach a plateau phase [2, 98]. Finally, the genetic aberration trisomy 21, expressed as Down syndrome, is often accompanied by AD dementia around the age of 35. Again, a coinciding elevation of iron can be observed in these individuals [2, 99].

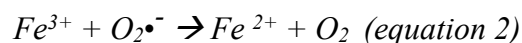
At this moment, iron dyshomeostasis is not included in the research framework of AD pathogenesis, nor considered as a diagnostic tool. However, increasing evidence for the role of iron is obtained by *in vitro*, *in vivo* and human studies. Several research outcomes even indicate the contribution of dysregulated iron to the earliest stages of AD.

#### **a) Relation between iron and oxidative stress**

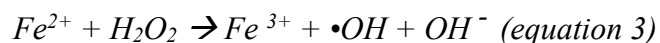
The ability of iron to exert many important functions in the body relies on its redox potential. It enables iron to exist in two forms, reduced  $Fe^{2+}$  and oxidized  $Fe^{3+}$ , and allows for the facilitation of electron-transfer reactions [19].

However, this redox behaviour also enables iron to act as a pro-oxidant to generate reactive oxygen species (ROS) by means of the 'Haber-Weiss reaction'.

According to equation 2,  $Fe^{3+}$  is reduced to  $Fe^{2+}$  by interaction with superoxide ( $O_2^{\bullet-}$ ).



In the second step, called the 'Fenton reaction', highly reactive hydroxyl radicals ( $\bullet OH$ ) are produced from hydrogen peroxide ( $H_2O_2$ ).



Finally, the net reaction produces  $\bullet OH$  from  $O_2^{\bullet-}$  and  $H_2O_2$ . (equation 3).



The resulting ROS contribute to the development of oxidative stress [12, 100]. This phenomenon is characterized by imbalanced pro- and antioxidant levels and disrupted redox signalling pathways [101, 102]. As a result, enhanced cell death, protein dysfunction and altered DNA and metabolism can be evoked, which all contribute to aging of the brain [103-107]. Compared to other organs, the brain is remarkably susceptible to oxidative stress due to several reasons. The particularly high oxygen consumption rate and energy demand, abundant levels of polyunsaturated fatty acids and redox active metals and confined antioxidant capacity, all play a role [108].

Fortunately, under physiological conditions the reaction rate of the Haber-Weiss reaction is low. However, under conditions of iron overload, iron acts as a catalyser to facilitate the reaction. Furthermore, a nonapoptotic cell death pathway depending on iron-related ROS accumulation, has been defined. This process, called ferroptosis, is still poorly understood [96, 109, 110]. Morphologically, ferroptotic cells can be recognized by altered mitochondrial appearance. The mitochondria demonstrate a smaller size and their cristae have a disorganized appearance [96, 110-112]. However, the functional relevance of these changes in the ferroptotic process and the cause are not known yet [96].

As ferroptosis requires iron, iron chelators have been shown to be potent inhibitors of this cell death pathway. Both  $Fe^{3+}$  and  $Fe^{2+}$  chelators have been found to be effective [96, 109]. Moreover, these ferroptotic inhibitors have been shown to exert a protective function in neurodegenerative disorders, including AD [109, 113].

#### Involvement of oxidative stress in Alzheimer's disease

Elevated levels of iron have been found in brain regions typically affected by AD pathology, including the hippocampus, cerebral cortex and nucleus basalis of Meynert [108]. Keller et al. and other researchers have proposed that iron-related oxidative damage constitutes one of the initial events in the onset of AD and contributes to its progression [103, 114, 115]. Their research elucidated the highest extent of oxidative damage in brain regions involved in cognitive dysfunction in AD and in regions with comprehensive neuronal degeneration [103-107, 114, 115]. Accordingly, several studies have found a link between oxidative stress and cognitive impairment [101, 103, 116].

In AD patients, cognitive decline has been correlated with loss of synapses. These essential structures of the nervous system allow for the propagation of electrical or chemical signals from one neuron to another and are involved in long-term potentiation (LTP) and depression (LTD)

[101, 117]. In AD patients, a typical inhibition of LTP and increase of LTD can be observed [101, 118]. *In vitro* and *in vivo* studies have demonstrated a direct correlation between oxidative stress and synaptic dysfunction. Moreover, synaptic loss is assumed to precede neuronal loss, which again indicates the role of oxidative stress early in the disease process [101, 119-121].

In addition, *in vitro* research using inducers of oxidative stress has confirmed its potential to cause neuronal death [103, 122, 123]. Keller et al. suggested a relation between increased protein oxidation and decreased cognitive performance [103]. They demonstrated signs of oxidative damage even in the MCI stage, indicating the importance of this mechanism in AD pathology and contributing to evidence for its involvement in the initial stages [103]. However, none of the researchers has been able to explain the role of oxidative damage in the onset and progression of AD.

Furthermore, mechanisms have been proposed to understand the role of oxidative stress in AD pathophysiology [2, 124]. Iron dyshomeostasis results in an increased  $Fe^{2+}/Fe^{3+}$  ratio. According to the previously discussed reactions,  $Fe^{2+}$  facilitates oxidative stress and causes damage to brain cells [2, 125]. In addition, lower  $Fe^{3+}$  concentrations cause indirect harm by promoting the production of excess  $O_2^{\bullet-}$ , and subsequent  $\bullet OH$ .  $O_2^{\bullet-}$  has also been found to have the ability to produce other toxic species by interaction with nitric oxide (NO) [2, 126]. This diffusible gas is hypothesized to delay A $\beta$  deposition as its levels are elevated in AD and inhibition promotes amyloid precursor protein (APP) expression and A $\beta$  production [2, 127]. Nevertheless, increased NO levels induce neuronal damage, prevent microtubule stabilisation by nitration of tau proteins and alter the production of iron regulatory proteins [2, 128].

Interestingly, the assessment of peripheral antioxidants is considered to provide reliable information on the oxidative conditions in humans [116, 129]. According to the study of Rinaldi et al., the plasma levels of antioxidants were similarly lower in MCI and AD patients compared to healthy controls. To exclude antioxidant depletion due to malnutrition, thorough nutritional assessment was performed for every subject. Moreover, malnutrition often occurs in late phase AD patients and the findings of this study showed diminished antioxidants even in early AD stages. The decrease in antioxidants included both non-enzymatic and enzymatic forms. An elevated induction of antioxidant enzymes would be expected with depletion of non-enzymatic antioxidant levels. However, MCI and AD patients appear to lack the ability to sufficiently activate antioxidant enzymes. This could be due to the high free radical production in patients, leading to rapid depletion of plasma antioxidants and absence of simultaneous enzymatic activation. Restoring the antioxidant levels in patients has been considered as a therapeutic option. *In vivo* experimentation with animal models of AD provided promising results. However, to date, clinical trials did not show significant beneficial effects in patients [116].

#### Mitochondria and iron dyshomeostasis in Alzheimer's disease

An important interplay between mitochondria and iron exists. A part of iron entering the body traverses these organelles, as mitochondria are key players in iron metabolism. They possess the ability to synthesize iron-sulfur clusters and heme prosthetic groups, which are vital for cell function as the electron transport chain highly depends on them [130].

With increased iron levels, mitochondria are exposed to more ROS, as a result of the redox-active iron pool [131]. This results in  $\bullet OH$ -mediated damage and eventually, mitochondrial dysfunction. Mitochondrial dysfunction impairs the production of ATP. As a consequence, the ability of neurons to exert their functions and to communicate with each other is affected. There

is a failure of the propagation of electrical signals, maintaining ionic gradients and enabling axonal anterograde and retrograde transport [16, 132]. In addition, mitochondrial dysfunction impairs the synthesis of iron-sulfur clusters and heme. This contributes to iron dyshomeostasis, which generates a pathological vicious cycle [16].

In its turn, mitochondrial malfunctioning enhances the production of free radicals [133, 134]. Mitochondria are the major source of ROS due to their active role in oxidative phosphorylation. During this process, ATP is produced by the conversion of oxygen into water. However, approximately 2% of oxygen yields  $O_2^{\bullet-}$  radicals, converted into  $H_2O_2$  by manganese superoxide dismutase.

Under normal conditions, free radical scavengers protect the cell by conversion into water [16, 108]. Unfortunately, in the presence of redox-active iron, reactive  $\bullet OH$  species are created via the previously mentioned Haber-Weiss reaction [108].

Next to the amyloid cascade hypothesis, the mitochondrial cascade hypothesis has been proposed for the development of AD. This hypothesis states that the decline of mitochondrial functioning is associated with the development of AD-related pathology and symptoms [101, 134]. Swerdlow et al. even suggested a relation between the severity of mitochondrial damage and the age of onset of the disease [134]. In addition, several studies have related mitochondrial dysfunction to AD pathophysiology. They have found detrimental effects on APP expression,  $A\beta$  accumulation and tau phosphorylation [134, 135].

#### Inflammation, mitochondrial dysfunction and iron dyshomeostasis in Alzheimer's disease

In addition to oxidative stress and mitochondrial dysfunction, Urrutia et al. considered inflammation as an important factor contributing to neuronal death in Alzheimer's disease. It is important to note that these are not fully separated phenomena and are related to each other in several ways [16, 136].

Important players in neuroinflammation are microglia and pro-inflammatory cytokines. Microglia are essential for inducing inflammatory responses as they are the residential immune cells of the brain [16, 137]. In several AD cases, a massive proliferation of these cells can be observed. As a result, their actions aiming to protect the brain are now leading to tissue damage. The activated microglia contribute to oxidative stress by two enzymes, namely NO synthase and NADPH oxidase [16].

The resulting inflammatory processes can lead to elevated levels of ROS, iron dyshomeostasis and mitochondrial dysfunction, which have all been linked to oxidative stress.

First, iron homeostasis can be affected by neuroinflammatory processes by means of the transcriptional modification of iron transporters. In particular, the DMT-1 is affected [16, 138]. Pro-inflammatory cytokines have been shown to increase the amount of this transporter and decrease ferroportin levels. This results in the accumulation of iron in the concerning cell, due to an elevated iron influx and diminished efflux [16, 139, 140].

Next, recent research has found the ability of inflammation to induce mitochondrial dysfunction in the central nervous system. Mainly a relation with toll-like receptors has been demonstrated, which have the ability to reduce mitochondrial oxygen consumption and cause oxidative stress. Moreover, these receptors can induce elevated ROS production by mitochondria. However, the involved molecular mechanisms still have to be elucidated [16, 141, 142].

In addition, mitochondria have been found to possess the capacity to modulate the immune response as well. In this way, mitochondria can activate the inflammatory response by means of novel pathways that remain to be elucidated [16, 143, 144].

#### Vicious cycle of multiple components leading to neuronal death

As a conclusion, a hypothesis is established suggesting a vicious cycle of five synergistic elements. Namely, oxidative stress, an exhausted antioxidant defense system, mitochondrial dysfunction, inflammation and iron dyshomeostasis [16].

Iron, mitochondrial dysfunction and inflammation all contribute to the generation of ROS. Whereas ROS are able to induce mitochondrial dysfunction, inflammation also damages the mitochondria by activating toll-like receptor signaling, again leading to ROS production. In addition, iron has the same effect by accumulating in the redox-active iron pool of the mitochondria and causing oxidative damage. Mitochondrial dysfunction, in its turn, promotes the production of ROS as well as iron dyshomeostasis. Finally, inflammation stimulates iron accumulation by promoting DMT-1 expression and diminishing ferroportin levels. Together with an insufficiently capable antioxidant defense system, these processes lead to an inevitable positive feedback loop causing neurodegeneration.

#### **b) Gender differences in susceptibility to Alzheimer's disease**

AD has been found to have a significantly higher incidence in women [145]. As age is a main risk factor for developing the disease, higher longevity of women has long been thought to be a causal factor for this finding. However, the prevalence of AD in females has been found to be higher in patients even in their sixties. This indicates the involvement of factors beyond merely sex difference.

The contribution of iron to this sex-dependent susceptibility to the development of AD seems unlikely at first sight as women tend to have lower iron values. Nevertheless, some research groups have hypothesized pathways to indicate its relevance. It has been hypothesized that men have a greater capacity in dealing with varying iron concentrations, due to their life long exposure to relatively high iron levels. By contrast, women in their reproductive life stage endure much lower iron loads compared to men. With the initiation of their menopause, iron starts to accumulate at a higher rate, causing damage to the brain tissue as its protective capacities are insufficient to deal with these elevations in iron concentrations [2].

A second hypothesis states that, due to the lower iron concentrations in the cerebral tissue of women, they solely have short-term iron storages available. This suggests the nearly continuous redox cycling of iron in women, increasing its ability to cause oxidative damage and to interact with protein aggregates in AD [2].

#### **c) $\beta$ -Amyloid neuropathology**

Amyloid plaques, consisting of deposited A $\beta$  fibrils, constitute one of the major hallmarks of AD. A $\beta$  peptides are derived from APP after cleavage by  $\beta$ -secretase (amyloidogenic pathway) and subsequent by  $\gamma$ -secretase [146]. Initially, the yielded A $\beta$  peptides exist as monomers. These are prone to aggregation into dimers, subsequently trimers, oligomers, protofibrils and finally fibrils. The latter finally deposit to generate amyloid plaques [146, 147].

Under physiological conditions, a second cleavage pathway of APP predominantly occurs. This pathway is called the secretory pathway (non-amyloidogenic) and involves APP cleavage by  $\alpha$ -secretase and subsequent  $\gamma$ -secretase. The former enzyme cleaves within the amino acid

sequence of the A $\beta$  peptide, precluding its formation. However, even when this pathway predominates, A $\beta$  peptides are still formed. Nevertheless, this is compensated for by clearance mechanisms [146, 148].

Interestingly, recent investigation has suggested an essential role of iron in the aggregation, oligomerization and amyloidosis of A $\beta$  peptides [15, 149-152]. They even claim that A $\beta$ -related toxicity is only established in the presence of an iron-rich environment. It is hypothesized that A $\beta$  has the ability to generate Fe<sup>2+</sup> from Fe<sup>3+</sup> by a reduction reaction, resulting in the generation of H<sub>2</sub>O<sub>2</sub>. The latter contributes to the production of ROS and subsequent oxidative damage [2, 153].

Furthermore, recent research suggests the co-localization of iron with amyloid plaques [154-157]. It is hypothesized that A $\beta$  incorporates iron to clear the excess of free iron in the brain [2, 153]. More results providing support for this hypothesis are obtained from *in vivo* studies using gene knock-out mice. When removing endogenous APP, elevated neuronal iron levels were observed and when overexpressing APP, iron was reduced [2, 158]. In the transgenic mouse model of AD *APP/PS1*, mutations are induced in both the *APP* gene and *PSEN1* gene (encoding  $\gamma$ -secretase). In this model iron overload was found to promote APP processing, amyloid plaque formation and was associated with cognitive decline [2, 159]. Nonetheless, this protective mechanism also has its pitfalls. As previously described, Fe<sup>3+</sup> bound to A $\beta$  is easily reduced to Fe<sup>2+</sup> iron, resulting in the production of ROS. The latter contributes to an environment stimulating the development of A $\beta$  oligomers and plaques [2, 153]. As a consequence, redox-active iron elements and A $\beta$  peptides can synergistically induce oxidative stress by producing ROS. A vicious cycle is created unavoidably leading to neuropathology. Nevertheless, a causal relationship has not been elucidated yet [101].

Other studies have demonstrated that iron can increase the deposition of amyloid plaques by a second mechanism. Namely, neuronal iron can promote the expression of APP. The translation of APP is suppressed by iron-responsive proteins. However, in the case of increasing cerebral iron concentrations, APP translation is promoted due to the interaction of iron with the iron-responsive element (IRE) of these iron regulatory proteins [12, 13, 159, 160]. In addition, iron overload stimulates amyloidogenic processing, resulting in increased A $\beta$  levels and eventually, insoluble A $\beta$  fibrils and plaques [2, 153].

Even more interesting, APP appears to have the ability to regulate iron homeostasis in the brain. APP exerts this function by interacting with ferroportin, affecting iron efflux [156, 161]. This is in agreement with the finding that neuronal iron levels increase in APP knockout models [156, 162].

These findings suggest a relation between iron and amyloid plaques. Further, they indicate the involvement of iron in an early stage of AD pathology. Additional support for this hypothesis was provided by Telling et al., who found iron present in diffuse A $\beta$  deposits. As these are considered to be immature plaques, they concluded that iron coincides with A $\beta$  very early in the disease progress [163, 164].

However, there is no conformity on the potential relation between iron and amyloid plaques. Researchers contradicting this hypothesis focus on results obtained from patients suffering from NBIA. In these cases, post-mortem analysis did not identify amyloid plaques as a typical pathological feature. Thus, they concluded that iron accumulation in the brain doesn't evoke A $\beta$  deposition and plaque formation. However, they did acknowledge the ability of iron to

accelerate the deposition of A $\beta$  [163, 165]. Moreover, the administration of iron chelators to restore iron dyshomeostasis has been found to diminish A $\beta$  aggregation and plaque load in animal models and humans. Even an improved cognitive performance was established [101]. As no agreement on this topic has been achieved, more research should be performed to improve the understanding of the relation between iron and amyloidogenesis. Nevertheless, a comprehensive amount of data indicates the relevance of iron, suggesting for the addition of the phenomenon of metallostasis in the amyloid cascade hypothesis.

#### **d) Tau neuropathology**

A second major hallmark of AD comprises neurofibrillary tangles, generated by the aggregation of tau proteins. Tau functions to stabilize microtubules in neurons and is regulated by its phosphorylation state [146, 166]. Microtubules constitute an essential part of the cytoskeleton and are indispensable for the maintenance of the neuronal structure and execution of axonal transport [146, 167]. Moreover, tau has been found to be involved in the transportation of APP to the neuronal surface and the facilitation of ferroportin iron export [2, 168].

Under physiological conditions, tau occurs in its soluble form. However, abnormal hyperphosphorylation results in the formation of insoluble tau, which is unable to bind to tubulin in the microtubules. As a consequence, they are precluded from exerting their functions, leading to cell death [146, 169, 170]. Moreover, insoluble tau is prone to aggregation into paired helical filaments, which deposit into neurofibrillary tangles [146, 170].

Similar to A $\beta$  deposition, colocalization of iron and intracellular neurofibrillary tangles has been demonstrated [2, 171]. Increased levels of cerebral iron diminish soluble tau concentrations, leading to neuronal iron retention due to the malfunctioning of ferroportin. In addition, loss of soluble tau prevents it from exerting its physiological function, stabilizing the microtubules. As a consequence, neurotransmitter transport, synapse stability and cellular health are affected [2, 172].

Moreover, *in vitro* experiments with neuronal cell cultures have provided proof for the induction of hyperphosphorylation of tau due to oxidative stress produced by Fe<sup>2+</sup>, and promotion of hyperphosphorylated tau aggregation by Fe<sup>3+</sup> [2, 173]. Iron-induced hyperphosphorylation of tau is thought to be mediated by an increase in glycogen synthase kinase 3 $\beta$  and/or cyclin-dependent kinase 5, which are important tau kinases, or by suppression of protein phosphatase 2, a tau phosphatase [12, 174].

#### **e) Genetic findings**

Several genes have been implicated in AD pathophysiology. *APP*, *PSEN1* and *PSEN2* are three identified causative genes and the *APOE* gene constitutes a genetic risk factor [175]. The latter encodes apolipoprotein E (APOE), of which three polymorphisms exist. First, the  $\epsilon$ 2 variant exerts a protective role, no association has been found with  $\epsilon$ 3, and  $\epsilon$ 4, identified in 40% of AD cases, has been linked to the onset and severity of AD dementia [2, 176-178]. APOE proteins have several functions, including cholesterol transport, A $\beta$  transferring, metabolism, aggregation and deposition [2, 179].

Bush et al characterized  $\epsilon$ 4 carriers by a strong relation between APOE protein and cerebrospinal fluid (CSF) ferritin levels. Furthermore, they observed major brain atrophy in patients with low APOE levels or high ferritin. After performing *in vivo* experiments with *APOE* knock-out mice, they concluded that APOE proteins decrease neuronal iron as these mice showed increased iron levels in the brain. Additional studies confirmed this finding by

exposing neurons to iron *in vitro* and by overexpressing the *APOE* gene *in vivo*. They found increased expression of the *APOE* gene and lower ferritin levels, respectively [2, 180]. In addition, human MRI studies of MCI patients demonstrated increased iron concentrations in *APOE*  $\epsilon$ 4 carriers, compared to MCI patients carrying other *APOE* variants [157, 181]. It is hypothesized that the  $\epsilon$ 4 variant reduces iron clearance and thus, potentially increases the risk of developing AD dementia [181, 182].

Next to these widely acknowledged AD-related genes, mutations in genes associated with iron often occur in AD as well. First, mutations in the gene encoding the iron-transporting protein, transferrin, are often observed in AD patients [181]. Second, human hemochromatosis (HFE) proteins, encoded by the *HFE* gene, have a function in iron absorption regulation via affecting the affinity of transferrin receptor 1. HFE proteins compete with iron-bound transferrin to bind to this receptor [2, 183]. Similar to the gene for transferrin, mutations in the *HFE* gene result in iron overload and are often involved in AD patients as well [2, 184-186]. Finally, the genetic sequence for the previously described DMT-1, is in close proximity to regions often affected in AD. Impairment of this iron transporter affects the transport of iron throughout the endothelial cell [2, 184].

#### **f) Knowledge from drugs**

As the involvement of iron in AD pathogenesis is a very recent finding, limited data of drugs influencing iron levels in AD are available. Huperzine A, a commonly used drug for AD, acts as a reversible acetylcholinesterase inhibitor and has an equivalent mode of action as donepezil, galantamine and rivastigmine [5, 187]. Several preclinical and clinical trials have demonstrated the efficacy of this drug [5, 188-191]. Interestingly, recent studies have demonstrated that Huperzine A treatment decreases iron levels in the brain. In an AD mouse model, treatment with this drug resulted in diminished amyloid plaque accumulation and hyperphosphorylation of tau. Moreover, when increasing iron, the beneficial effects provided by this drug were abolished. This provides additional indications for the important role of iron in AD pathogenesis [2, 192].

A second drug indicating the relevance of iron, is deferoxamine. This is a  $\text{Fe}^{3+}$  chelator applied to treat individuals with iron overload. McLachlan his research group was the first to use this drug to treat AD. The results of their clinical trial included a delayed clinical progression of the disease and improved behavioural functioning after administration for 24 months [2, 193].

A few years later Savory et al, followed by Prasanthi and Guo's research groups performed *in vivo* studies utilizing the same drug. They all agreed that deferoxamine decreased the amount of amyloid plaques, tau pathology and behavioural alterations [2, 194-197].

Although these results sound very promising, no human follow-up study has been performed. Nevertheless, Dr. Scott Ayton has started a clinical trial of five years in 2017, based on his positive findings on iron involvement in AD. The results of his research will undoubtedly render major contributions to the current knowledge of the relation between iron and AD [182].

#### **g) Knowledge from diet**

Regarding AD, it has been demonstrated that subjects with a strict adherence to the previously discussed Mediterranean diet have a 40-60% lower chance to develop the disease and show delayed cognitive decline. Even less strict adherence showed a reduced risk, indicating a potential dose-response effect [198-200]. Moreover, a reduced risk to develop MCI and decreased progression from MCI to AD have been linked to this dietary pattern. Both showing a dose-response effect as well [199]. Furthermore, Sofi et al found an overall reduced risk of 13% of the development of neurodegenerative diseases [43].

To date, these findings cannot be explained or attributed to specific dietary factors yet, as a tremendous number of factors and confounders can play a role. First, it is uncertain whether the beneficial effect of the Mediterranean diet on AD development should be attributed to single nutritional components, or rather to their interactions and dietary patterns. Second, there are increasing indications for the involvement of vascular factors in the risk for developing AD [198-201]. The Mediterranean diet pattern has been shown to reduce the incidence of vascular risk factors like hypertension and dyslipidemia [198, 202, 203]. Scarmeas et al included vascular variables in their models to relate the diet of the subjects to the incidence of AD. However, there was no change in their results compared to the outcome of the models excluding vascular risk factors. Their findings could be explained by underestimation of these factors due to evaluating them by self-report [198].

Nevertheless, other, nonvascular factors could also be involved in the beneficial effects of this diet. As mentioned before, iron overload has the potential to induce oxidative stress. This results in neuronal death and is increasingly related to the pathogenesis of MCI and AD [103, 108, 116, 199, 204]. Interestingly, the concerning diet comprises low iron levels and plentiful components with antioxidant properties, like olive oil [199, 205]. The combined effect provides reduced oxidative damage to brain tissue [198, 199, 206].

## **5. Conclusion**

It can be concluded that there are many indications of the importance of cerebral iron dyshomeostasis in AD. However, this subject is only in its infancy and requires more extensive verification. Several important questions require explanation. First of all, is iron dyshomeostasis a primary or rather a secondary factor of the patho-etiology of AD? Second, is cerebral iron dyshomeostasis related to systemic iron levels? Finally, what is the relation between iron, amyloidosis, neurofibrillary tangle formation and cognition?

With this project, the latter question will be examined. It has the potential to increase the understanding of the pathology of AD and contribute to the discovery of potential new drug targets.



## Materials and method

### 1. Study design

This was a cross-sectional study designed to compare brain iron load in control, MCI and AD populations. The study also sought to quantify the association between brain iron load and protein aggregates associated with AD. Data was collected at the McGill University Research Centre for Studies in Aging (MCSA). Patients were enrolled at the MCSA study if they were diagnosed with AD or MCI by a panel of neurologists based on their cognitive evaluation and the presence of both A $\beta$ /tau neuropathology. Age-matched healthy controls (CN) were also recruited. Only patients showing both A $\beta$  and tau deposits were included in this study. In total, 32 AD patients (including 15 late onset (LOAD) and 17 EOAD patients), 105 age-matched controls, 22 young controls and 21 MCI patients were used for this study. All individuals were subjected to extensive clinical examinations at the McGill University Research Centre for Studies in Aging.

To evaluate iron load, quantitative MRI techniques were applied. Apparent transverse relaxation rate ( $R_2^*$ ) was assessed solely for the brain grey matter. A $\beta$  and tau deposition were examined by utilizing positron emission tomography (PET). Finally, the mini-mental state examination (MMSE) scores, were used as a proxy for cognitive function. Group comparison allowed for assessing group differences on iron content. Association analyses were performed to examine the relationship between iron deposition, age, amyloid plaques, tau aggregation and cognitive decline in the grey matter of the brain.

### 2. Magnetic resonance acquisition and processing protocols

To obtain  $T_2^*$ -weighted multi-echo, gradient echo data, two protocols were used at two different image acquisition sites. At the Cerebral Imaging Centre (CIC) of the Douglas Mental Health University Institute, the Siemens® ‘MAGNETOM Trio 3T’ scanner was utilized with ‘Total imaging matrix (Tim) technology’. For the measurements a Tx/Rx 15-Channel Knee Coil was used and the *syngo* MR B17 software was applied. A 12-echo sequence was utilized to determine the magnitude and phase with a repetition time (TR) of 44.00 ms (echo times (TE): TE1=2.84 ms, TE12=39.80 ms, echo spacing: 3.36 ms). In addition, slice thickness was 1.00 mm, the excitation flip angle was 15 degrees and the field of view was 180 mm x 192 mm x 144 mm. Brain slices were obtained in transversal slice orientation. Secondly, at the Montreal Neurological Institute (MNI), a Siemens® ‘MAGNETOM Prisma 3T’ was used with Tim 4G technology. This scanner is equipped with an XR 80/200 gradient coil. For this protocol, a 7-echo sequence was applied to measure the magnitude and phase (TE1=5.00 ms, TE7=35.00 ms, echo spacing: 5 ms). The TR was 40.00 ms. Other imaging parameters included slice thickness of 1.00 mm, a flip angle of 17 degrees and a field of view of 176 mm x 224 mm x 160 mm.

In addition,  $T_1$ -weighted images were obtained by a protocol with a TR of 2300 ms, TE of 2.96 ms and an inversion time (TI) of 900 ms. Slice thickness was 1 mm, flip angle 9 degrees and the field of view dimensions were 176 mm x 240 mm x 256 mm.

Anatomical  $T_1$ -weighted images (with magnetization-preparation radio-frequency pulses and rapid gradient (MP-RAGE) readout; 1 mm<sup>3</sup> isotropic resolution), were processed using the standard FreeSurfer pipeline (<https://surfer.nmr.mgh.harvard.edu/>). Native space grey matter segmentation was performed by using the ‘Desikan-Killiany-Tourville (DKT) atlas to define the region of interest (ROI) [207]. All other images (PET and multi-echo  $T_2^*$ ) were co-registered to the  $T_1$ -weighted images prior to image processing.

To calculate  $R_2^*$ , a mono-exponential fit was applied on a voxel-wise basis. Quantitative iron levels in the brain were obtained by fitting an exponential across the echo time of each grey matter voxel using MATLAB fit function with the non-linear least squares method.

In human brain imaging, magnetic susceptibility artifacts at air-tissue interfaces can result in erroneous  $R_2^*$  values in the vicinity of the frontal sinus and ear canal regions. The goodness of fit of the  $T_2^*$  decay was used to partially identify these artifacts. In particular, the goodness of fit was calculated for every voxel and a threshold of 95% ( $R^2 < 0.95$ ) was applied. A high threshold was chosen to remove artifacts that showed a similar exponential decay due to scaling of the magnitude of the signal dropout as a function of echo time. However, a discrimination between real  $T_2^*$  decay from tissue and artifacts was possible due to a faster decay of the latter and greater oscillation at later echo times (rendering a lower goodness of fit). The iron values for grey matter voxels having  $R^2 < 0.95$  were averaged in each region of the DKT atlas. Similarly, standardized uptake value ratio (SUVR) images for tau and  $A\beta$  were averaged in every region of the DKT atlas, allowing for the regional analysis of iron,  $A\beta$  and tau values.

The iron values were registered to the DKT atlas and merged with the PET values to allow for regional analysis of iron,  $A\beta$  and tau values in 76 regions (Supplementary Table 1).

### **3. Positron emission tomography acquisition and processing protocols**

PET scans were acquired with a Siemens® High Resolution Research Tomograph (HRRT). For  $A\beta$  and tau detection, the [ $^{18}\text{F}$ ]AZD4694 and [ $^{18}\text{F}$ ]MK6240 tracer were used, respectively. [ $^{18}\text{F}$ ]MK6240 images were acquired 90-110 minutes after intravenous bolus injection and scans were reconstructed with the OSEM algorithm on a 4D volume with four frames (4 x 300s) [208]. [ $^{18}\text{F}$ ]AZD4694 images were acquired 40-70 minutes post-injection and scans were reconstructed with the OSEM algorithm on a 4D volume with three frames (3 x 600s) [209]. Immediately following each PET acquisition, a six-minute transmission scan was conducted with a rotating  $^{137}\text{Cs}$  point source for attenuation correction. Additionally, the images underwent correction for dead time, decay, and random and scattered coincidences [208, 210, 211].  $T_1$ -weighted images were non-uniformity and field-distortion corrected and processed using an in-house pipeline. Next, PET images were automatically registered to the  $T_1$ -weighted image space, and the  $T_1$ -weighted images were linearly and non-linearly registered to the ADNI template space. Subsequently, a PET non-linear registration was performed using the linear and non-linear transformations from the  $T_1$ -weighted image to the ADNI space and the PET to  $T_1$ -weighted image registration. The PET images were spatially smoothed to achieve a final resolution of 8mm full-width at half maximum [208, 212].

[ $^{18}\text{F}$ ]MK6240 SUVR maps were generated using the inferior cerebellar grey matter as a reference region and [ $^{18}\text{F}$ ]AZD4694 SUVR maps were generated using the cerebellar grey matter as a reference region. Additional information concerning the imaging methods pipeline can be found elsewhere [208, 213, 214].

### **4. Mini-mental state examination**

The MMSE was used to quantitatively estimate general cognitive function of subjects enrolled in our study. The MMSE examination includes questions grouped into seven categories, which each reflect different cognitive domains. Orientation to time (5 points), to place (5 points), registration of three words (3 points), attention and calculation (5 points), recall of three words (3 points), language (8 points) and finally visual construction (1 point) were all evaluated. The tested maximum score for the MMSE was 30 [215]. A score of 24 was considered as a cut-off for dementia [216].

## **5. Genetic analysis**

Determination of *APOE* genotype was performed using the polymerase chain reaction (PCR) amplification technique, followed by restriction enzyme digestion, standard gel resolution and visualization processes. Full details of this procedure can be found elsewhere [217].

## **6. Statistical analysis**

Statistical analysis was performed using 'MATLAB' software by MathWorks®. Multiple least squares linear regression models were used to evaluate the main hypothesis for each region independently. The relevance of adding confounders in the models was tested. Confounders were defined as variables correlating with both the independent and dependent variable. Finally, correction for multiple comparison was applied using the function 'mafdr' in 'MATLAB' which estimated a false discovery rate (FDR) [218].



## Results

Demographic and clinical features of the studied population are summarized in Table 2. In total, 180 subjects were examined. Twenty-two young controls were included with age ranging from 20 to 26 years. One hundred and five age-matched controls were recruited with age between 53 and 86. The MCI group included 21 patients with age ranging from 61 to 82. Finally, 32 AD patients with age between 44 and 87 were studied (including 15 LOAD and 17 EOAD patients). Every patient group included more females than males. An overview of the *APOE* variant distribution in our cohort can be found in the supplementary material (Supplementary Table 2).

**Table 2. Demographics and clinical features**

	CN(Y)	CN	MCI	AD EOAD	LOAD
Population	22	105	21	17	15
Age (years)	23.0±1.6	71.5±6.4	73.6±5.4	61.8±5.4	75.1±4.6
Gender (M/F)	8/14	35/70	8/12	7/10	6/9
MMSE	29.8±0.5	29.1±1.1	27.5±1.8	17.1±6.9	22.1±3.8
APOE (% ε4 carrier)	26.7	31.7	42.1	66.7	40.0
Site (CIC/MNI)	1/21	12/93	6/15	7/10	8/7

Data are expressed as mean ± standard deviation.

### 1. The site of acquisition affects brain iron quantification

For this analysis, solely aged controls were used. The images for 12 of them were acquired at the CIC site and 93 at the MNI site. Significant differences in iron values could be found for the MNI and CIC MRI acquisition sites (Table 3). In the left and right fusiform, left and right inferior temporal, left and right medial orbitofrontal, left and right parahippocampal, right isthmus cingulate, right lateral orbitofrontal and right transverse temporal cortex higher values could be found at the MNI site (Figure 5). Only the left cuneus showed lower iron values at the MNI site.

**Table 3. P- and t-values of regions showing significant differences between sites of acquisition**

Region	Hemisphere	p-value	t-value
Cuneus	Left	0.02	-2.53
Fusiform	Left	0.02	2.68
	Right	0.01	3.10
Inferior temporal	Left	0.00	4.37
	Right	0.01	3.07
Medial orbitofrontal	Left	0.01	3.29
	Right	0.00	3.87
Parahippocampal	Left	0.02	2.55
	Right	0.03	2.34
Isthmus cingulate	Right	0.01	3.07
Lateral orbitofrontal	Right	0.00	3.55
Transverse temporal cortex	Right	0.01	2.98

P- and t-values are rounded to two decimal places.

### Differences in brain iron values according to site of acquisition

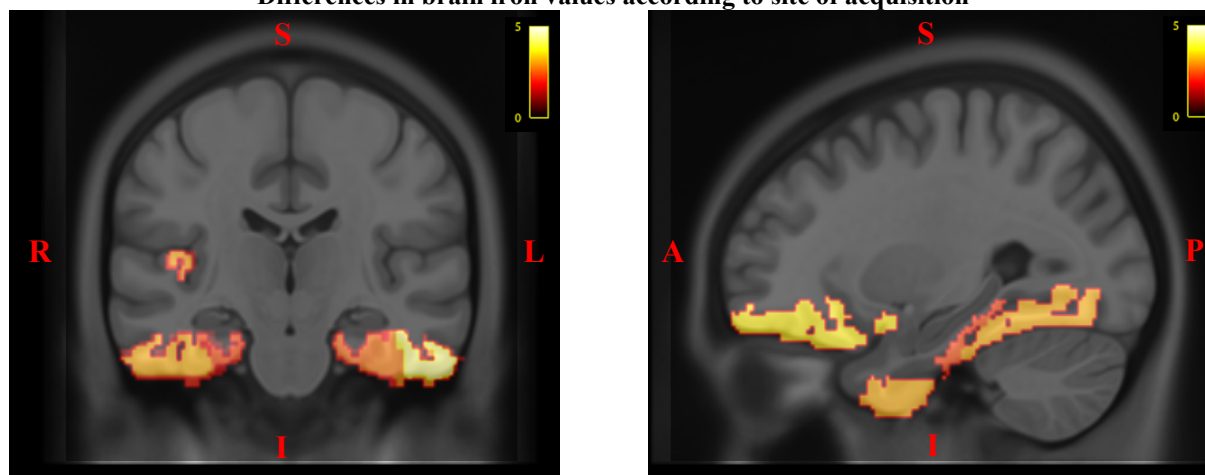


Figure 5 Frontal and sagittal images showing higher iron values at the MNI site compared to the CIC site in several grey matter regions (left and right fusiform, left and right inferior temporal, left and right medial orbitofrontal, left and right parahippocampal, right isthmus cingulate, right lateral orbitofrontal and right transverse temporal cortex). An intensity scale of zero to five was used.

## 2. The brain does not show sex differences in iron values

For this analysis, only aged controls were included. No sex differences were found in brain iron load (Figure 6).

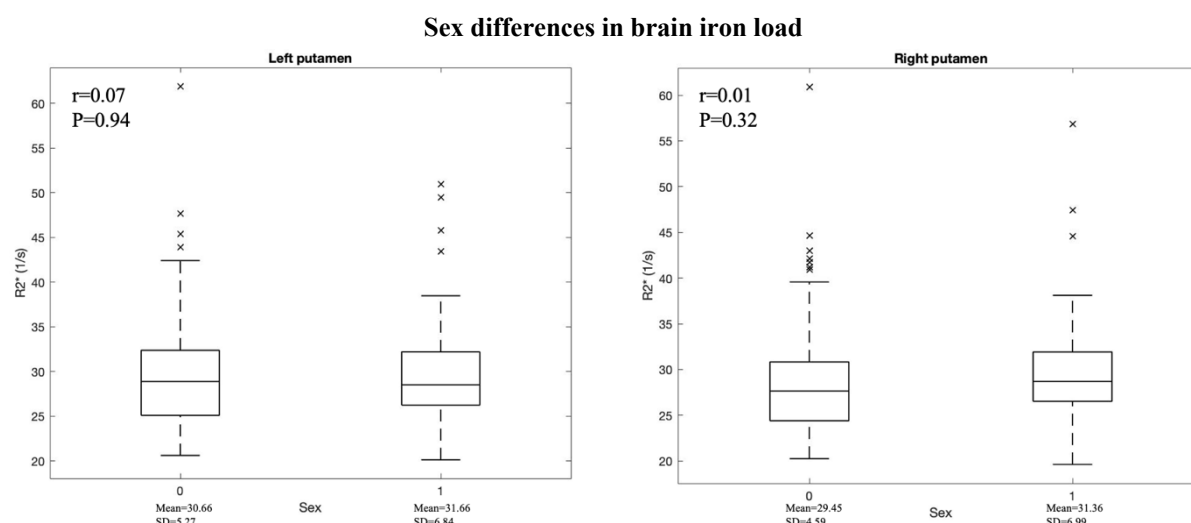


Figure 6 Boxplots showing no significant differences ( $p > 0.05$ ) between the brain iron load in females (0) and males (1). Data of the left and right putamen are provided as an example. The mean, standard deviation (SD), correlation coefficient ( $r$ ) and  $p$ -value are displayed. Diagonal crosses represent outliers.

## 3. Iron tends to accumulate in the healthy aging brain

For this analysis, young and aged healthy controls were used. In this population, elderly subjects showed significantly higher iron levels compared to younger participants in the vast majority of studied brain regions (Figure 7A and Supplementary Table 3). The highest levels could be found in the left and right caudate (Figure 8), left and right putamen (Figure 8), left and right pallidum (Figure 8), left and right caudal middle frontal, left and right pars opercularis, left and right precentral, left and right superior frontal, right supramarginal and right transverse temporal cortex (Figure 7B and Table 4). Nevertheless, several cortical regions showed comparable iron accumulation. In 74 of the studied 76 regions a positive relation was found. Solely in the left entorhinal and right lateral orbitofrontal cortex weak negative relations could be established (Table 4).

**Table 4. P- and t-values of regions showing the most significant brain iron load changes in healthy aging**

Region	Hemisphere	p-value	t-value
Entorhinal	Left	0.01	-0.19
Caudate	Left	5.47E-10	6.09
	Right	4.47E-11	6.75
Putamen	Left	9.29E-13	7.61
	Right	4.38E-12	7.23
Pallidum	Left	5.99E-11	6.64
	Right	6.15E-11	6.66
Caudal middle frontal	Left	1.92E-10	6.37
	Right	5.42E-11	6.64
Lateral orbitofrontal	Right	1.79E-3	-1.29
Pars opercularis	Left	7.22E-15	8.76
	Right	6.87E-14	8.15
Precentral	Left	1.76E-14	8.47
	Right	4.16E-12	7.28
Superior frontal	Left	1.84E-10	6.36
	Right	5.85E-10	6.09
Supramarginal	Right	7.57E-10	6.01
Transverse temporal	Right	1.72E-10	6.36

P- and t-values are rounded to two decimals places.

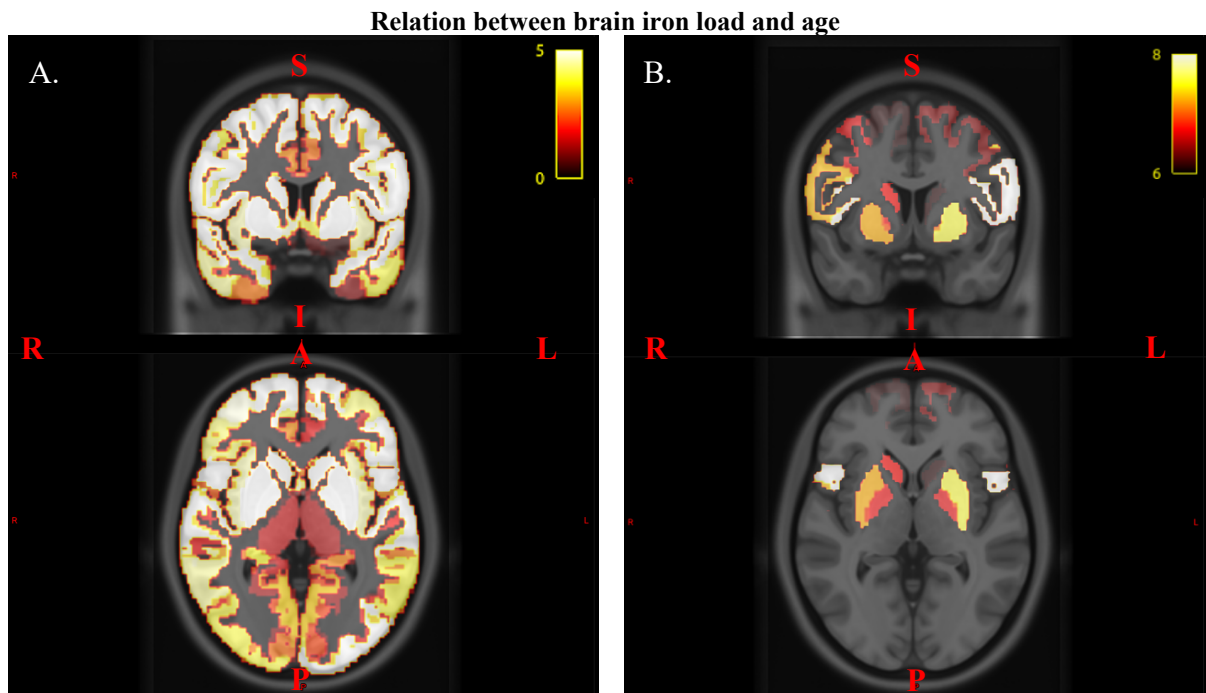


Figure 7 Frontal and transverse images showing brain grey matter regions with higher iron load with increasing age. An intensity scale of zero to five was used (A). The highest levels could be found in the left and right caudate, left and right putamen, left and right pallidum, left and right caudal middle frontal, left and right pars opercularis, left and right precentral, left and right superior frontal, right supramarginal and right transverse temporal cortex. An intensity scale of six to eight was used (B).

### Relation between brain iron load and age

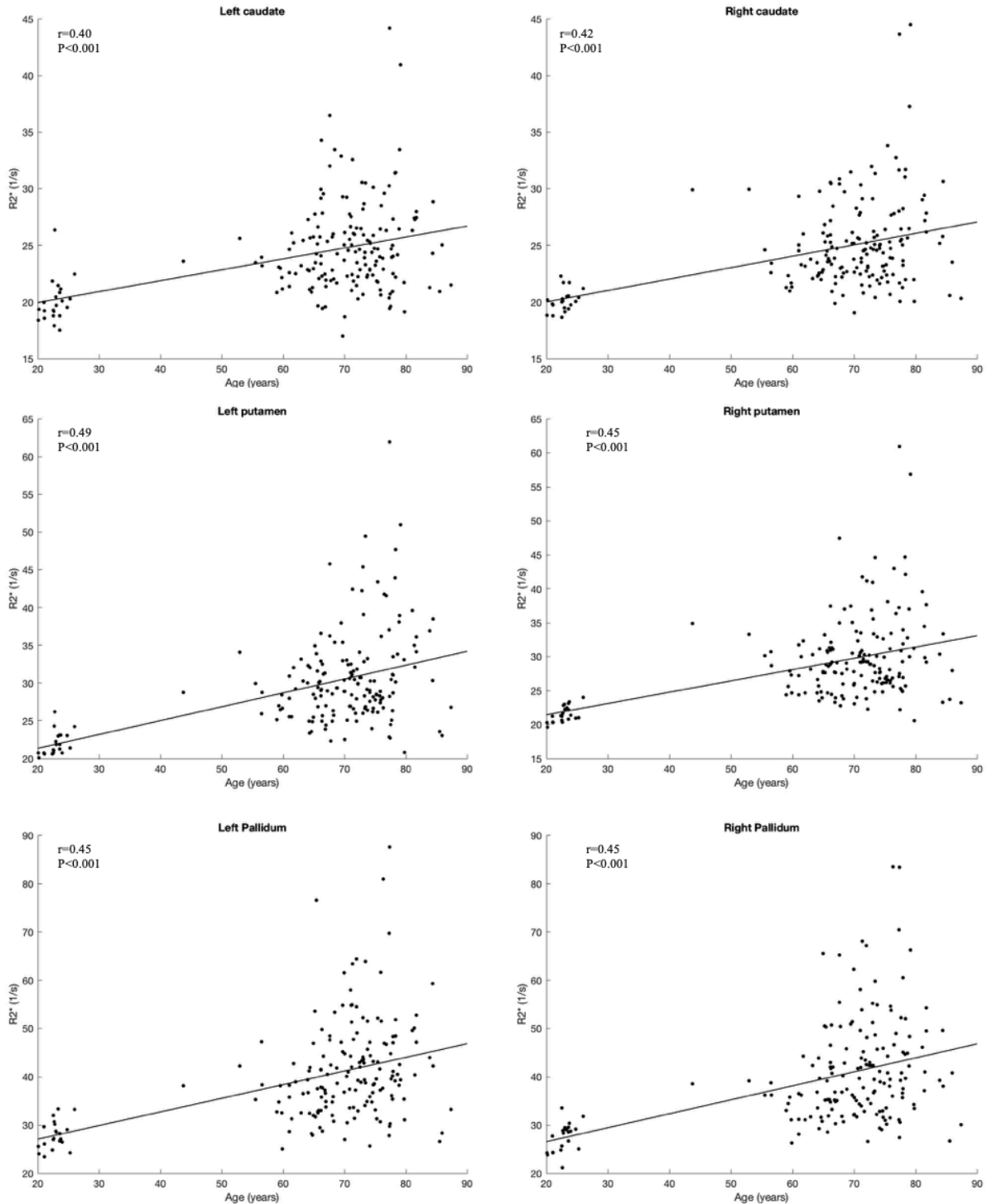


Figure 8 Scatterplots showing the extremely significant relation between brain iron load and age in the left and right caudate, putamen and pallidum ( $p < 0.001$ ). With increasing age, increased levels of brain iron can be observed. The  $r$ - and  $p$ -value are displayed.

#### 4. Alzheimer's disease patients show differences in iron load compared to controls

For this analysis, aged controls and patients (including MCI, LOAD and EOAD patients) were included. When comparing iron values between aged controls and patients (MCI and AD patients together), no significant relation could be found (Figure 9).

### Brain iron differences between controls and patients

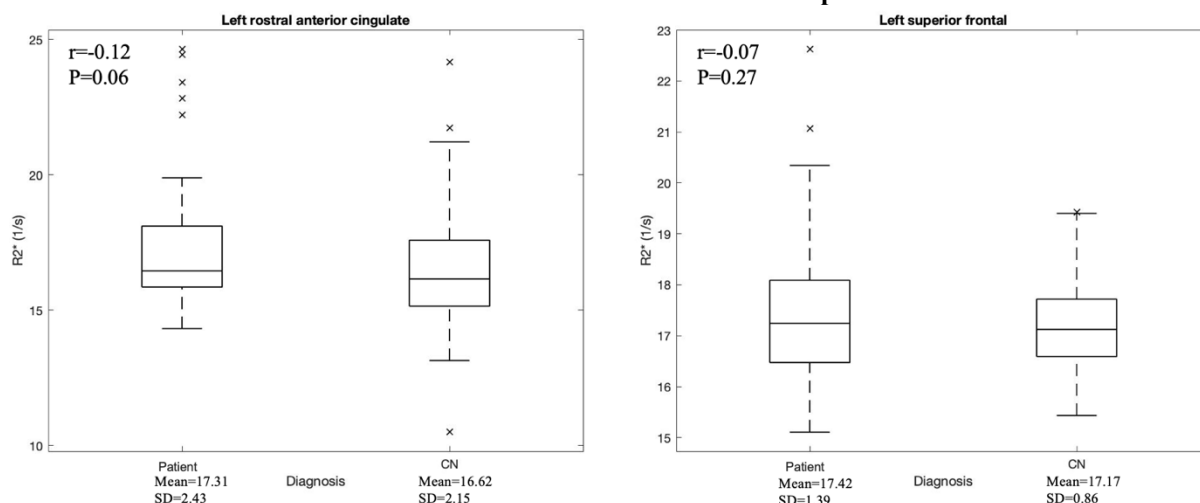


Figure 9 Boxplots showing the lack of differences ( $p > 0.05$ ) in brain iron load between aged controls and patients (including MCI and AD patients). Data of the left rostral anterior cingulate and superior frontal cortex have been displayed as an example. Mean, SD,  $r$ - and  $p$ -value are provided. Diagonal crosses represent outliers.

Nonetheless, LOAD patients demonstrated lower iron levels than controls in the left cuneus, left isthmus cingulate (Figure 10), left lingual (Figure 10), left paracentral, left pericalcarine, left precentral, left precuneus and left superior parietal cortex (Figure 11 and Table 5). By contrast, EOAD patients showed higher iron load than controls in the left rostral anterior cingulate (Figure 12), left and right superior frontal (Figure 12) and right caudal middle frontal cortex (Figure 13). Between these two groups a negative relation could also be found in the left thalamus proper (Table 6). No relations between controls and MCI patients or between MCI and AD patients could be found. All analyses were corrected for the site of acquisition.

**Table 5. P- and t-values of regions showing significant differences between controls and LOAD patients**

Region	Hemisphere	p-value	t-value
Cuneus	Left	2.48E-3	-4.18
Isthmus cingulate	Left	0.03	-3.10
Lingual	Left	0.01	-3.83
Paracentral	Left	0.02	-3.08
Pericalcarine	Left	0.03	-2.87
Precentral	Left	0.03	-2.86
Precuneus	Left	0.04	-3.12
Superior parietal	Left	0.03	-2.88

P- and t-values are rounded to two decimal places.

**Table 6. P- and t-values of regions showing significant differences between controls and EOAD patients**

Region	Hemisphere	p-value	t-value
Thalamus proper	Left	0.04	-3.03
Rostral anterior cingulate	Left	0.04	3.18
Superior frontal	Left	0.03	3.47
	Right	0.05	2.80
Caudal middle frontal	Right	0.04	2.93

P- and t-values are rounded to two decimal places.

### Differences in brain iron load between LOAD patients and controls

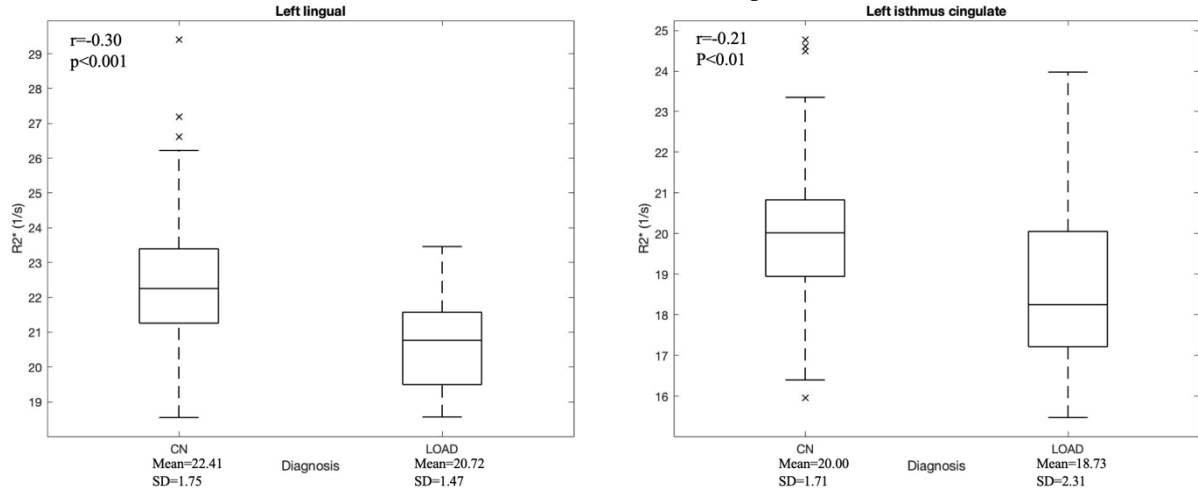


Figure 10 Boxplots showing lower iron load in the left lingual (extremely significant,  $p < 0.001$ ) and isthmus cingulate cortex (very significant  $p < 0.01$ ) of LOAD patients compared to aged controls. Mean, SD,  $r$ - and  $p$ -value are provided. Diagonal crosses represent outliers.

### Differences in brain iron load between LOAD patients and controls

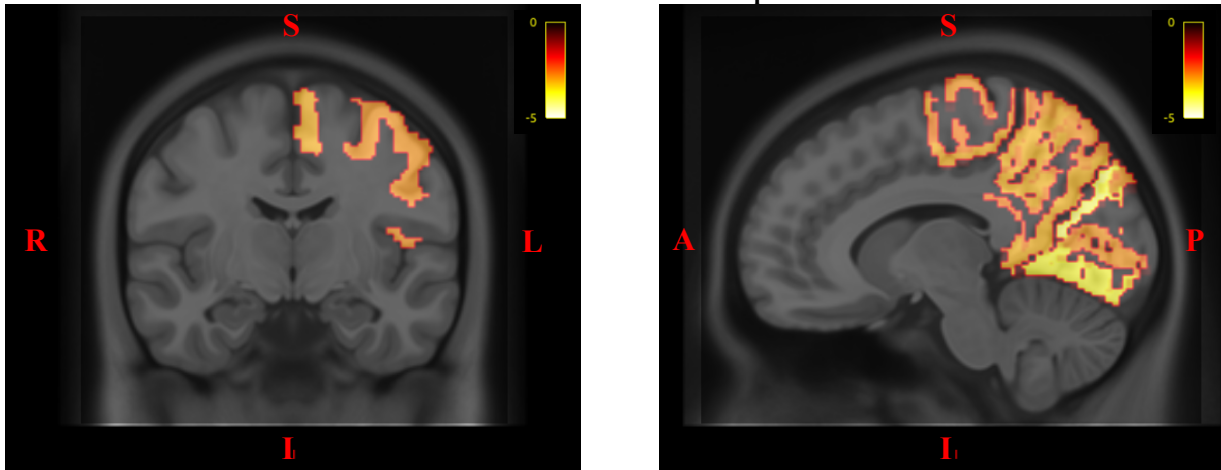


Figure 11 Frontal and sagittal images showing lower iron levels in LOAD patients compared to controls in the left cuneus, left isthmus cingulate, left lingual, left paracentral, left pericalcarine, left precentral, left precuneus and left superior parietal cortex. An intensity scale of minus five to zero was used.

### Differences in brain iron load between EOAD patients and controls

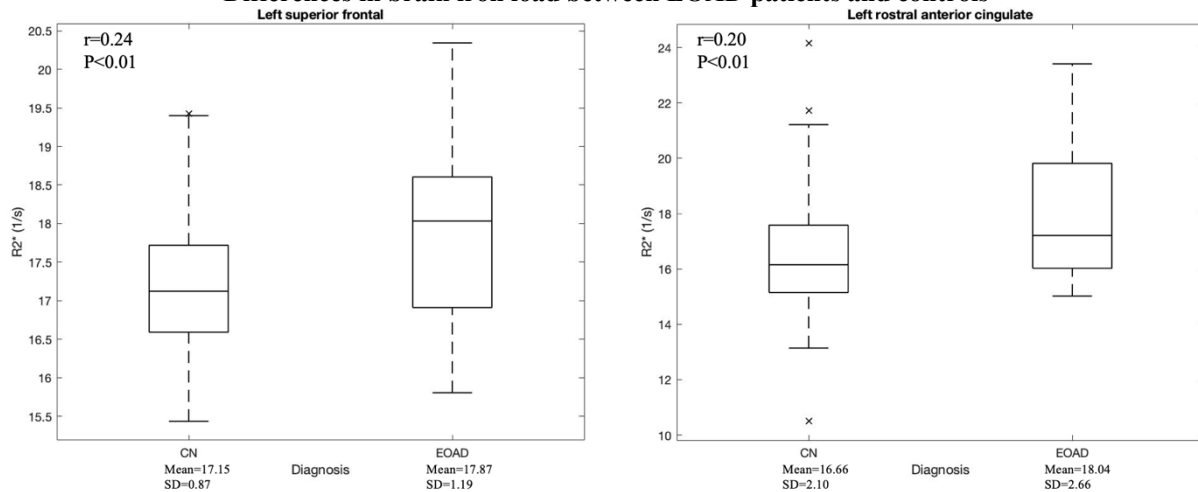


Figure 12 Boxplots showing increased iron load in the left superior frontal and rostral anterior cingulate cortex in EOAD patients compared to controls (very significant,  $p < 0.01$ ). Mean, SD,  $r$ - and  $p$ -value are provided. Diagonal crosses are outliers.

### Differences in brain iron load between EOAD patients and controls

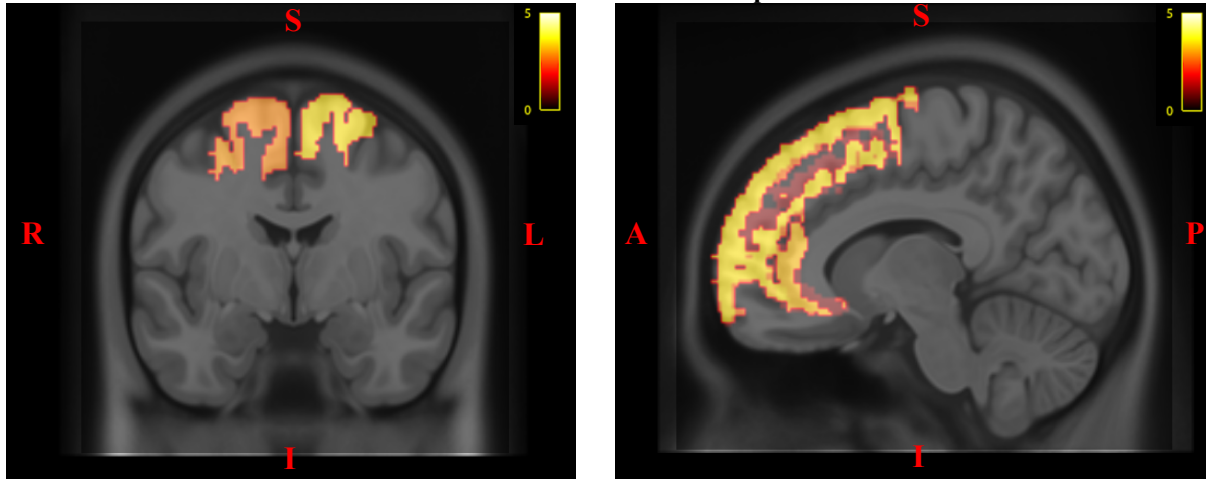


Figure 13 Frontal and sagittal images showing higher iron load in EOAD patients compared to controls in the left rostral anterior cingulate, left and right superior frontal and right caudal middle frontal cortex. An intensity scale of zero to five was used.

## 5. Iron load is not related to $\beta$ -amyloid deposition

For this analysis, aged controls and patients (including MCI, LOAD and EOAD patients) were included. No relation was established for iron load and regional  $A\beta$  nor global  $A\beta$  values (Figure 14). All analyses were corrected for age and site of acquisition.

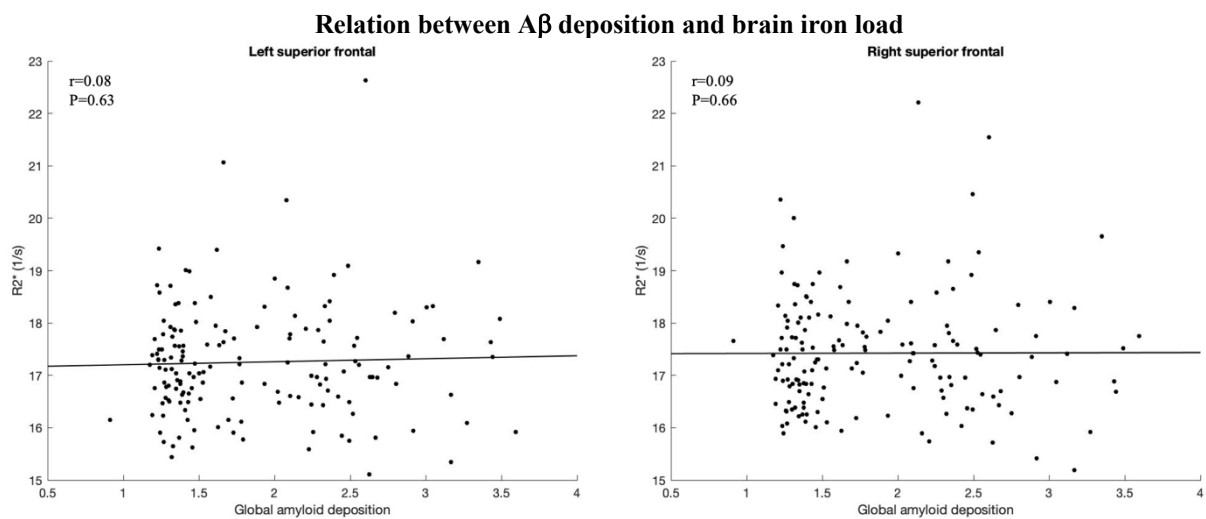


Figure 14 Scatterplots showing the absence of a significant relation ( $p > 0.05$ ) between brain iron load and global brain  $A\beta$  deposition (SUVR). Data of the left and right superior frontal cortex are provided as an example. Correlation coefficient  $r$  and  $p$ -value are displayed.

## 6. Iron load relates to global tau load

For this analysis, aged controls and patients (including MCI, LOAD and EOAD patients) were used. No regional relations between iron and tau deposits were established. However, when considering iron deposition and the global tau load in the brain, lower iron load in the left thalamus proper ( $p=0.03$ ,  $t=-3.61$ ) was found for higher total brain tau levels (Figure 15). The analysis was corrected for age and site of acquisition.

### Relation between brain iron load and total tau deposition

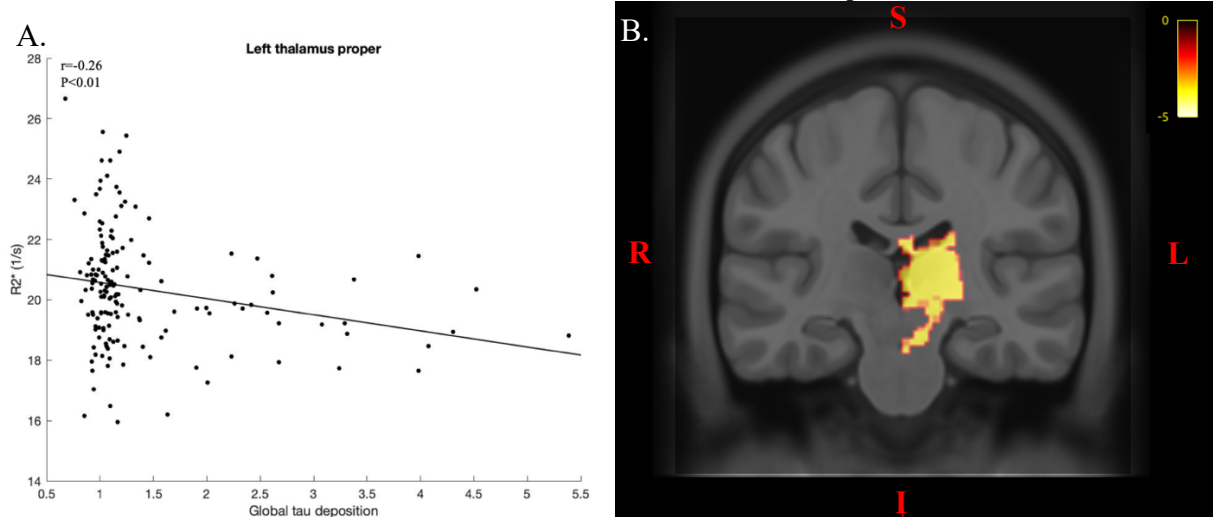


Figure 15 Scatterplot showing the negative very significant relation ( $p < 0.01$ ) between brain iron load and global tau deposition (SUVR). R- and p-value are provided (A). Frontal image showing lower iron levels in the left thalamus proper with higher total brain tau load. An intensity scale of minus five to zero was used (B).

### 7. Iron values relate to MMSE scores

For this analysis, aged controls and patients (MCI, LOAD and EOAD patients) were included. For higher MMSE scores, higher iron values could be observed in the left thalamus proper ( $p = 0.04$ ,  $t = 3.41$ ) (Figure 16). The analysis was corrected for age and site of acquisition.

### Relation between brain iron load and MMSE score

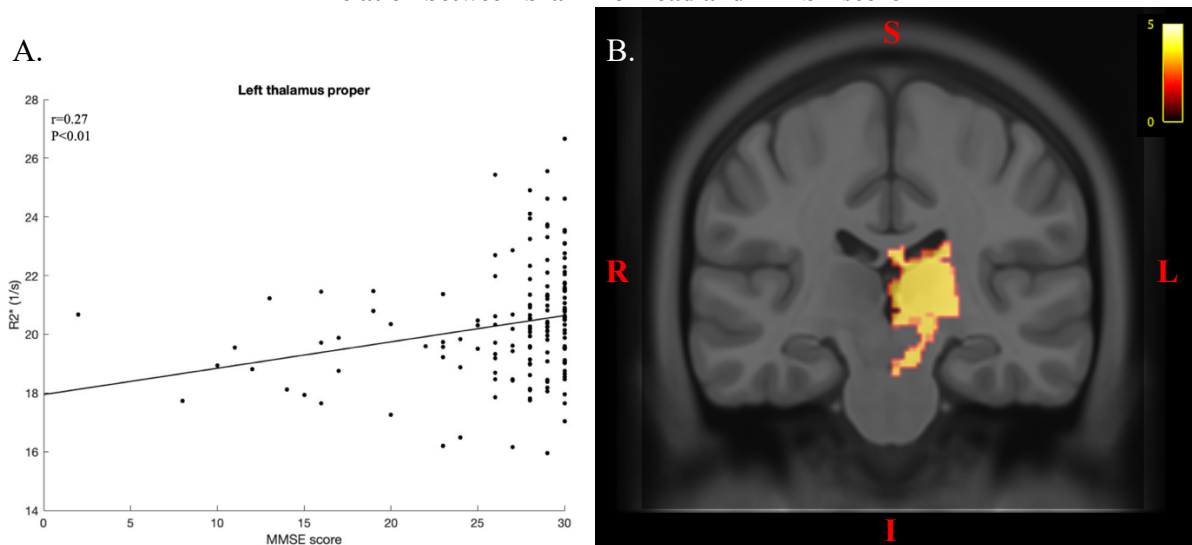


Figure 16 Scatterplot showing the very significant relation ( $p < 0.01$ ) between brain iron load and MMSE score in the left thalamus proper (A). Frontal image showing higher iron load for higher MMSE scores in the left thalamus proper. An intensity scale of zero to five was used (B).

### 8. Iron values differ for varying APOE $\epsilon 4$ variants

For this analysis, aged controls and patients (MCI, LOAD and EOAD patients) were used. No relation could be found for iron load between  $\epsilon 4$  carriers and non-carriers (Figure 17). The iron values of non-carriers and carriers of two  $\epsilon 4$  variants (homozygotes) were also not significantly different (Figure 18).

### Differences in brain iron load between carriers and non-carriers of the $\epsilon 4$ APOE allele

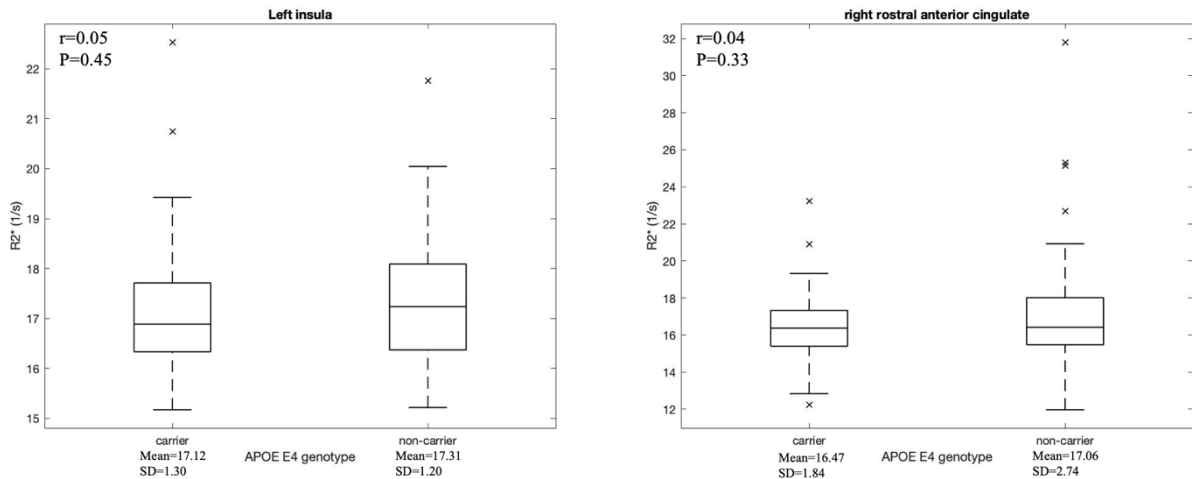


Figure 17 Boxplots showing no significant differences ( $p > 0.05$ ) in brain iron load between carriers and non-carriers of the  $\epsilon 4$  APOE allele. Data of the left insula and right rostral anterior cingulate cortex are provided as an example. Mean, SD,  $r$ - and  $p$ -value are provided. Diagonal crosses represent outliers.

### Differences in brain iron load between homozygotes and non-carriers of the $\epsilon 4$ APOE allele

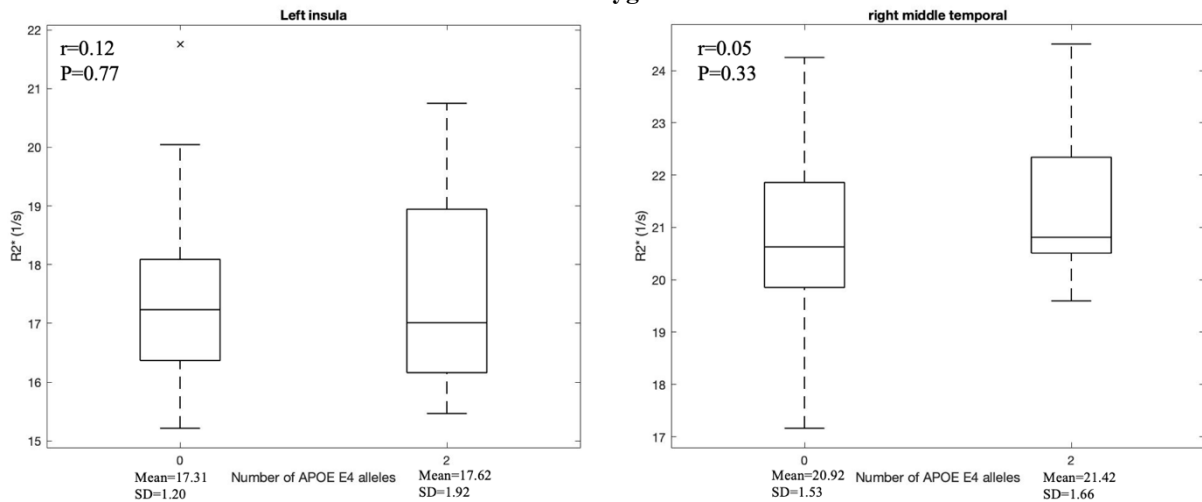


Figure 18 Boxplots showing no significant differences ( $p > 0.05$ ) in brain iron load between homozygotes and non-carriers of the  $\epsilon 4$  APOE allele. Data of the left insula and right middle temporal cortex are provided as an example. Mean, SD,  $r$ - and  $p$ -value are provided. Diagonal crosses indicate outliers.

Lower iron load was found in carriers of one  $\epsilon 4$  allele, compared to non-carriers in the left caudal middle frontal, left cuneus, left lateral occipital, left lateral orbitofrontal, left and right paracentral, left pars opercularis, left pars orbitalis, left and right pars triangularis, left precentral, left and right insula, right putamen, right caudal anterior cingulate, right medial orbitofrontal, right middle temporal, right posterior cingulate, right rostral anterior cingulate, right rostral middle frontal, right superior parietal and right superior temporal cortex (Figure 19 and Table 7). Contrary, higher iron values were observed in the left rostral anterior cingulate cortex (Supplementary Figure 2 and Table 7).

Although carriers of two  $\epsilon 4$  variants demonstrated lower iron load compared to carriers of one  $\epsilon 4$  allele in the left and right entorhinal, left and right putamen, left and right pallidum, left and right inferior temporal, left and right lateral orbitofrontal, left and right medial orbitofrontal, left and right parahippocampal, left and right rostral anterior cingulate, right amygdala, right thalamus proper, right fusiform and right superior temporal cortex (Figure 20 and Table 8). All other grey matter regions showed higher iron values in subjects homozygous for the  $\epsilon 4$  allele

(Figure 22 and Supplementary Table 4). The highest values were found in the left caudal middle frontal, left inferior parietal, left isthmus cingulate, left lingual, left postcentral, left posterior cingulate, left and right precuneus, left superior parietal (Figure 21), left superior temporal, left supramarginal (Figure 21), left transverse temporal and right middle temporal cortex (Table 9).

**Table 7. P- and t-values of regions showing significant differences in iron load between carriers of one  $\epsilon 4$  allele and non-carriers**

Region	Hemisphere	p-value	t-value
Caudal middle frontal	Left	0.04	-1.17
Cuneus	Left	0.04	-1.19
Lateral occipital	Left	0.04	-0.86
Lateral orbitofrontal	Left	0.04	-0.96
Paracentral	Left	0.04	-0.96
	Right	0.04	-0.96
Pars opercularis	Left	0.04	-0.95
Pars orbitalis	Left	0.04	-1.14
Pars triangularis	Left	0.04	-1.15
	Right	0.04	-0.98
Precentral	Left	0.04	-1.15
Rostral anterior cingulate	Left	0.04	0.91
	Right	0.04	-1.25
Insula	Left	0.04	-1.23
	Right	0.04	-1.17
Putamen	Right	0.04	-0.87
Caudal anterior cingulate	Right	0.04	-0.81
Medial orbitofrontal	Right	0.04	-0.82
Middle temporal	Right	0.04	-1.21
Posterior cingulate	Right	0.04	-0.92
Rostral middle frontal	Right	0.04	-1.22
Superior parietal	Right	0.04	-1.10
Superior temporal	Right	0.04	-1.03

P- and t-values are rounded to two decimal places.

#### Brain iron load differences between carriers of one *APOE* $\epsilon 4$ allele and non-carriers

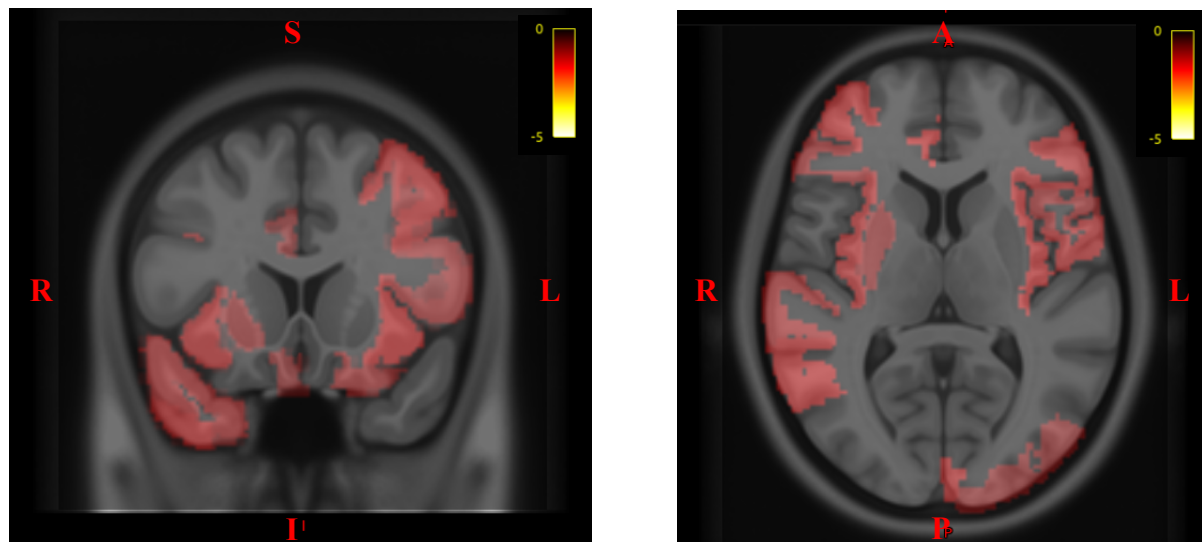


Figure 19 Frontal and transverse images showing lower iron values in carriers of one  $\epsilon 4$  allele compared to non-carriers in the left caudal middle frontal, left cuneus, left lateral occipital, left lateral orbitofrontal, left and right paracentral, left pars opercularis, left pars orbitalis, left pars and right triangularis, left precentral, left and right insula, right putamen, right caudal anterior cingulate, right medial orbitofrontal, right middle temporal, right posterior cingulate, right rostral anterior cingulate, right rostral middle frontal, right superior parietal and right superior temporal cortex. An intensity scale of minus five to zero was used.

**Table 8. P- and t-values of regions showing significant differences in iron load between heterozygotes and homozygotes of the  $\epsilon 4$  allele**

Region	Hemisphere	p-value	t-value
Entorhinal	Left	0.04	-1.70
	Right	0.04	-0.06
Putamen	Left	0.04	-0.38
	Right	0.04	-0.60
Pallidum	Left	0.04	-1.20
	Right	0.04	-0.35
Inferior temporal	Left	0.04	-1.20
	Right	0.04	-0.35
Lateral orbitofrontal	Left	0.04	-1.33
	Right	0.04	-0.76
Medial orbitofrontal	Left	0.04	-1.62
	Right	0.04	-1.22
Parahippocampal	Left	0.04	-0.88
	Right	0.04	-0.39
Rostral anterior cingulate	Left	0.04	-0.21
	Right	0.04	-0.74
Amygdala	Right	0.04	-0.14
Thalamus proper	Right	0.04	-0.25
Fusiform	Right	0.04	-0.82
Superior temporal	Right	0.04	-0.07

P- and t-values are rounded to two decimal places.

**Brain iron load differences between homozygotes and heterozygotes of the *APOE*  $\epsilon 4$  allele (negative scale)**

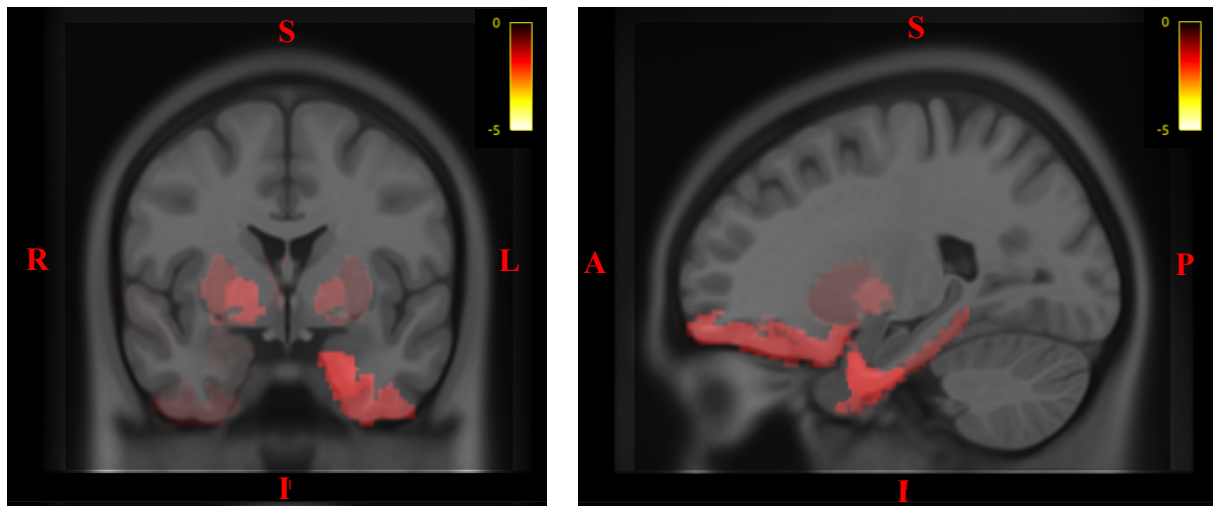


Figure 20 Frontal and sagittal images showing lower iron load in homozygotes compared to heterozygotes of the *APOE*  $\epsilon 4$  allele carriers in the left and right entorhinal, left and right putamen, left and right pallidum, left and right inferior temporal, left and right lateral orbitofrontal, left and right medial orbitofrontal, left and right parahippocampal, left and right rostral anterior cingulate, right amygdala, right thalamus proper, right fusiform and right superior temporal cortex. An intensity scale of minus five to zero was used.

**Table 9. P- and t-values of regions showing the most significant differences in brain iron load between homozygotes and heterozygotes of the  $\epsilon 4$  allele**

Region	Hemisphere	p-value	t-value
Caudal middle frontal	Left	0.03	1.91
Inferior parietal	Left	0.03	2.11
Isthmus cingulate	Left	0.03	2.11
Lingual	Left	0.04	1.67
Postcentral	Left	0.04	1.72
Posterior cingulate	Left	0.04	1.52
Precuneus	Left	0.03	2.72
	Right	0.03	1.58
Superior parietal	Left	0.03	2.19
Superior temporal	Left	0.04	1.64
Supramarginal	Left	0.02	2.64
Transverse temporal	Left	0.03	2.29
Middle temporal	Right	0.04	1.59

P- and t-values are rounded to two decimal places.

**Differences in brain iron load between homozygotes and heterozygotes of the  $\epsilon 4$  APOE allele**

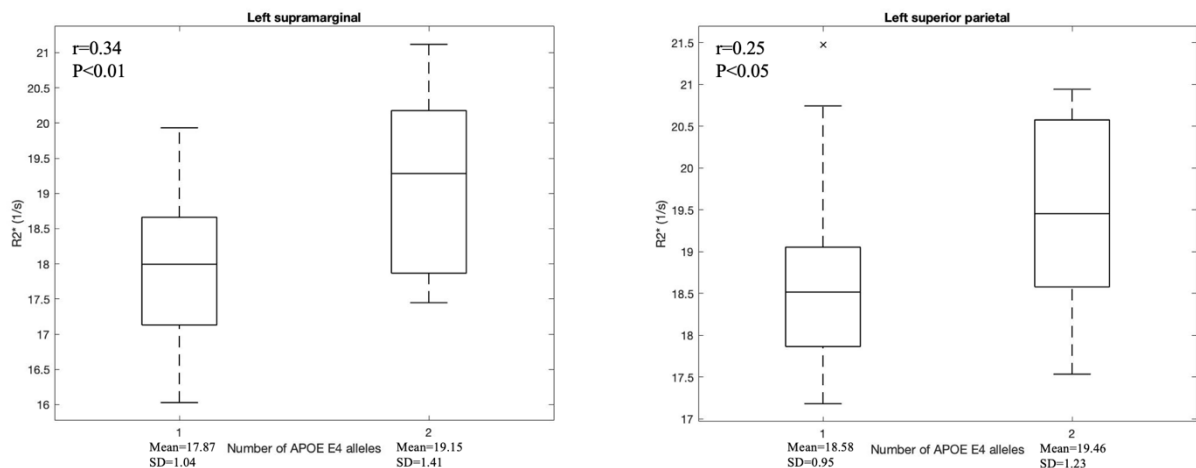


Figure 21 Boxplots showing increased brain iron load in carriers of two  $\epsilon 4$  APOE alleles compared to carriers of one  $\epsilon 4$  APOE allele in the left supramarginal (very significant,  $p > 0.01$ ) and left superior parietal cortex (significant,  $p < 0.05$ ). Mean, SD,  $r$ - and  $p$ -value are provided. Diagonal crosses represent outliers.

**Brain iron load differences between homozygotes and heterozygotes of the APOE  $\epsilon 4$  allele (positive scale)**

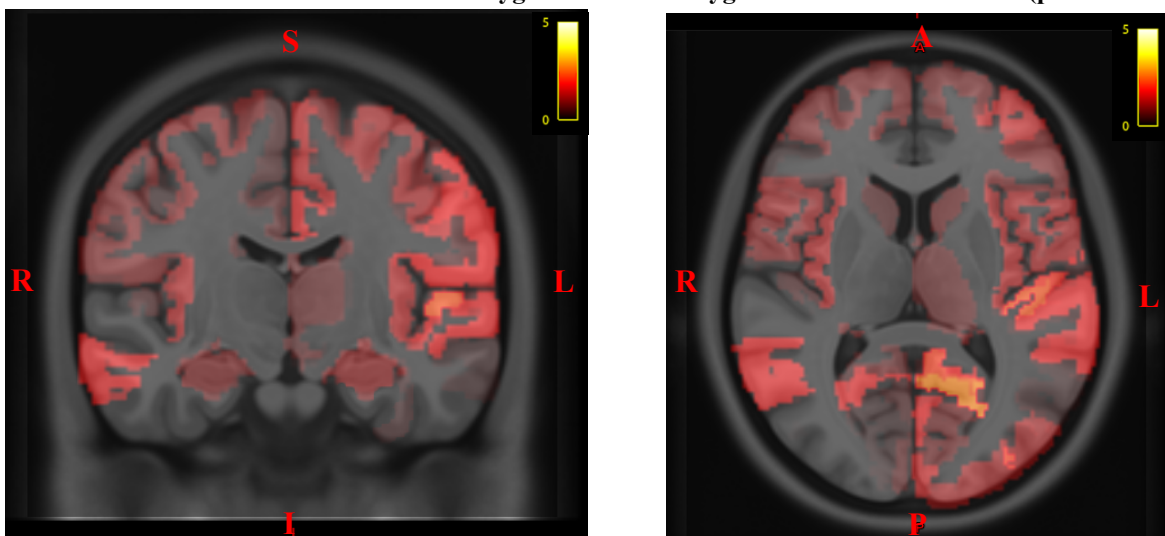


Figure 22 Frontal and transverse images showing higher brain iron load in homozygotes compared to heterozygotes for the  $\epsilon 4$  allele. The strongest relation was found in the left caudal middle frontal, left inferior parietal, left isthmus cingulate, left lingual, left postcentral, left posterior cingulate, left and right precuneus, left superior parietal, left superior temporal, left supramarginal, left transverse temporal and right middle temporal cortex. An intensity scale of zero to five was used.

## Discussion

To our knowledge, this project presents one of the most extensive *in vivo* studies of brain iron levels in healthy controls, MCI and AD patients. We have assessed iron values by quantitative multi-echo  $R_2^*$  mapping techniques. This method has been validated for the acquisition of *in vivo* brain iron load by a post-mortem study, showing a linear correlation between  $R_2^*$  and iron concentration [76].

Since the MRI images were acquired at two different sites (MNI and CIC) with differing protocols, the potential differences in the iron images were evaluated. At the MNI site, a protocol was applied including seven echoes, whereas at the CIC site, twelve echoes were used. We found higher iron values at the MNI site in the left and right fusiform, left and right inferior temporal, left and right medial orbitofrontal, left and right parahippocampal, right isthmus cingulate, right lateral orbitofrontal and right transverse temporal cortex. Only the left cuneus showed lower iron values at the MNI site. These regions have typically been found to be affected by artifacts. Although we corrected for artifacts, we acknowledge that some could still be present due to limitations of our correcting method. As a result, our findings were more robust in the regions showing no differences between the two sites.

Next, we did not find any differences in brain iron between male and female subjects. This result implies that the sex differences of systemic iron, are not reflected in the brain. These results contradict previous studies suggesting an effect of sex on brain iron load [34, 53]. We are not the first research group to contradict this hypothesis. Xu et al. also did not observe any sex differences in brain iron levels [219]. Furthermore, we question the claim that systemic iron levels change similarly to brain iron levels. To improve the understanding of their potential relation, more research into the topic should be done.

We provide further evidence for the recognized feature of brain iron accumulation with age. In particular, we replicate previous findings of a shift of iron to the basal ganglia with increasing age and extend this to iron deposition in a comprehensive part of the brain grey matter [13, 88, 92, 93]. Together with the basal ganglia, the caudal middle frontal cortex, pars opercularis, precentral and superior frontal cortex on both sides of the brain, show the highest iron accumulation with the process of healthy aging. We conclude that in healthy aging individuals, a predominant subcortical accumulation of iron occurs, with additional significant frontal depositions.

With increasing age, iron mainly accumulates in the form of hemosiderin and ferritin [94, 220]. It is hypothesized that, due to these elevations in iron deposition, more free ionic iron is released. These ions can participate in the Haber-Weiss reaction, leading to the production of ROS [13, 94]. Several studies have linked this event to the lower cognitive ability of elderly [220-224]. Thompson and Jahanshad thus suggested that iron can be considered as a ‘double-edged sword’. It is essential for the development of the brain in the initial stages of life, but promotes brain aging at older ages [225].

Next, we evaluated brain iron load according to diagnosis. We found lower iron values in the cuneus, isthmus cingulate, lingual, paracentral, pericalcarine, precentral, precuneus and superior parietal cortex of LOAD patients compared to healthy controls. These findings were only established in the left hemisphere of the brain. Nevertheless, EOAD patients showed higher levels compared to controls in the left rostral anterior cingulate, left and right superior frontal and right caudal middle frontal cortex and a negative relation in the left thalamus proper.

We conclude a predominant change in iron load in the cortical regions of AD patients that may be linked to AD onset status.

The lower iron load found in LOAD patients, contradicts other studies. We hypothesize that increase in brain iron alone may not contribute to the pathophysiology of AD, but rather the occurrence of a dysregulated iron metabolism and transport results in initiation of AD pathophysiology. Iron excess results in oxidative stress, leading to cell death. Iron insufficiency in the brain can also play a significant role in neuronal degeneration, due to its importance to several cell functions. Connor et al. found a decrease in transferrin in LOAD patients, leading to a decreased mobility of iron and, thus, an insufficient availability in the brain [226]. This could explain the lower iron load in LOAD patients that we have found. However, more research should be performed to elicit the changes of iron levels in AD patients.

In addition, LOAD patients showed a hemispheric asymmetry in brain iron changes. Lower brain iron values compared to controls could only be found in the left hemisphere. This hemispheric asymmetry in  $R_2^*$  relaxometry has been noticed before by other researchers [219, 227, 228]. Xu et al. measured shorter  $T_2$  in the left hemisphere of healthy controls and associated this with higher iron load [219]. They attribute this neurochemical difference in iron load to the distinct functions localized in the left or right hemispheres [219, 229].

Several studies have indicated a leftward asymmetry of the dopamine system in the brain, associated with increased dopamine production in the left hemisphere [230-232]. Iron has been found to be colocalized with dopaminergic neurons in the substantia nigra, owing to its essential functions as a cofactor for tyrosine hydroxylase, an enzyme important for dopamine synthesis [219, 233]. As a consequence, the iron requirements in the left hemisphere are higher than in the right hemisphere. Moreover, the capacity of dopaminergic neurons to transport iron has been suggested, resulting in an additional leftward asymmetry in the brain regions receiving dopaminergic projections from the substantia nigra [219, 234].

To our knowledge,  $T_2$  hemispheric asymmetry hasn't been examined yet in AD patients. Whether dopaminergic dysfunction is involved in AD pathophysiology is still under debate. Perez et al. suggested a causal role for  $A\beta$  deposition on dopaminergic pathology [235, 236]. Interestingly, it has been hypothesized that dopamine has a protective role against amyloidosis and oxidative stress [235, 237]. Our findings, showing lower iron load in the left hemisphere of LOAD patients, may indicate an associated dysfunctional dopaminergic system. More research should be performed to elucidate the role of hemispheric iron asymmetry in AD patients.

The findings for EOAD patients support current literature on iron deposition in AD pathophysiology. Increased brain iron load found in the patients results in the generation of ROS and subsequent oxidative stress. A vicious cycle arises, involving iron dyshomeostasis, oxidative stress, mitochondrial dysfunction and inflammation, eventually resulting in neuronal death. Moreover, an environment that promotes  $A\beta$  and tau aggregation is produced.

Finally, we found no differences in iron load when comparing MCI patients to controls or AD patients. This can indicate two possibilities. First, iron values in MCI patients might be of intermediate extent between controls and AD patients, without a clear regional trend, resulting in the absence of any significant relation.

Second, iron dyshomeostasis might only be detectable by our MRI technique in the later stages of AD. Several studies have indicated the importance of iron deposition in the initial stages of AD [2, 164]. We, thus, encourage the validation of MRI techniques for the detection of iron dyshomeostasis in the initial stages of AD.

We obtained A $\beta$  and tau values by analysing PET images and compared these levels to brain iron load. Iron levels in specific brain regions were compared to regional or total brain levels of the protein aggregates. No relations were found between iron load and regional nor total brain A $\beta$  load. This contradicts the proposed iron involvement in the amyloid cascade hypothesis [154-157]. As mentioned before, this topic requires extensive examination to elucidate the relation between iron and A $\beta$  deposition. Our results are in accordance with previous findings from a population suffering from NBIA. These patients showed iron accumulation without accompanying A $\beta$  aggregation [163, 165]. However, it is hypothesized that free iron forms are associated with A $\beta$  aggregates, which are not detectable by our iron quantitation technique.

Furthermore, Peters et al. concluded that iron-rich brain regions are significantly less affected by amyloidosis than regions with lower iron concentrations and vice versa [2, 88]. They hypothesized that low-iron regions are more susceptible to the dyshomeostasis of iron compared to regions with high iron content, as the latter have a greater capacity to maintain iron equilibrium. As mentioned before, iron ions have the ability to upregulate APP translation, contributing to amyloidosis. This theory also indicates the inability of our technique to detect iron associated with amyloidosis.

Nevertheless, the relation between iron dyshomeostasis and A $\beta$  deposition remains unclear. Current literature acknowledges a relation between iron deposition and amyloidogenesis in the brain [2, 238]. More research should be performed to elicit the nature of this relation and to elucidate whether our results are cohort-specific.

Next, no relation was found between regional iron and tau levels. Nonetheless, brain iron load was found to be related to total tau levels in the left thalamus proper. Higher iron levels were found to relate to lower total tau levels in the brain. This contradicts previous findings [2, 171]. Increased iron load is deemed to deplete soluble tau concentrations, leading to the destabilization of microtubules and increased iron retention, contributing to a vicious cycle [2, 172].

When we considered total tau levels and iron values in the separated patient groups, no relations could be found. This suggests that the established relationship was not valid and probably due to other factors or lack of power. Nevertheless, Ahmadi et al. performed an electrochemical study of iron-tau interactions, showing the association of Fe<sup>2+</sup> and Fe<sup>3+</sup> with tau proteins. Fe<sup>2+</sup> is considered to promote tau hyperphosphorylation, whereas Fe<sup>3+</sup> is associated with the aggregation of hyperphosphorylated tau proteins [2, 173]. As mentioned before, these ions can't be detected by our MRI technique. Thus, we propose to use techniques with higher resolution to determine the relation between iron and tau deposits [239].

MMSE scores were used to investigate the relation between iron load and cognitive ability. Higher scores were found to relate to higher iron levels in the left thalamus proper. Previous studies rather predict a negative relation, assuming lower cognitive abilities with higher iron levels [220, 240].

Similar to the total tau results, we analyzed MMSE scores in separate patient groups. We could not confirm our previously established relation between MMSE score and iron, suggesting again the involvement of other factors or lack of power.

We also investigated the relation between brain iron load and the *APOE* genotype of the subjects. To our knowledge, we present the largest study linking iron load to *APOE* genotype. The  $\epsilon 4$  variant is commonly found in AD patients and is associated with the age of onset and expression of the disease [2, 176-178]. Researchers, who performed an MRI study showing increased brain iron load in patients carrying this variant, proposed a causal role of the  $\epsilon 4$  *APOE* variant in the reduction of clearance of iron in the brain [181, 182].

We did not find a relation when comparing iron values between non-carriers and carriers of the  $\epsilon 4$  allele. The same result was found for the comparison of non-carriers and carriers of two  $\epsilon 4$  variants.

When comparing iron values between non-carriers and carriers of one  $\epsilon 4$  variant, lower levels could be found in the left caudal middle frontal, left cuneus, left lateral occipital, left lateral orbitofrontal, left and right paracentral, left pars opercularis, left pars orbitalis, left and right pars triangularis, left precentral, left and right insula, right putamen, right caudal anterior cingulate, right medial orbitofrontal, right middle temporal, right posterior cingulate, right rostral anterior cingulate, right rostral middle frontal, right superior parietal and right superior temporal cortex of the carriers of one  $\epsilon 4$  variant.

This contradicts the findings of van Bergen, showing higher cerebral iron in MCI patients carrying the  $\epsilon 4$  allele [157]. However, their study only included 22 controls and 15 MCI patients, which rises questions on the validity of their study. Our study covered a lot more subjects, including 104 non-carriers and 61 carriers. Nevertheless, we did find higher iron levels in the left rostral anterior cingulate cortex for these subjects. However, more research should be performed to truly understand the link between cerebral iron load and *APOE* genotype.

Carriers of two  $\epsilon 4$  variants showed lower iron levels in left and right entorhinal, left and right putamen, left and right pallidum, left and right inferior temporal, left and right lateral orbitofrontal, left and right medial orbitofrontal, left and right parahippocampal, left and right rostral anterior cingulate, right amygdala, right thalamus proper, right fusiform, right superior temporal cortex and higher levels in all remaining regions compared to carriers of one allele. The regions at the front of the brain near the sagittal sinus associated with lower iron values are questionable, as these regions are often affected by artifacts. As only six homozygous patients were included, these results cannot be fully trusted (Supplementary Table 2). Nevertheless, these are interesting findings and should be investigated further.

## **1. Strengths and limitations**

One of the strengths of our study is the number of included subjects. A second strength is the inclusion of age-matched controls for the AD patients. However, the different subgroups are not equally distributed, as the vast majority of the subjects (58%) are aged controls. This study only includes a limited number of patients (29%), reducing the robustness of our research. Nevertheless, the addition of young controls can be considered as a strength of our study and increases the validity of hypothesis testing of the relation between iron and age.

In addition to the confined number of included patients, 50% of the AD patients were suffering from an atypical form. Of these, 43% were found to show signs of posterior cortical atrophy (PCA) and 25% of primary progressive aphasia (PPA).

PCA patients are characterized by atrophy in the parietal, occipital and temporal lobes. This is typically expressed by progressive deterioration of literacy, visuospatial and visuoperceptual skills [241]. Only a few studies have been performed to examine A $\beta$  deposition in PCA patients. Four small-scale studies agreed on an increased deposition of A $\beta$  in the parietal and occipital lobes in PCA patients compared to the deposition seen in typical AD [242-245]. However, research with larger populations did not demonstrate any differences in A $\beta$  deposition between PCA and typical AD [246, 247]. Regarding tau deposition, very limited research has been performed. Day et al. claimed an increased vulnerability of the posterior regions to tau accumulation in PCA patients [248]. Nevertheless, many regions commonly affected in typical AD, showed also tau accumulation in these PCA patients. Moreover, they only included five PCA patients and all of them demonstrated only a very mild clinical picture to enable the investigation of the earliest stages of the disease. We conclude that, to date, insufficient evidence exists to reject the acceptance of a pathophysiological similarity between PCA and typical AD. Thus, we do not consider the inclusion of PCA patients in our study as a significant limitation. Nonetheless, more research should be performed to understand the similarities and disparities between these two pathologies.

PPA is a syndrome characterized by issues involving language. The diagnosis of PPA is established when the subject demonstrates impairment of word usage and comprehension, while, initially, other areas like memory, visuospatial skills and reasoning are relatively spared [249, 250]. Contrary to the neuropathology of PCA, only a small percentage of PPA patients shows similarities to the pathophysiology of typical AD [249, 251]. Some patients lack amyloidosis, show unusual neurofibrillary tangle distributions and ‘nonspecific focal atrophy’, referring to focal neurodegeneration in superficial cortical layers [249]. Moreover, no relation has been found between the *APOE*  $\epsilon$ 4 variant and the prevalence of the syndrome [249, 252]. Thus, significant differences have been found between the clinical picture and neuropathology of PPA and typical AD patients, prejudicing the robustness of our research. Nevertheless, only four PPA patients were included in our study, limiting the potential confounding effects of the differing neuropathology on our results.

Next, the majority of data acquisitions took place at the MNI site, which was associated with a different protocol than at the CIC site. The acquisition of the MRI images was initially performed at the CIC site, which later on was transferred to the MNI site for practical reasons. We did not recommend changing the protocol and this change was out of our hands. However, we corrected for potential effects of the acquisition site on our results when necessary, limiting erroneous findings due to this confounding factor.

Furthermore, we did not match the subject groups for sex and *APOE* genotype. Our cohort includes more women than men. This difference is particularly noticeable in the control groups. As we are mainly concerned about pathological differences between men and women, we do not consider the unequal sex distribution in controls as a significant confounding factor. Moreover, we did not find any significant sex differences for brain iron load, limiting the confounding effect of this group inequality for our analyses.

Next, our cohort includes mainly non-carriers of the *APOE*  $\epsilon$ 4 allele (58%). 31% of the population carries one  $\epsilon$ 4 allele and only 3% is homozygous for this variant. As a result, the accuracy of our results considering the homozygous subjects, is very restricted and cannot be used to draw valid conclusions.

During the visual evaluation of the  $R_2^*$  images, we noticed the presence of magnetic susceptibility artifacts. These were mainly apparent near the edges of the brain tissue, as a result of the air-tissue interfaces. The artifactual regions showed abnormally high  $R_2^*$  values and comprised some portions of the cerebral cortex. We decided to apply a threshold to every voxel, based on the goodness of fit of their  $T_2^*$  decay to an exponential decay model. We chose a sufficiently high threshold (95%), as the artifacts often showed substantial goodness of fit values as well. They resembled an exponential decay due to scaling of the magnitude of the signal decrease as a function of echo time.

First, we tried analyzing the images in a voxel-wise manner. However, this could only be established by creating a mask based solely on the voxels of all subjects above the applied threshold. In other words, if a voxel showed a goodness of fit below the threshold in only one patient, it was not included in the mask. As a result, the obtained mask could not be used for our analyses as the majority of cortical voxels were excluded. We thus decided to continue our work in a region-wise manner. The values of all failing voxels in a specific region of the DKT atlas were substituted by the average of the values of the passing voxels in that same region. In this way, we did not lose as many voxels as with the voxel-wise method.

A major challenge for the *in vivo* imaging of iron in the brain arises from the varying magnetic properties of different biochemical forms of iron. Our MRI technique is only sensitive to iron associated with ferritin and hemosiderin [71, 80]. Nonetheless, the free, redox-active forms of iron, constituting the labile iron pool and incapable of influencing the MRI signal, are potentially of more profound interest of researchers. It is hypothesized that a dynamic equilibrium exists between the volume of iron load in this pool and the measurable ferritin and hemosiderin quantity. This would enable the detection of the accumulation of detrimental free iron ions. However, it is uncertain whether this equilibrium truly exists. Moreover, alterations in chemical forms of iron might be of high importance as well, next to the accumulation of iron in the brain [84].

Although the MRI  $R_2^*$  contrast has been found to be linearly correlated to iron concentration by Langkammer et al., other factors can contribute to the obtained signal intensity too. The two most important confounding factors on the  $R_2^*$  signal are tissue water and myelin content [20, 253]. Lower water contents cause an increase in the  $R_2^*$ . Myelin shows diamagnetic properties and tends to elevate  $R_2^*$  values, as seen in the anterior commissure, internal capsule and fornix [20, 254]. Dusek et al. concluded a decreased reliability of the use of  $R_2^*$  values for measuring iron in the case of pathologies increasing the water content in the brain. With neuronal loss, a hallmark of AD, water levels increase. Potentially, this can partly explain our findings of lower iron load in LOAD patients. However, we did not assess neuronal loss in the included subjects, precluding the option to correct for this confounding factor in our analyses.

In addition, one can consider other metal ions, like copper, manganese and calcium, as confounding factors in the measurement of brain iron load. Nevertheless, under physiological conditions, copper and manganese do not reach the high concentrations necessary to influence MRI-based  $R_2^*$  measurements [20, 71, 255, 256]. In some pathological cases, like chronic liver diseases, however, the concentration of these metals can increase significantly [20, 257]. Thus, it is important to rule out diseases affecting other metal concentrations when assessing iron levels. For this study, we did not have access to the full clinical state of the included subjects. As a result, subjects with potential confounding metals were not rejected.

In contrast to copper and manganese, calcium can exert diamagnetic effects on the MRI signal under physiological circumstances [20, 258]. Its concentrations are similar to iron and evenly increase with age. As a result, we consider calcium as a potential confounder for our results [20, 259]. As iron has paramagnetic properties and calcium diamagnetic ones, opposite signal intensities can be obtained in filtered phase images [260]. As this technique extends beyond the scope of this thesis, we did not focus on discriminating iron and calcium values in our images.

Unfortunately, we did not have access to information regarding the dietary patterns and intake of supplements of the subjects. As mentioned before, several studies have indicated the effect of diet on brain iron levels [13, 33-36]. Moreover, dietary patterns have been found to have the capacity to affect the incidence and progression of neurodegenerative diseases [198-200]. Thus, our inability to correct for the effects of dietary factors on brain iron levels can be considered as a significant limitation of our study. Furthermore, we did not have access to data on systemic iron levels of the included subjects. As a result, we could not correct for the body iron state of the subjects nor could we confirm the difference in systemic iron concentrations between females and males. As we did not find any sex differences of brain iron load, it would have been instructive to compare the systemic and brain iron values.

Nevertheless, the study of Scarmes et al. did not find significant relations between systemic and brain iron levels [198]. Moreover, multiple factors, confounders and interactions between them are potentially involved, making this relation very complex. Further research should be performed to characterize the effects of dietary factors on brain iron load to understand its relevance in brain-related studies [34].

In addition, other factors than dietary patterns can affect iron in the body too. Mainly vascular health affects iron deposition in the brain. Del C Valdés Hernández et al. found that history of stroke is significantly related to the accumulation of iron in the brain [220]. Next, hypercholesterolemia showed a significant relation with increased iron levels in the corpus striatum [220, 261]. Hypertension, diabetes and cardiovascular diseases are also assumed to affect brain iron load. However, more research should be performed to confirm this assumption [220].

## **2. Future perspectives**

As we acknowledge the involvement of iron dyshomeostasis in healthy aging and AD pathophysiology, further research on this topic is of great importance. It will lead to a better understanding of aging of the brain and the pathophysiology of AD. This, eventually, contributes to the discovery of novel therapeutic targets and a potential treatment for this highly prevalent disease.

In our opinion, there is a great need for the development of a golden standard technique in assessing brain iron levels *in vivo*. First, it is important to correctly define the effects on the measured signal of the different biochemical forms of iron and how to discriminate them. For pathological research, particularly the redox-active free iron ions are of great interest. Their potential dynamic equilibrium with currently measurable iron forms should be further characterized, or, ideally, their direct measurement should be enabled. Moreover, when studying iron in the pathophysiology of AD, the ability of this golden standard technique should be validated for detecting changes in iron levels early in the disease process.

We assessed brain iron load by  $R_2^*$  relaxometry, which is one of the most often applied techniques in this research area. Nevertheless, this iron quantitation method requires optimization. First, to ameliorate the discrimination between artifactual and true signal decay, we propose to characterize the artifactual decay in more detail, based on the shape of its curve. We identified a faster decay and greater oscillations at longer echo times for the artifactual voxels. Voxels showing this curve shape can then be excluded from the analyses.

Second, a voxel-wise analysis is more desirable than a region-wise one, as it allows for more detailed examination of brain iron levels. Unfortunately, this technique is more complex and may, in some cases, be subject to artifacts generated in the  $T_2^*$ -weighted images. We propose to blur the voxels that have goodness of fit values below the predetermined threshold to obtain a functional mask.

Next, this methodology can be confounded by increased water content due to neuronal loss in AD patients. We propose to assess brain atrophy by ‘Voxel-Based Morphometry’, an automated technique which identifies differences in volume in a voxel-wise manner [262]. Any changes in brain volume can then be corrected for in the analyses.

Furthermore, the validity of the  $R_2^*$  values for representing iron levels can be improved by discriminating the contribution of iron and calcium to the MRI signal. We propose to acquire filtered phase images, as paramagnetic iron and diamagnetic calcium can be characterized by focussing on phase.

Next to our iron quantification technique, others have been proposed with both advantages and disadvantages. We consider two of them as useful alternatives for our research question. First, ‘Susceptibility-Weighted Imaging’ (SWI) is similar to  $R_2^*$  relaxometry as it obtains its signal by spin dephasing due to local field inhomogeneities. Nonetheless, it adds phase information, which enhances the contrast of the image [20, 263, 264]. However, artifacts at air-tissue interfaces can also occur with this technique, as the phase values are not only affected by iron content but also by differences in the magnetic susceptibility of the surrounding tissue [20, 265]. With this technique, the obtained values can be affected by diamagnetic tissue components, similar to the  $R_2^*$  relaxometry technique [20, 266, 267]. Thus, a correction for artifacts and diamagnetic influences is also required with this technique.

A second technique we propose as a relevant alternative is ‘Quantitative Susceptibility Mapping’ (QSM). Similar to SWI, this MRI technique uses phase information in addition to magnitude information to improve contrast between tissues [268-270]. QSM involves advanced post-processing techniques which provide images with voxels linearly related to the tissue magnetic susceptibility. An important difference between SWI and  $R_2^*$  relaxometry, is the provision by QSM of maps showing relative susceptibility differences rather than absolute values. As a consequence, a reference region must be assigned, for instance the CSF [20, 271]. QSM has a higher specificity by its differentiation between iron and calcium deposition [20, 272].

Next, performing longitudinal analyses, rather than cross-sectional ones, would be interesting. In this way, iron changes compared to baseline can be evaluated in healthy aging individuals and AD patients. It allows for a thorough investigation of the relation between brain iron and the onset and progression of AD pathophysiology. Furthermore, it enables to examine the relation between brain iron levels and the expression of disease-characteristic symptoms.

In addition to methods to optimize the MRI protocol, we suggest developing surveys to assess the dietary patterns and general health status of the subjects included in the study. It has been suggested that iron intake (from food or supplements) affects brain iron levels. Moreover, pathologies like iron deficiency, chronic liver diseases and vascular diseases, all have been found to be related to cerebral iron.

Whether systemic iron and cerebral iron are linked still remains to be confirmed. More research should be performed to elucidate this research question and identify factors influencing brain iron levels.



## Conclusion

We provide an *in vivo* cross-sectional study analysing brain iron load in healthy aging and AD pathophysiology including an extensive study population. Our results support the subcortical deposition of iron in healthy elderly people and we have found similar iron levels in other grey matter regions. No sex differences in brain iron load are demonstrated by this study, raising questions about the link between systemic and brain iron levels. Next, LOAD patients show lower brain iron, while EOAD patients show higher brain iron levels compared to healthy aged controls, particularly in cortical regions. We hypothesize this may be a result of the involvement of severe iron dyshomeostasis in AD patients. In this study, MCI patients do not show differences in brain iron deposition compared to healthy aged controls and AD patients. This is potentially due to the inability of our imaging technique to detect changes in iron load early in the disease process. Finally, regarding *APOE* genotype, we demonstrate lower brain iron load in carriers of one  $\epsilon 4$  *APOE* allele compared to non-carriers and higher iron load in homozygotes compared to heterozygotes. This finding also supports the relevance of iron dyshomeostasis in AD pathophysiology.

As a conclusion, we acknowledge the involvement of iron dyshomeostasis in healthy aging and AD pathophysiology. We encourage further research on this topic and on the development of a golden standard technique in measuring brain iron levels *in vivo* to obtain validated and trustworthy results. This will improve the understanding of the pathophysiology of AD and might contribute to the development of highly desired novel therapies.



## **Acknowledgements**

First, I would like to thank my promoter, Prof. Dr. P. Rosa-Neto, for welcoming me into his lab in Canada and for believing in me from the day I started. I am very grateful for all the opportunities he was willing to give me and for his passionate approach to being a thesis promoter. Second, I want to thank my internal promoter, Prof. Dr. S. Engelborghs, who enthusiastically introduced me to Prof. Rosa-Neto and was always ready to help me with any questions or problems I encountered. I would also like to thank Méliissa Savard for her contributions to this project and for guiding me through this learning process. All the other lab members were also a big support to me and helped me out when I encountered complications. I am also very thankful for Prof. Dr. D. Rudko for offering a collaboration to establish this project and for helping me with any questions I had. Finally, I would like to thank my family and friends for always believing in me and supporting me throughout this year.



## References

1. 2018 *Alzheimer's disease facts and figures*. *Alzheimer's & Dementia*, 2018. **14**(3): p. 367-429.
2. Peters, D.G., J.R. Connor, and M.D. Meadowcroft, *The relationship between iron dyshomeostasis and amyloidogenesis in Alzheimer's disease: Two sides of the same coin*. (1095-953X (Electronic)).
3. Brookmeyer, R., et al., *Forecasting the global burden of Alzheimer's disease*. (1552-5279 (Electronic)).
4. Hippus, H. and G. Neundörfer, *The discovery of Alzheimer's disease*. *Dialogues in clinical neuroscience*, 2003. **5**(1): p. 101-108.
5. Yang, G., et al., *Huperzine A for Alzheimer's disease: a systematic review and meta-analysis of randomized clinical trials*. (1932-6203 (Electronic)).
6. Jessen, F., *Subjective and objective cognitive decline at the pre-dementia stage of Alzheimer's disease*. (1433-8491 (Electronic)).
7. Hughes, T.F., M. Snitz Be Fau - Ganguli, and M. Ganguli, *Should mild cognitive impairment be subtyped?* (1473-6578 (Electronic)).
8. Larner, A.J., *Getting it wrong: the clinical misdiagnosis of Alzheimer's disease*. *International Journal of Clinical Practice*, 2004. **58**(11): p. 1092-1094.
9. McKhann, G., et al., *Clinical diagnosis of Alzheimer's disease: report of the NINCDS-ADRDA Work Group under the auspices of Department of Health and Human Services Task Force on Alzheimer's Disease*. *Neurology*, 1984. **34**(7): p. 939-44.
10. Jack, C.R., Jr., et al., *NIA-AA Research Framework: Toward a biological definition of Alzheimer's disease*. *Alzheimer's & dementia : the journal of the Alzheimer's Association*, 2018. **14**(4): p. 535-562.
11. Jack, C.R., Jr., et al., *A/T/N: An unbiased descriptive classification scheme for Alzheimer disease biomarkers*. *Neurology*, 2016. **87**(5): p. 539-547.
12. Lane, D.J.R., S. Ayton, and A.I. Bush, *Iron and Alzheimer's Disease: An Update on Emerging Mechanisms*. (1875-8908 (Electronic)).
13. Ashraf, A., M. Clark, and P.W. So, *The Aging of Iron Man*. (1663-4365 (Print)).
14. Duck, K.A. and J.R. Connor, *Iron uptake and transport across physiological barriers*. *Biometals : an international journal on the role of metal ions in biology, biochemistry, and medicine*, 2016. **29**(4): p. 573-591.
15. Masaldan, S., et al., *Striking while the iron is hot: Iron metabolism and ferroptosis in neurodegeneration*. (1873-4596 (Electronic)).
16. Urrutia, P.J., N.P. Mena, and M.T. Nunez, *The interplay between iron accumulation, mitochondrial dysfunction, and inflammation during the execution step of neurodegenerative disorders*. *Front Pharmacol*, 2014. **5**: p. 38.
17. Pauling, L., *General Chemistry*. Third ed. 1988, New York: Dover.
18. Winter We Fau - Bazydlo, L.A.L., N.S. Bazydlo La Fau - Harris, and N.S. Harris, *The molecular biology of human iron metabolism*. (0007-5027 (Print)).
19. Belaidi, A.A. and A.I. Bush, *Iron neurochemistry in Alzheimer's disease and Parkinson's disease: targets for therapeutics*. (1471-4159 (Electronic)).
20. Dusek, P., M. Dezortova, and J. Wuerfel, *Imaging of iron*. *Int Rev Neurobiol*, 2013. **110**: p. 195-239.
21. Mackenzie, B. and M.D. Garrick, *Iron Imports. II. Iron uptake at the apical membrane in the intestine*. (0193-1857 (Print)).
22. Adisetiyo, V., et al., *In vivo assessment of age-related brain iron differences by magnetic field correlation imaging*. *Journal of magnetic resonance imaging : JMRI*, 2012. **36**(2): p. 322-331.
23. Vymazal, J., J.W. Urgosik D Fau - Bulte, and J.W. Bulte, *Differentiation between hemosiderin- and ferritin-bound brain iron using nuclear magnetic resonance and magnetic resonance imaging*. (0145-5680 (Print)).
24. Haacke, E.M., et al., *Imaging iron stores in the brain using magnetic resonance imaging*. (0730-725X (Print)).
25. Singh, N., et al., *Brain iron homeostasis: from molecular mechanisms to clinical significance and therapeutic opportunities*. (1557-7716 (Electronic)).
26. Griffiths, P.D. and A.R. Crossman, *Distribution of iron in the basal ganglia and neocortex in postmortem tissue in Parkinson's disease and Alzheimer's disease*. (1013-7424 (Print)).
27. Drayer B Fau - Burger, P., et al., *MRI of brain iron*. (0361-803X (Print)).
28. Abbott, N.J., et al., *Structure and function of the blood-brain barrier*. (1095-953X (Electronic)).
29. McCarthy, R.C. and D.J. Kosman, *Ferroportin and exocytosomal ferroxidase activity are required for brain microvascular endothelial cell iron efflux*. (1083-351X (Electronic)).
30. McCarthy, R.C. and D.J. Kosman, *Glial cell ceruloplasmin and hepcidin differentially regulate iron efflux from brain microvascular endothelial cells*. (1932-6203 (Electronic)).

31. Simpson, I.A., et al., *A novel model for brain iron uptake: introducing the concept of regulation*. Journal of cerebral blood flow and metabolism : official journal of the International Society of Cerebral Blood Flow and Metabolism, 2015. **35**(1): p. 48-57.
32. Skjorringe, T., et al., *Divalent metal transporter 1 (DMT1) in the brain: implications for a role in iron transport at the blood-brain barrier, and neuronal and glial pathology*. (1662-5099 (Print)).
33. Institute of Medicine Panel on, M., in *Dietary Reference Intakes for Vitamin A, Vitamin K, Arsenic, Boron, Chromium, Copper, Iodine, Iron, Manganese, Molybdenum, Nickel, Silicon, Vanadium, and Zinc*. 2001, National Academies Press (US).  
Copyright 2001 by the National Academy of Sciences. All rights reserved.: Washington (DC).
34. Hagemeyer, J., et al., *Effects of diet on brain iron levels among healthy individuals: an MRI pilot study*. (1558-1497 (Electronic)).
35. Youdim, M.B., *Brain iron deficiency and excess; cognitive impairment and neurodegeneration with involvement of striatum and hippocampus*. (1029-8428 (Print)).
36. Agrawal, S., et al., *Impact of high iron intake on cognition and neurodegeneration in humans and in animal models: a systematic review*. Nutrition reviews, 2017. **75**(6): p. 456-470.
37. Mascitelli, L., M.R. Goldstein, and L.R. Zacharski, *Iron, oxidative stress, and the mediterranean diet*. Am J Med, 2014. **127**(9): p. e49.
38. Castro-Quezada, I., B. Román-Viñas, and L. Serra-Majem, *The Mediterranean diet and nutritional adequacy: a review*. Nutrients, 2014. **6**(1): p. 231-248.
39. Zacharski, L.R., G. Shamayeva, and B.K. Chow, *Effect of controlled reduction of body iron stores on clinical outcomes in peripheral arterial disease*. Am Heart J, 2011. **162**(5): p. 949-957.e1.
40. de Abreu-Silva, E., et al., *Diet and Inflammation: Effects of Macronutrients and Dietary Patterns*. Vol. 2. 2015. 7-13.
41. Bach-Faig, A., et al., *Mediterranean diet pyramid today. Science and cultural updates*. Public Health Nutr, 2011. **14**(12a): p. 2274-84.
42. Willett, W.C., et al., *Mediterranean diet pyramid: a cultural model for healthy eating*. Am J Clin Nutr, 1995. **61**(6 Suppl): p. 1402s-1406s.
43. Sofi, F., et al., *Accruing evidence on benefits of adherence to the Mediterranean diet on health: an updated systematic review and meta-analysis*. Am J Clin Nutr, 2010. **92**(5): p. 1189-96.
44. Couto, E., et al., *Mediterranean dietary pattern and cancer risk in the EPIC cohort*. Br J Cancer, 2011. **104**(9): p. 1493-9.
45. Salas-Salvado, J., et al., *Prevention of diabetes with Mediterranean diets: a subgroup analysis of a randomized trial*. Ann Intern Med, 2014. **160**(1): p. 1-10.
46. Estruch, R., et al., *Primary Prevention of Cardiovascular Disease with a Mediterranean Diet*. New England Journal of Medicine, 2013. **368**(14): p. 1279-1290.
47. Mitrou, P.N., et al., *Mediterranean dietary pattern and prediction of all-cause mortality in a US population: results from the NIH-AARP Diet and Health Study*. Arch Intern Med, 2007. **167**(22): p. 2461-8.
48. Sofi, F., et al., *Mediterranean diet and health*. BioFactors, 2013. **39**(4): p. 335-342.
49. Dwork, A.J., *Effects of diet and development upon the uptake and distribution of cerebral iron*. Journal of the Neurological Sciences, 1995. **134**: p. 45-51.
50. Pinero, D.J., et al., *Variations in dietary iron alter brain iron metabolism in developing rats*. J Nutr, 2000. **130**(2): p. 254-63.
51. Kastman, E.K., et al., *A Calorie-Restricted Diet Decreases Brain Iron Accumulation and Preserves Motor Performance in Old Rhesus Monkeys*. The Journal of Neuroscience, 2012. **32**: p. 11897-11904.
52. Jellen, L.C., et al., *Iron deficiency alters expression of dopamine-related genes in the ventral midbrain in mice*. Neuroscience, 2013. **252**: p. 13-23.
53. Hagemeyer, J., et al., *Effect of Age on MRI Phase Behavior in the Subcortical Deep Gray Matter of Healthy Individuals*. American Journal of Neuroradiology, 2013. **34**: p. 2144-2151.
54. Hirota, K., *An intimate crosstalk between iron homeostasis and oxygen metabolism regulated by the hypoxia-inducible factors (HIFs)*. Free Radic Biol Med, 2019. **133**: p. 118-129.
55. Du, F., et al., *Hepcidin Suppresses Brain Iron Accumulation by Downregulating Iron Transport Proteins in Iron-Overloaded Rats*. (1559-1182 (Electronic)).
56. McLean, E., et al., *Worldwide prevalence of anaemia, WHO Vitamin and Mineral Nutrition Information System, 1993-2005*. (1368-9800 (Print)).
57. Radlowski, E.C. and R.W. Johnson, *Perinatal iron deficiency and neurocognitive development*. Frontiers in human neuroscience, 2013. **7**: p. 585-585.
58. Jáuregui-Lobera, I., *Iron deficiency and cognitive functions*. Neuropsychiatric disease and treatment, 2014. **10**: p. 2087-2095.

59. Falkingham, M., et al., *The effects of oral iron supplementation on cognition in older children and adults: a systematic review and meta-analysis*. (1475-2891 (Electronic)).
60. Gregory, A., Hayflick, S. *Neurodegeneration with Brain Iron Accumulation Disorders Overview*. 2013; Available from: <https://www.ncbi.nlm.nih.gov/books/NBK121988/>.
61. Dusi, S., et al., *Exome sequence reveals mutations in CoA synthase as a cause of neurodegeneration with brain iron accumulation*. *Am J Hum Genet*, 2014. **94**(1): p. 11-22.
62. Al-Semari, A. and S. Bohlega, *Autosomal-recessive syndrome with alopecia, hypogonadism, progressive extra-pyramidal disorder, white matter disease, sensory neural deafness, diabetes mellitus, and low IGF1*. *Am J Med Genet A*, 2007. **143a**(2): p. 149-60.
63. Yoshida, K., et al., *A mutation in the ceruloplasmin gene is associated with systemic hemosiderosis in humans*. *Nat Genet*, 1995. **9**(3): p. 267-72.
64. Curtis, A.R., et al., *Mutation in the gene encoding ferritin light polypeptide causes dominant adult-onset basal ganglia disease*. *Nat Genet*, 2001. **28**(4): p. 350-4.
65. Schneider, S.A., et al., *ATP13A2 mutations (PARK9) cause neurodegeneration with brain iron accumulation*. *Mov Disord*, 2010. **25**(8): p. 979-84.
66. Kruer, M.C., et al., *Defective FA2H leads to a novel form of neurodegeneration with brain iron accumulation (NBIA)*. *Ann Neurol*, 2010. **68**(5): p. 611-8.
67. Hogarth, P., et al., *New NBIA subtype: genetic, clinical, pathologic, and radiographic features of MPAN*. *Neurology*, 2013. **80**(3): p. 268-75.
68. Zhou, B., et al., *A novel pantothenate kinase gene (PANK2) is defective in Hallervorden-Spatz syndrome*. *Nat Genet*, 2001. **28**(4): p. 345-9.
69. Schild, H.H., *MRI made easy*. 1990, Berlin: Schering AG.
70. Stryer, L., *Chapter 7. Myoglobin and hemoglobin*, in *Biochemistry*. 1988, W.H. Freeman: New York.
71. Schenck, J.F., *Magnetic resonance imaging of brain iron*. *Journal of the Neurological Sciences*, 2003. **207**(1): p. 99-102.
72. Gutiérrez, L., et al., *Quantitative magnetic analysis reveals ferritin-like iron as the most predominant iron-containing species in the murine Hfe-haemochromatosis*. *Biochimica et Biophysica Acta (BBA) - Molecular Basis of Disease*, 2012. **1822**(7): p. 1147-1153.
73. Pauling, L. and C.D. Coryell, *The Magnetic Properties and Structure of Hemoglobin, Oxyhemoglobin and Carbonmonoxyhemoglobin*. *Proc Natl Acad Sci U S A*, 1936. **22**(4): p. 210-6.
74. Jensen, J.H. and R. Chandra, *Strong field behavior of the NMR signal from magnetically heterogeneous tissues*. *Magn Reson Med*, 2000. **43**(2): p. 226-36.
75. Yablonskiy, D.A. and E.M. Haacke, *Theory of NMR signal behavior in magnetically inhomogeneous tissues: the static dephasing regime*. *Magn Reson Med*, 1994. **32**(6): p. 749-63.
76. Langkammer, C., et al., *Quantitative MR imaging of brain iron: a postmortem validation study*. *Radiology*, 2010. **257**(2): p. 455-62.
77. *The Chemistry of Contrast Agents in Medical Magnetic Resonance Imaging*. Second ed. 2013: John Wiley & Sons.
78. Marques, J.P., et al., *On the origin of the MR image phase contrast: An in vivo MR microscopy study of the rat brain at 14.1 T*. *NeuroImage*, 2009. **46**(2): p. 345-352.
79. Bradbury, M.W., *Transport of iron in the blood-brain-cerebrospinal fluid system*. *J Neurochem*, 1997. **69**(2): p. 443-54.
80. Chrichton, R., *Inorganic Biochemistry of Iron Metabolism: From Molecular Mechanisms to Clinical Consequences*. Second ed. 2001: John Wiley & Sons.
81. Koenig, S.H., et al., *Relaxometry of ferritin solutions and the influence of the Fe<sup>3+</sup> core ions*. *Magnetic Resonance in Medicine*, 1986. **3**(5): p. 755-767.
82. Vymazal, J., et al., *T1 and T2 of ferritin solutions: Effect of loading factor*. *Magnetic Resonance in Medicine*, 1996. **36**(1): p. 61-65.
83. Vymazal, J., et al., *The relation between brain iron and NMR relaxation times: An in vitro study*. *Magnetic Resonance in Medicine*, 1996. **35**(1): p. 56-61.
84. Wood, J.C., *Impact of iron assessment by MRI*. *Hematology Am Soc Hematol Educ Program*, 2011. **2011**: p. 443-50.
85. Bartzokis, G., et al., *Gender and iron genes may modify associations between brain iron and memory in healthy aging*. (1740-634X (Electronic)).
86. Bartzokis, G., et al., *Brain ferritin iron as a risk factor for age at onset in neurodegenerative diseases*. (0077-8923 (Print)).
87. Ghadery, C., et al., *R2\* mapping for brain iron: associations with cognition in normal aging*. (1558-1497 (Electronic)).
88. Hallgren B Fau - Sourander, P. and P. Sourander, *The effect of age on the non-haemin iron in the human brain*. (0022-3042 (Print)).

89. Bartzokis, G., *Alzheimer's disease as homeostatic responses to age-related myelin breakdown*. (1558-1497 (Electronic)).
90. Horowitz, M.P. and J.T. Greenamyre, *Mitochondrial iron metabolism and its role in neurodegeneration*. (1875-8908 (Electronic)).
91. Zlokovic, B.V., *Neurovascular mechanisms of Alzheimer's neurodegeneration*. (0166-2236 (Print)).
92. Connor, J.R. and S.L. Menzies, *Relationship of iron to oligodendrocytes and myelination*. (0894-1491 (Print)).
93. Connor, J.R., et al., *Cellular distribution of transferrin, ferritin, and iron in normal and aged human brains*. (0360-4012 (Print)).
94. Hebbrecht, G., W. Maenhaut, and J.D. Reuck, *Brain trace elements and aging*. Nuclear Instruments and Methods in Physics Research Section B: Beam Interactions with Materials and Atoms, 1999. **150**(1): p. 208-213.
95. Ramos, P., et al., *Iron levels in the human brain: a post-mortem study of anatomical region differences and age-related changes*. (1878-3252 (Electronic)).
96. Magtanong, L. and S.J. Dixon, *Ferroptosis and Brain Injury*. (1421-9859 (Electronic)).
97. Koedam, E.L., et al., *Early-versus late-onset Alzheimer's disease: more than age alone*. (1875-8908 (Electronic)).
98. Mullan, M., et al., *Age of onset in familial early onset Alzheimer's disease correlates with genetic aetiology*. American Journal of Medical Genetics, 1993. **48**(3): p. 129-130.
99. Roth, G.M., et al., *Premature aging in persons with Down syndrome: MR findings*. (0195-6108 (Print)).
100. Kehrer, J.P., *The Haber-Weiss reaction and mechanisms of toxicity*. (0300-483X (Print)).
101. Tonnie, E. and E. Trushina, *Oxidative Stress, Synaptic Dysfunction, and Alzheimer's Disease*. J Alzheimers Dis, 2017. **57**(4): p. 1105-1121.
102. Jones, D.P., *Redefining oxidative stress*. Antioxid Redox Signal, 2006. **8**(9-10): p. 1865-79.
103. Keller, J.N., et al., *Evidence of increased oxidative damage in subjects with mild cognitive impairment*. Neurology, 2005. **64**(7): p. 1152-6.
104. Perry, G., et al., *Is oxidative damage the fundamental pathogenic mechanism of Alzheimer's and other neurodegenerative diseases?* Free Radic Biol Med, 2002. **33**(11): p. 1475-9.
105. Markesbery, W.R. and J.M. Carney, *Oxidative alterations in Alzheimer's disease*. Brain Pathol, 1999. **9**(1): p. 133-46.
106. Markesbery, W.R., *Oxidative stress hypothesis in Alzheimer's disease*. Free Radic Biol Med, 1997. **23**(1): p. 134-47.
107. Sayre, L.M., M.A. Smith, and G. Perry, *Chemistry and biochemistry of oxidative stress in neurodegenerative disease*. Curr Med Chem, 2001. **8**(7): p. 721-38.
108. Lovell, M.A. and W.R. Markesbery, *Oxidative damage in mild cognitive impairment and early Alzheimer's disease*. J Neurosci Res, 2007. **85**(14): p. 3036-40.
109. Stockwell, B.R., et al., *Ferroptosis: A Regulated Cell Death Nexus Linking Metabolism, Redox Biology, and Disease*. (1097-4172 (Electronic)).
110. Dixon, S.J., et al., *Ferroptosis: an iron-dependent form of nonapoptotic cell death*. (1097-4172 (Electronic)).
111. Yagoda, N., et al., *RAS-RAF-MEK-dependent oxidative cell death involving voltage-dependent anion channels*. (1476-4687 (Electronic)).
112. Friedmann Angeli, J.P., et al., *Inactivation of the ferroptosis regulator Gpx4 triggers acute renal failure in mice*. (1476-4679 (Electronic)).
113. Hambright, W.S., et al., *Ablation of ferroptosis regulator glutathione peroxidase 4 in forebrain neurons promotes cognitive impairment and neurodegeneration*. (2213-2317 (Electronic)).
114. Zhu, X., et al., *Oxidative stress signalling in Alzheimer's disease*. Brain Res, 2004. **1000**(1-2): p. 32-9.
115. Nunomura, A., et al., *Oxidative damage is the earliest event in Alzheimer disease*. J Neuropathol Exp Neurol, 2001. **60**(8): p. 759-67.
116. Rinaldi, P., et al., *Plasma antioxidants are similarly depleted in mild cognitive impairment and in Alzheimer's disease*. Neurobiol Aging, 2003. **24**(7): p. 915-9.
117. Szule, J.A., J.H. Jung, and U.J. McMahan, *The structure and function of 'active zone material' at synapses*. Philosophical transactions of the Royal Society of London. Series B, Biological sciences, 2015. **370**(1672): p. 20140189.
118. Jang, S.S. and H.J. Chung, *Emerging Link between Alzheimer's Disease and Homeostatic Synaptic Plasticity*. Neural Plast, 2016. **2016**: p. 7969272.
119. Terry, R.D., et al., *Physical basis of cognitive alterations in Alzheimer's disease: synapse loss is the major correlate of cognitive impairment*. Ann Neurol, 1991. **30**(4): p. 572-80.
120. Robinson, J.L., et al., *Perforant path synaptic loss correlates with cognitive impairment and Alzheimer's disease in the oldest-old*. Brain, 2014. **137**(Pt 9): p. 2578-87.

121. DeKosky, S.T. and S.W. Scheff, *Synapse loss in frontal cortex biopsies in Alzheimer's disease: correlation with cognitive severity*. *Ann Neurol*, 1990. **27**(5): p. 457-64.
122. Mattson, M.P. and R.J. Mark, *Excitotoxicity and excitoprotection in vitro*. *Adv Neurol*, 1996. **71**: p. 1-30; discussion 30-5.
123. Coyle, J.T. and P. Puttfarcken, *Oxidative stress, glutamate, and neurodegenerative disorders*. *Science*, 1993. **262**(5134): p. 689-95.
124. Piloni, N.E., et al., *Acute iron overload and oxidative stress in brain*. (1879-3185 (Electronic)).
125. Koppenol, W.H., *The Haber-Weiss cycle--70 years later*. (1351-0002 (Print)).
126. Aliaga, M., et al., *Superoxide-dependent reduction of free Fe<sup>3+</sup> and release of Fe<sup>2+</sup> from ferritin by the physiologically-occurring Cu(I)-glutathione complex*. Vol. 19. 2011. 534-41.
127. Austin, S.A., A.V. Santhanam, and Z.S. Katusic, *Endothelial nitric oxide modulates expression and processing of amyloid precursor protein*. *Circulation research*, 2010. **107**(12): p. 1498-1502.
128. Kummer, M.P., et al., *Nitration of tyrosine 10 critically enhances amyloid beta aggregation and plaque formation*. (1097-4199 (Electronic)).
129. Polidori, M.C., et al., *Profiles of antioxidants in human plasma*. *Free Radic Biol Med*, 2001. **30**(5): p. 456-62.
130. Rouault, T.A. and W.H. Tong, *Iron-sulphur cluster biogenesis and mitochondrial iron homeostasis*. *Nat Rev Mol Cell Biol*, 2005. **6**(4): p. 345-51.
131. Petrat, F., H. de Groot, and U. Rauen, *Subcellular distribution of chelatable iron: a laser scanning microscopic study in isolated hepatocytes and liver endothelial cells*. *The Biochemical journal*, 2001. **356**(Pt 1): p. 61-69.
132. Su, K., D. Bourdette, and M. Forte, *Mitochondrial dysfunction and neurodegeneration in multiple sclerosis*. *Front Physiol*, 2013. **4**: p. 169.
133. Markesbery, W.R., *The Role of Oxidative Stress in Alzheimer Disease*. *Archives of Neurology*, 1999. **56**(12): p. 1449-1452.
134. Swerdlow, R.H., J.M. Burns, and S.M. Khan, *The Alzheimer's disease mitochondrial cascade hypothesis: progress and perspectives*. *Biochim Biophys Acta*, 2014. **1842**(8): p. 1219-31.
135. Swerdlow, R.H., *Mitochondria and Cell Bioenergetics: Increasingly Recognized Components and a Possible Etiologic Cause of Alzheimer's Disease*. *Antioxidants & Redox Signaling*, 2012. **16**(12): p. 1434-1455.
136. Hirsch, E.C. and S. Hunot, *Neuroinflammation in Parkinson's disease: a target for neuroprotection?* *Lancet Neurol*, 2009. **8**(4): p. 382-97.
137. Colton, C. and D.M. Wilcock, *Assessing activation states in microglia*. *CNS Neurol Disord Drug Targets*, 2010. **9**(2): p. 174-91.
138. Paradkar, P.N. and J.A. Roth, *Nitric oxide transcriptionally down-regulates specific isoforms of divalent metal transporter (DMT1) via NF-kappaB*. *J Neurochem*, 2006. **96**(6): p. 1768-77.
139. Urrutia, P., et al., *Inflammation alters the expression of DMT1, FPN1 and hepcidin, and it causes iron accumulation in central nervous system cells*. *J Neurochem*, 2013. **126**(4): p. 541-9.
140. Wang, J., et al., *Pro-inflammatory cytokines modulate iron regulatory protein 1 expression and iron transportation through reactive oxygen/nitrogen species production in ventral mesencephalic neurons*. *Biochim Biophys Acta*, 2013. **1832**(5): p. 618-25.
141. Djafarzadeh, S., et al., *Toll-like receptor-3-induced mitochondrial dysfunction in cultured human hepatocytes*. *Mitochondrion*, 2011. **11**(1): p. 83-8.
142. Xie, Z., C.J. Smith, and L.J. Van Eldik, *Activated glia induce neuron death via MAP kinase signaling pathways involving JNK and p38*. *Glia*, 2004. **45**(2): p. 170-9.
143. Lee, Y.W., W.H. Lee, and P.H. Kim, *Oxidative mechanisms of IL-4-induced IL-6 expression in vascular endothelium*. *Cytokine*, 2010. **49**(1): p. 73-79.
144. Shi, H.X., et al., *Mitochondrial ubiquitin ligase MARCH5 promotes TLR7 signaling by attenuating TANK action*. *PLoS Pathog*, 2011. **7**(5): p. e1002057.
145. Vina, J. and A. Lloret, *Why women have more Alzheimer's disease than men: gender and mitochondrial toxicity of amyloid-beta peptide*. *J Alzheimers Dis*, 2010. **20 Suppl 2**: p. S527-33.
146. De-Paula, V.J., et al., *Alzheimer's disease*. *Subcell Biochem*, 2012. **65**: p. 329-52.
147. Recuero, M., et al., *Abeta production as consequence of cellular death of a human neuroblastoma overexpressing APP*. *FEBS Lett*, 2004. **570**(1-3): p. 114-8.
148. Roberts, G.W., et al., *Beta amyloid protein deposition in the brain after severe head injury: implications for the pathogenesis of Alzheimer's disease*. *J Neurol Neurosurg Psychiatry*, 1994. **57**(4): p. 419-25.
149. Huang, X., et al., *Trace metal contamination initiates the apparent auto-aggregation, amyloidosis, and oligomerization of Alzheimer's Aβ peptides*. *JBIC Journal of Biological Inorganic Chemistry*, 2004. **9**(8): p. 954-960.

150. Liu, B., et al., *Iron promotes the toxicity of amyloid beta peptide by impeding its ordered aggregation*. J Biol Chem, 2011. **286**(6): p. 4248-56.
151. Mantyh, P.W., et al., *Aluminum, Iron, and Zinc Ions Promote Aggregation of Physiological Concentrations of  $\beta$ -Amyloid Peptide*. Journal of Neurochemistry, 1993. **61**(3): p. 1171-1174.
152. Schubert, D. and M. Chevion, *The Role of Iron in Beta Amyloid Toxicity*. Biochemical and Biophysical Research Communications, 1995. **216**(2): p. 702-707.
153. Everett, J., et al., *Ferrous iron formation following the co-aggregation of ferric iron and the Alzheimer's disease peptide beta-amyloid (1-42)*. (1742-5662 (Electronic)).
154. Gong, N.J., et al., *Imaging beta amyloid aggregation and iron accumulation in Alzheimer's disease using quantitative susceptibility mapping MRI*. Neuroimage, 2019. **191**: p. 176-185.
155. Telling, N.D., et al., *Iron Biochemistry is Correlated with Amyloid Plaque Morphology in an Established Mouse Model of Alzheimer's Disease*. Cell Chem Biol, 2017. **24**(10): p. 1205-1215.e3.
156. Liu, J.-L., et al., *Iron and Alzheimer's Disease: From Pathogenesis to Therapeutic Implications*. Frontiers in neuroscience, 2018. **12**: p. 632-632.
157. van Bergen, J.M., et al., *Colocalization of cerebral iron with Amyloid beta in Mild Cognitive Impairment*. (2045-2322 (Electronic)).
158. Maynard, C.J., et al., *Overexpression of Alzheimer's disease amyloid-beta opposes the age-dependent elevations of brain copper and iron*. (0021-9258 (Print)).
159. Rogers, J.T., et al., *An iron-responsive element type II in the 5'-untranslated region of the Alzheimer's amyloid precursor protein transcript*. (0021-9258 (Print)).
160. Ward, R.J., et al., *The role of iron in brain ageing and neurodegenerative disorders*. The Lancet. Neurology, 2014. **13**(10): p. 1045-1060.
161. Kawahara, M., M. Kato-Negishi, and K. Tanaka, *Cross talk between neurometals and amyloidogenic proteins at the synapse and the pathogenesis of neurodegenerative diseases*. Metallomics, 2017. **9**(6): p. 619-633.
162. Duce, J.A., et al., *Iron-export ferroxidase activity of beta-amyloid precursor protein is inhibited by zinc in Alzheimer's disease*. Cell, 2010. **142**(6): p. 857-67.
163. Ayton, S., S.A. James, and A.I. Bush, *Nanoscale Imaging Reveals Big Role for Iron in Alzheimer's Disease*. (2451-9448 (Electronic)).
164. Telling, N.D., et al., *Iron Biochemistry is Correlated with Amyloid Plaque Morphology in an Established Mouse Model of Alzheimer's Disease*. (2451-9448 (Electronic)).
165. Kruer, M.C., *The neuropathology of neurodegeneration with brain iron accumulation*. (2162-5514 (Electronic)).
166. Kosik, K.S., *The molecular and cellular biology of tau*. Brain Pathol, 1993. **3**(1): p. 39-43.
167. Lindwall, G. and R.D. Cole, *Phosphorylation affects the ability of tau protein to promote microtubule assembly*. J Biol Chem, 1984. **259**(8): p. 5301-5.
168. Lei, P., et al., *Tau deficiency induces parkinsonism with dementia by impairing APP-mediated iron export*. (1546-170X (Electronic)).
169. Wang, J.Z., I. Grundke-Iqbal, and K. Iqbal, *Kinases and phosphatases and tau sites involved in Alzheimer neurofibrillary degeneration*. Eur J Neurosci, 2007. **25**(1): p. 59-68.
170. Hanger, D.P., et al., *The complex relationship between soluble and insoluble tau in tauopathies revealed by efficient dephosphorylation and specific antibodies*. FEBS Letters, 2002. **531**(3): p. 538-542.
171. Rao, S.S. and P.A.J.F.i.m.n. Adlard, *Untangling Tau and Iron: Exploring the Interaction Between Iron and Tau in Neurodegeneration*. 2018. **11**.
172. Guo, J.L. and V.M. Lee, *Seeding of normal Tau by pathological Tau conformers drives pathogenesis of Alzheimer-like tangles*. (1083-351X (Electronic)).
173. Munoz, P., et al., *Effect of iron on the activation of the MAPK/ERK pathway in PC12 neuroblastoma cells*. (0716-9760 (Print)).
174. Jin Jung, K., et al., *Oxidative stress induces inactivation of protein phosphatase 2A, promoting proinflammatory NF-kappaB in aged rat kidney*. (1873-4596 (Electronic)).
175. Bekris, L.M., et al., *Genetics of Alzheimer disease*. Journal of geriatric psychiatry and neurology, 2010. **23**(4): p. 213-227.
176. Conejero-Goldberg, C., et al., *APOE2 enhances neuroprotection against Alzheimer's disease through multiple molecular mechanisms*. (1476-5578 (Electronic)).
177. Farrer, L.A., et al., *Effects of age, sex, and ethnicity on the association between apolipoprotein E genotype and Alzheimer disease. A meta-analysis. APOE and Alzheimer Disease Meta Analysis Consortium*. (0098-7484 (Print)).
178. Huang, Y. and L. Mucke, *Alzheimer mechanisms and therapeutic strategies*. (1097-4172 (Electronic)).
179. Kanekiyo, T., H. Xu, and G. Bu, *ApoE and Abeta in Alzheimer's disease: accidental encounters or partners?* (1097-4199 (Electronic)).

180. Bush, A.I., et al., *EVIDENCE FOR APOE PROTECTING AGAINST BRAIN IRON OVERLOAD*. *Alzheimer's & Dementia: The Journal of the Alzheimer's Association*, 2014. **10**(4): p. P878.
181. van Duijn, S., et al., *Cortical Iron Reflects Severity of Alzheimer's Disease*. *Journal of Alzheimer's disease* : JAD, 2017. **60**(4): p. 1533-1545.
182. Ayton, S.A.-O., N.A.-O. Faux, and A.A.-O. Bush, *Ferritin levels in the cerebrospinal fluid predict Alzheimer's disease outcomes and are regulated by APOE*. (2041-1723 (Electronic)).
183. Nandar, W., et al., *A mutation in the HFE gene is associated with altered brain iron profiles and increased oxidative stress in mice*. (0006-3002 (Print)).
184. Jamieson, S.E., et al., *Candidate gene association study of solute carrier family 11a members 1 (SLC11A1) and 2 (SLC11A2) genes in Alzheimer's disease*. (0304-3940 (Print)).
185. Loeffler, D.A., et al., *Transferrin and iron in normal, Alzheimer's disease, and Parkinson's disease brain regions*. (0022-3042 (Print)).
186. Mariani, S., et al., *Effects of hemochromatosis and transferrin gene mutations on peripheral iron dyshomeostasis in mild cognitive impairment and Alzheimer's and Parkinson's diseases*. (1663-4365 (Print)).
187. Wang Ye Fau - Yue, D.X., X.C. Yue Dx Fau - Tang, and X.C. Tang, *[Anti-cholinesterase activity of huperzine A]*. (0253-9756 (Print)).
188. Fu, L.M. and J.T. Li, *A systematic review of single chinese herbs for Alzheimer's disease treatment*. (1741-4288 (Electronic)).
189. Rafii, M.S., et al., *A phase II trial of huperzine A in mild to moderate Alzheimer disease*. (1526-632X (Electronic)).
190. Zhang, Z., et al., *[Clinical efficacy and safety of huperzine Alpha in treatment of mild to moderate Alzheimer disease, a placebo-controlled, double-blind, randomized trial]*. (0376-2491 (Print)).
191. Liu Fugen, F.Y. and Z.J. Gao Zhixu, *Double-blind control treatment of huperzine-A and placebo in 28 patients with Alzheimer disease*. *药物流行病学杂志* (Chinese Journal of Pharmacoepidemiology), 1995. **4**(4): p. 196-198.
192. Huang, X.T., et al., *Reducing iron in the brain: a novel pharmacologic mechanism of huperzine A in the treatment of Alzheimer's disease*. (1558-1497 (Electronic)).
193. Crapper McLachlan, D.R., et al., *Intramuscular desferrioxamine in patients with Alzheimer's disease*. (0140-6736 (Print)).
194. Guo, C., et al., *Deferoxamine inhibits iron induced hippocampal tau phosphorylation in the Alzheimer transgenic mouse brain*. (1872-9754 (Electronic)).
195. Guo, C., et al., *Intranasal deferoxamine reverses iron-induced memory deficits and inhibits amyloidogenic APP processing in a transgenic mouse model of Alzheimer's disease*. (1558-1497 (Electronic)).
196. Prasanthi, J.R., et al., *Deferiprone reduces amyloid-beta and tau phosphorylation levels but not reactive oxygen species generation in hippocampus of rabbits fed a cholesterol-enriched diet*. (1875-8908 (Electronic)).
197. Savory, J., et al., *Reversal by desferrioxamine of tau protein aggregates following two days of treatment in aluminum-induced neurofibrillary degeneration in rabbit: implications for clinical trials in Alzheimer's disease*. (0161-813X (Print)).
198. Scarmeas, N., et al., *Mediterranean diet, Alzheimer disease, and vascular mediation*. *Arch Neurol*, 2006. **63**(12): p. 1709-17.
199. Scarmeas, N., et al., *Mediterranean diet and mild cognitive impairment*. *Arch Neurol*, 2009. **66**(2): p. 216-25.
200. Scarmeas, N., et al., *Mediterranean diet and risk for Alzheimer's disease*. *Ann Neurol*, 2006. **59**(6): p. 912-21.
201. Breteler, M.M., *Vascular risk factors for Alzheimer's disease: an epidemiologic perspective*. *Neurobiol Aging*, 2000. **21**(2): p. 153-60.
202. Lorigeril, M.d., et al., *Mediterranean Diet, Traditional Risk Factors, and the Rate of Cardiovascular Complications After Myocardial Infarction*. *Circulation*, 1999. **99**(6): p. 779-785.
203. Panagiotakos, D.B., et al., *Status and management of hypertension in Greece: role of the adoption of a Mediterranean diet: the Attica study*. *J Hypertens*, 2003. **21**(8): p. 1483-9.
204. Mecocci, P., *Oxidative stress in mild cognitive impairment and Alzheimer disease: a continuum*. *J Alzheimers Dis*, 2004. **6**(2): p. 159-63.
205. Alarcon de la Lastra, C., et al., *Mediterranean diet and health: biological importance of olive oil*. *Curr Pharm Des*, 2001. **7**(10): p. 933-50.
206. Cummings, J.L., *Alzheimer's disease*. *N Engl J Med*, 2004. **351**(1): p. 56-67.
207. Klein, A. and J. Tourville, *101 labeled brain images and a consistent human cortical labeling protocol*. *Front Neurosci*, 2012. **6**: p. 171.

208. Pascoal, T.A., et al., *In vivo quantification of neurofibrillary tangles with [(18)F]MK-6240*. *Alzheimers Res Ther*, 2018. **10**(1): p. 74.
209. Cselenyi, Z., et al., *Clinical validation of 18F-AZD4694, an amyloid-beta-specific PET radioligand*. *J Nucl Med*, 2012. **53**(3): p. 415-24.
210. Hudson, H.M. and R.S. Larkin, *Accelerated image reconstruction using ordered subsets of projection data*. *IEEE Trans Med Imaging*, 1994. **13**(4): p. 601-9.
211. Costes, N., et al., *Motion correction of multi-frame PET data in neuroreceptor mapping: simulation based validation*. *Neuroimage*, 2009. **47**(4): p. 1496-505.
212. Mazziotta, J., et al., *A probabilistic atlas and reference system for the human brain: International Consortium for Brain Mapping (ICBM)*. *Philosophical transactions of the Royal Society of London. Series B, Biological sciences*, 2001. **356**(1412): p. 1293-1322.
213. Pascoal, T.A., et al., *Synergistic interaction between amyloid and tau predicts the progression to dementia*. *Alzheimers Dement*, 2017. **13**(6): p. 644-653.
214. Pascoal, T.A., et al., *Amyloid- $\beta$  and hyperphosphorylated tau synergy drives metabolic decline in preclinical Alzheimer's disease*. *Molecular psychiatry*, 2017. **22**(2): p. 306-311.
215. Tombaugh, T.N. and N.J. McIntyre, *The mini-mental state examination: a comprehensive review*. *J Am Geriatr Soc*, 1992. **40**(9): p. 922-35.
216. Kochhann, R., et al., *The Mini Mental State Examination: Review of cutoff points adjusted for schooling in a large Southern Brazilian sample*. *Dement Neuropsychol*, 2010. **4**(1): p. 35-41.
217. Saykin, A.J., et al., *Genetic studies of quantitative MCI and AD phenotypes in ADNI: Progress, opportunities, and plans*. *Alzheimers Dement*, 2015. **11**(7): p. 792-814.
218. D. Storey, J., *A Direct Approach to False Discovery Rates*. Vol. 64. 2002. 479-498.
219. Xu, X., Q. Wang, and M. Zhang, *Age, gender, and hemispheric differences in iron deposition in the human brain: an in vivo MRI study*. *Neuroimage*, 2008. **40**(1): p. 35-42.
220. Del C Valdés Hernández, M., et al., *Brain iron deposits and lifespan cognitive ability*. *Age (Dordrecht, Netherlands)*, 2015. **37**(5): p. 100-100.
221. Rodrigue, K.M., et al., *The role of hippocampal iron concentration and hippocampal volume in age-related differences in memory*. *Cereb Cortex*, 2013. **23**(7): p. 1533-41.
222. Daugherty, A.M., E.M. Haacke, and N. Raz, *Striatal iron content predicts its shrinkage and changes in verbal working memory after two years in healthy adults*. *J Neurosci*, 2015. **35**(17): p. 6731-43.
223. van Es, A.C., et al., *Caudate nucleus hypointensity in the elderly is associated with markers of neurodegeneration on MRI*. *Neurobiol Aging*, 2008. **29**(12): p. 1839-46.
224. Sullivan, E.V., et al., *Relevance of Iron Deposition in Deep Gray Matter Brain Structures to Cognitive and Motor Performance in Healthy Elderly Men and Women: Exploratory Findings*. *Brain Imaging Behav*, 2009. **3**(2): p. 167-175.
225. Thompson, P.M. and N. Jahanshad, *Ironing out neurodegeneration: is iron intake important during the teenage years?* *Expert Rev Neurother*, 2012. **12**(6): p. 629-31.
226. Connor, J.R., et al., *Regional distribution of iron and iron-regulatory proteins in the brain in aging and Alzheimer's disease*. *J Neurosci Res*, 1992. **31**(2): p. 327-35.
227. Steen, R.G., W.E. Reddick, and R.J. Ogg, *More than meets the eye: significant regional heterogeneity in human cortical T1*. *Magn Reson Imaging*, 2000. **18**(4): p. 361-8.
228. Supprian, T., et al., *MRI T2 relaxation times of brain regions in schizophrenic patients and control subjects*. *Psychiatry Res*, 1997. **75**(3): p. 173-82.
229. Tucker, D.M. and P.A. Williamson, *Asymmetric neural control systems in human self-regulation*. *Psychol Rev*, 1984. **91**(2): p. 185-215.
230. de la Fuente-Fernandez, R., et al., *Nigrostriatal dopamine system and motor lateralization*. *Behav Brain Res*, 2000. **112**(1-2): p. 63-8.
231. Glick, S.D., D.A. Ross, and L.B. Hough, *Lateral asymmetry of neurotransmitters in human brain*. *Brain Res*, 1982. **234**(1): p. 53-63.
232. Wagner, H.N., Jr., et al., *Imaging dopamine receptors in the human brain by positron tomography*. *Science*, 1983. **221**(4617): p. 1264-6.
233. Beard, J., *Iron deficiency alters brain development and functioning*. *J Nutr*, 2003. **133**(5 Suppl 1): p. 1468s-72s.
234. Faucheux, B.A., et al., *Autoradiographic localization and density of [125I]ferrotransferrin binding sites in the basal ganglia of control subjects, patients with Parkinson's disease and MPTP-lesioned monkeys*. *Brain Res*, 1995. **691**(1-2): p. 115-24.
235. Martorana, A. and G. Koch, *"Is dopamine involved in Alzheimer's disease?"*. *Frontiers in aging neuroscience*, 2014. **6**: p. 252-252.
236. Perez, S.E., et al., *Nigrostriatal dysfunction in familial Alzheimer's disease-linked APP<sup>swe</sup>/PS1<sup>DeltaE9</sup> transgenic mice*. *J Neurosci*, 2005. **25**(44): p. 10220-9.

237. Himeno, E., et al., *Apomorphine treatment in Alzheimer mice promoting amyloid-beta degradation*. Ann Neurol, 2011. **69**(2): p. 248-56.
238. Leskovjan, A.C., et al., *Increased brain iron coincides with early plaque formation in a mouse model of Alzheimer's disease*. Neuroimage, 2011. **55**(1): p. 32-8.
239. Ahmadi, S., et al., *Electrochemical studies of tau protein-iron interactions—Potential implications for Alzheimer's Disease*. Electrochimica Acta, 2017. **236**: p. 384-393.
240. Ghadery, C., et al., *R2\* mapping for brain iron: associations with cognition in normal aging*. Neurobiol Aging, 2015. **36**(2): p. 925-32.
241. Crutch, S.J., et al., *Posterior cortical atrophy*. The Lancet. Neurology, 2012. **11**(2): p. 170-178.
242. Formaglio, M., et al., *In vivo demonstration of amyloid burden in posterior cortical atrophy: a case series with PET and CSF findings*. J Neurol, 2011. **258**(10): p. 1841-51.
243. Kambe, T., et al., *Posterior cortical atrophy with [11C] Pittsburgh compound B accumulation in the primary visual cortex*. Vol. 257. 2009. 469-71.
244. Ng, S.Y., et al., *Evaluating atypical dementia syndromes using positron emission tomography with carbon 11 labeled Pittsburgh Compound B*. Arch Neurol, 2007. **64**(8): p. 1140-4.
245. Tenovuo, O., et al., *Posterior cortical atrophy: a rare form of dementia with in vivo evidence of amyloid-beta accumulation*. J Alzheimers Dis, 2008. **15**(3): p. 351-5.
246. de Souza, L.C., et al., *Similar amyloid-beta burden in posterior cortical atrophy and Alzheimer's disease*. Brain, 2011. **134**(Pt 7): p. 2036-43.
247. Rosenbloom, M.H., et al., *Distinct clinical and metabolic deficits in PCA and AD are not related to amyloid distribution*. Neurology, 2011. **76**(21): p. 1789-96.
248. Day, G.S., et al., *Tau-PET Binding Distinguishes Patients With Early-stage Posterior Cortical Atrophy From Amnesic Alzheimer Disease Dementia*. Alzheimer disease and associated disorders, 2017. **31**(2): p. 87-93.
249. Mesulam, M.-M., *Primary progressive aphasia*. Annals of Neurology, 2001. **49**(4): p. 425-432.
250. Mesulam, M.M. and S. Weintraub, *Spectrum of primary progressive aphasia*. Baillieres Clin Neurol, 1992. **1**(3): p. 583-609.
251. Galton, C.J., et al., *Atypical and typical presentations of Alzheimer's disease: a clinical, neuropsychological, neuroimaging and pathological study of 13 cases*. Brain, 2000. **123 Pt 3**: p. 484-98.
252. Mesulam, M.M., et al., *Apolipoprotein E genotypes in primary progressive aphasia*. Neurology, 1997. **49**(1): p. 51-5.
253. Kamman, R.L., et al., *Nuclear magnetic resonance relaxation in experimental brain edema: Effects of water concentration, protein concentration, and temperature*. Magnetic Resonance in Medicine, 1988. **6**(3): p. 265-274.
254. Curnes, J.T., et al., *MR imaging of compact white matter pathways*. American Journal of Neuroradiology, 1988. **9**(6): p. 1061-1068.
255. Schenck, J.F., *The role of magnetic susceptibility in magnetic resonance imaging: MRI magnetic compatibility of the first and second kinds*. Medical Physics, 1996. **23**(6): p. 815-850.
256. Vymazal, J., et al., *Frequency dependence of MR relaxation times I. Paramagnetic ions*. Journal of Magnetic Resonance Imaging, 1993. **3**(4): p. 637-640.
257. Vymazal, J., et al., *T1 and T2 alterations in the brains of patients with hepatic cirrhosis*. American Journal of Neuroradiology, 1996. **17**(2): p. 333-336.
258. Riederer, P., et al., *Transition Metals, Ferritin, Glutathione, and Ascorbic Acid in Parkinsonian Brains*. Journal of Neurochemistry, 1989. **52**(2): p. 515-520.
259. Casanova, M.F. and J.M. Araque, *Mineralization of the basal ganglia: implications for neuropsychiatry, pathology and neuroimaging*. Psychiatry Research, 2003. **121**(1): p. 59-87.
260. Wu, Z., et al., *Identification of calcification with MRI using susceptibility-weighted imaging: a case study*. Journal of magnetic resonance imaging : JMRI, 2009. **29**(1): p. 177-182.
261. Ong, W.Y. and B. Halliwell, *Iron, atherosclerosis, and neurodegeneration: a key role for cholesterol in promoting iron-dependent oxidative damage?* Ann N Y Acad Sci, 2004. **1012**: p. 51-64.
262. Whitwell, J.L., *Voxel-Based Morphometry: An Automated Technique for Assessing Structural Changes in the Brain*. The Journal of Neuroscience, 2009. **29**: p. 9661-9664.
263. Ogg, R.J., et al., *The correlation between phase shifts in gradient-echo MR images and regional brain iron concentration*. Magnetic Resonance Imaging, 1999. **17**(8): p. 1141-1148.
264. Reichenbach, J.R., et al., *Theory and application of static field inhomogeneity effects in gradient-echo imaging*. Journal of Magnetic Resonance Imaging, 1997. **7**(2): p. 266-279.
265. Chen, Z., et al., *An optimised framework for reconstructing and processing MR phase images*. NeuroImage, 2010. **49**(2): p. 1289-1300.
266. Gupta, R.K., et al., *Differentiation of calcification from chronic hemorrhage with corrected gradient echo phase imaging*. J Comput Assist Tomogr, 2001. **25**(5): p. 698-704.

267. Yamada, N., et al., *Intracranial calcification on gradient-echo phase image: depiction of diamagnetic susceptibility*. Radiology, 1996. **198**(1): p. 171-178.
268. de Rochefort, L., et al., *Quantitative MR susceptibility mapping using piece-wise constant regularized inversion of the magnetic field*. Magnetic Resonance in Medicine, 2008. **60**(4): p. 1003-1009.
269. Schweser, F., et al., *Quantitative imaging of intrinsic magnetic tissue properties using MRI signal phase: An approach to in vivo brain iron metabolism?* NeuroImage, 2011. **54**(4): p. 2789-2807.
270. Shmueli, K., et al., *Magnetic susceptibility mapping of brain tissue in vivo using MRI phase data*. Magnetic Resonance in Medicine, 2009. **62**(6): p. 1510-1522.
271. Cheng, Y.-C.N., J. Neelavalli, and E.M. Haacke, *Limitations of calculating field distributions and magnetic susceptibilities in MRI using a Fourier based method*. Physics in medicine and biology, 2009. **54**(5): p. 1169-1189.
272. Reichenbach, J.R., *The future of susceptibility contrast for assessment of anatomy and function*. Neuroimage, 2012. **62**(2): p. 1311-5.
273. Beck, K.L., et al., *Dietary determinants of and possible solutions to iron deficiency for young women living in industrialized countries: a review*. Nutrients, 2014. **6**(9): p. 3747-76.
274. Cole, S.K., W.Z. Billewicz, and A.M. Thomson, *Sources of variation in menstrual blood loss*. J Obstet Gynaecol Br Commonw, 1971. **78**(10): p. 933-9.
275. Finch, C.A., et al., *Ferrokinetics in man*. Medicine (Baltimore), 1970. **49**(1): p. 17-53.
276. Green, R., et al., *Body iron excretion in man: a collaborative study*. Am J Med, 1968. **45**(3): p. 336-53.
277. Luo, X., et al., *Modulation of Dcytb (Cybrd 1) expression and function by iron, dehydroascorbate and Hif-2alpha in cultured cells*. Biochim Biophys Acta, 2014. **1840**(1): p. 106-12.
278. McKie, A.T., et al., *An iron-regulated ferric reductase associated with the absorption of dietary iron*. Science, 2001. **291**(5509): p. 1755-9.
279. Vlachodimitropoulou, E., R.J. Naftalin, and P.A. Sharp, *Quercetin is a substrate for the transmembrane oxidoreductase Dcytb*. Free Radic Biol Med, 2010. **48**(10): p. 1366-9.
280. Canonne-Hergaux, F., et al., *Cellular and subcellular localization of the Nramp2 iron transporter in the intestinal brush border and regulation by dietary iron*. Blood, 1999. **93**(12): p. 4406-17.
281. Gunshin, H., et al., *Cloning and characterization of a mammalian proton-coupled metal-ion transporter*. Nature, 1997. **388**(6641): p. 482-8.
282. Le Blanc, S., M.D. Garrick, and M. Arredondo, *Heme carrier protein 1 transports heme and is involved in heme-Fe metabolism*. Am J Physiol Cell Physiol, 2012. **302**(12): p. C1780-5.
283. Raffin, S.B., et al., *Intestinal absorption of hemoglobin iron-heme cleavage by mucosal heme oxygenase*. The Journal of clinical investigation, 1974. **54**(6): p. 1344-1352.
284. West, A.R. and P.S. Oates, *Subcellular location of heme oxygenase 1 and 2 and divalent metal transporter 1 in relation to endocytotic markers during heme iron absorption*. J Gastroenterol Hepatol, 2008. **23**(1): p. 150-8.
285. Williams, E.W. and W.A. Hemmings, *Intestinal uptake and transport of proteins in the adult rat*. Proc R Soc Lond B Biol Sci, 1978. **203**(1151): p. 177-89.
286. Donovan, A., et al., *The iron exporter ferroportin/Slc40a1 is essential for iron homeostasis*. Cell Metab, 2005. **1**(3): p. 191-200.
287. Han, O. and E.Y. Kim, *Colocalization of ferroportin-1 with hephaestin on the basolateral membrane of human intestinal absorptive cells*. J Cell Biochem, 2007. **101**(4): p. 1000-10.
288. Bedard, Y.C., P.H. Pinkerton, and G.T. Simon, *Uptake of circulating iron by the duodenum of normal mice and mice with altered iron stores, including sex-linked anemia: high resolution radioautographic study*. Lab Invest, 1976. **34**(6): p. 611-5.
289. Nemeth, E., et al., *Hepcidin regulates cellular iron efflux by binding to ferroportin and inducing its internalization*. Science, 2004. **306**(5704): p. 2090-3.
290. Vanoaica, L., et al., *Intestinal ferritin H is required for an accurate control of iron absorption*. Cell Metab, 2010. **12**(3): p. 273-82.

## Supplementary material

### Iron uptake in humans

Iron is obtained from dietary sources and absorbed by the gut enterocytes. A distinction is made between heme and non-heme iron. The latter is the most common source of iron and can be obtained from plant sources like peas, fruits and vegetables. Although heme iron contributes less to the dietary source of iron, it has a high bioavailability and is present in meat and fish [273].

Excretion of iron is limited. The three main processes for iron excretion are menstruation, shedding of the intestinal epithelium and skin exfoliation. Only small amounts are expelled from the body via urine and faeces [14, 274-276]. As a result, the key modulator of the concentrations of iron throughout the body is the gut.

The uptake process of iron by the intestines can be divided into three main stages (Supplementary Figure 1). First, uptake of iron from the intestinal lumen takes place. For non-heme iron, this requires the reduction of the  $\text{Fe}^{3+}$  into  $\text{Fe}^{2+}$  by duodenal cytochrome B (DcytB) [14, 277-279]. The resulting  $\text{Fe}^{2+}$  is then transported into the enterocyte across the apical membrane via DMT-1 [14, 21, 280, 281]. Whereas for heme iron, heme carrier protein 1 (HCP1) is suggested to transfer the iron into the enterocytes. However, the exact uptake mechanism remains unclear [14, 282]. After entering the enterocyte, heme iron is converted into  $\text{Fe}^{2+}$  by heme oxygenase. This, together with the entered  $\text{Fe}^{2+}$  derived from non-heme iron, constitute to the labile iron pool of the enterocytes [14, 283, 284]. Finally, a third form of iron bound to ferritin, which is a storage protein for iron, can directly enter and leave the enterocyte without any conversions. Nevertheless, this pathway also requires more extensive examination [14, 285].

In the second stage, iron is transferred to the basolateral membrane or stored by ferritin. In the final stage,  $\text{Fe}^{2+}$  is transported across the basolateral membrane into the blood circulation. This is mediated by the iron transport protein, ferroportin [14, 286]. In addition, the  $\text{Fe}^{2+}$  is again converted into  $\text{Fe}^{3+}$  by hephaestin, a ferroxidase linked to ferroportin. Apo-transferrin can then incorporate the resulting  $\text{Fe}^{3+}$ , which facilitates its distribution throughout the body [14, 287].

### Intestinal iron uptake regulation

As the intestinal uptake of iron determines the levels throughout the body, extensive regulatory mechanisms are required. Bedard et al. suggested the involvement of crypt cells, which are part of the intestinal gland and mature into enterocytes. These cells have access to iron present in the blood circulation, which enables them to act as sensors of the systemic iron load. When the latter increases, more iron accumulates in the crypt cells. This affects the levels of iron management proteins (e.g. ferritin) present in these cells, which results in the alteration of iron transport after enterocyte maturation [14, 288].

In addition, ferroportin in the basolateral membrane is regulated by hepcidin (Supplementary Figure 1). This peptide causes a reduction of iron release in the blood, by decreasing ferroportin expression of enterocytes. This is achieved by the internalization of ferroportin, which is then degraded by the proteasome. When systemic iron levels increase, hepcidin is secreted by the liver. As a result, iron absorption is decreased, and normal systemic levels are gradually reached. In the case of iron deficiency, levels of circulating hepcidin are decreased to increase iron absorption [14, 289].

Furthermore, Vanoaica et al. demonstrated the importance of ferritin in the regulation mechanisms. Animals genetically deprived from ferritin showed an increased iron absorption.

As a result, hepcidin levels were elevated, but this did not induce a decreased ferroportin expression. Moreover, the expression was increased. These results indicate the relevance of intracellular communication in iron absorption [14, 290].

## Supplementary tables

**Supplementary Table 1. 76 regions analysed in this study**

<b>Region</b>	
left hippocampus	right hippocampus
left entorhinal	right entorhinal
left amygdala	right amygdala
left thalamus proper	right thalamus proper
left caudate	right caudate
left putamen	right putamen
left pallidum	right pallidum
left accumbens area	right accumbens area
left caudal anterior cingulate	right caudal anterior cingulate
left caudal middle frontal	right caudal middle frontal
left cuneus	right cuneus
left fusiform	right fusiform
left inferior parietal	right inferior parietal
left inferior temporal	right inferior temporal
left isthmus cingulate	right isthmus cingulate
left lateral occipital	right lateral occipital
left lateral orbitofrontal	right lateral orbitofrontal
left lingual	right lingual
left medial orbitofrontal	right medial orbitofrontal
left middle temporal	right middle temporal
left parahippocampal	right parahippocampal
left paracentral	right paracentral
left pars opercularis	right pars opercularis
left pars orbitalis	right pars orbitalis
left pars triangularis	right pars triangularis
left pericalcarine	right pericalcarine
left postcentral	right postcentral
left posterior cingulate	right posterior cingulate
left precentral	right precentral
left precuneus	right precuneus
left rostral anterior cingulate	right rostral anterior cingulate
left rostral middle frontal	right rostral middle frontal
left superior frontal	right superior frontal
left superior parietal	right superior parietal
left superior temporal	right superior temporal
left supramarginal	right supramarginal
left transverse temporal	right transverse temporal
left insula	right insula

76 grey matter regions of the DKT atlas were analysed in this study.

**Supplementary Table 2. Overview of APOE variant distribution**

	CN(Y)	CN	MCI	LOAD	EOAD	TOTAL
	22	105	21	15	17	180
<b>0 E4</b>	11	69	10	9	5	104
<b>1 E4</b>	4	31	8	5	7	55
<b>2 E4</b>	0	1	1	1	3	6
<b>Not known</b>	7	4	2	0	2	15

**Supplementary Table 3. Regions affected by iron load changes in the healthy aging process**

Region	p-value	t-value
left hippocampus	7.78E-05	2.77
left entorhinal	0.01	-0.19
left amygdala	1.32E-04	2.54
left thalamus proper	2.01E-03	1.22
left caudate	5.47E-10	6.09
left putamen	9.29E-13	7.61
left pallidum	5.99E-11	6.64
left accumbens area	1.42E-06	4.04
left caudal anterior cingulate	1.20E-04	2.59
left caudal middle frontal	1.92E-10	6.37
left cuneus	8.72E-09	5.42
left fusiform	4.58E-05	2.97
left inferior parietal	1.71E-07	4.65
left inferior temporal	3.06E-03	0.94
left isthmus cingulate	4.70E-05	2.96
left lateral occipital	4.28E-08	5.03
left lateral orbitofrontal	0.01	0.31
left lingual	1.57E-05	3.32
left medial orbitofrontal	4.73E-03	0.60
left middle temporal	1.50E-06	4.00
left parahippocampal	1.48E-03	1.41
left paracentral	2.81E-07	4.50
left pars opercularis	7.22E-15	8.76
left pars orbitalis	8.92E-05	2.71
left pars triangularis	2.57E-09	5.74
left pericalcarine	2.75E-04	2.24
left postcentral	9.94E-08	4.79
left posterior cingulate	1.27E-03	1.50
left precentral	1.76E-14	8.47
left precuneus	5.18E-07	4.32
left rostral anterior cingulate	9.15E-04	1.69
left rostral middle frontal	5.34E-07	4.30
left superior frontal	1.84E-10	6.36
left superior parietal	2.47E-09	5.73
left superior temporal	3.79E-09	5.62
left supramarginal	9.12E-08	4.82
left transverse temporal	3.20E-09	5.66
left insula	1.84E-07	4.61
right hippocampus	2.36E-06	3.87
right entorhinal	1.34E-04	2.54
right amygdala	5.16E-07	4.32
right thalamus proper	1.59E-03	1.37
right caudate	4.47E-11	6.75
right putamen	4.38E-12	7.23
right pallidum	6.15E-11	6.66
right accumbens area	9.31E-08	4.84
right caudal anterior cingulate	6.95E-05	2.81
right caudal middle frontal	5.42E-11	6.64
right cuneus	1.49E-04	2.49
right fusiform	2.59E-07	4.52
right inferior parietal	6.54E-08	4.93
right inferior temporal	1.05E-04	2.65
right isthmus cingulate	1.22E-03	1.53

right lateral occipital	1.48E-06	4.01
right lateral orbitofrontal	1.79E-03	-1.29
right lingual	1.40E-05	3.36
right medial orbitofrontal	6.08E-03	0.37
right middle temporal	2.80E-07	4.49
right parahippocampal	5.02E-04	1.98
right paracentral	9.90E-08	4.79
right pars opercularis	6.87E-14	8.15
right pars orbitalis	2.71E-04	2.24
right pars triangularis	5.40E-07	4.29
right pericalcarine	1.21E-04	2.58
right postcentral	2.03E-08	5.23
right posterior cingulate	5.74E-04	1.91
right precentral	4.16E-12	7.28
right precuneus	1.24E-06	4.07
right rostral anterior cingulate	6.14E-05	2.86
right rostral middle frontal	8.84E-08	4.85
right superior frontal	5.85E-10	6.09
right superior parietal	3.67E-07	4.42
right superior temporal	2.65E-08	5.15
right supramarginal	7.57E-10	6.01
right transverse temporal	1.72E-10	6.36
right insula	1.83E-07	4.62

---

P- and t-values are rounded to two decimal places.

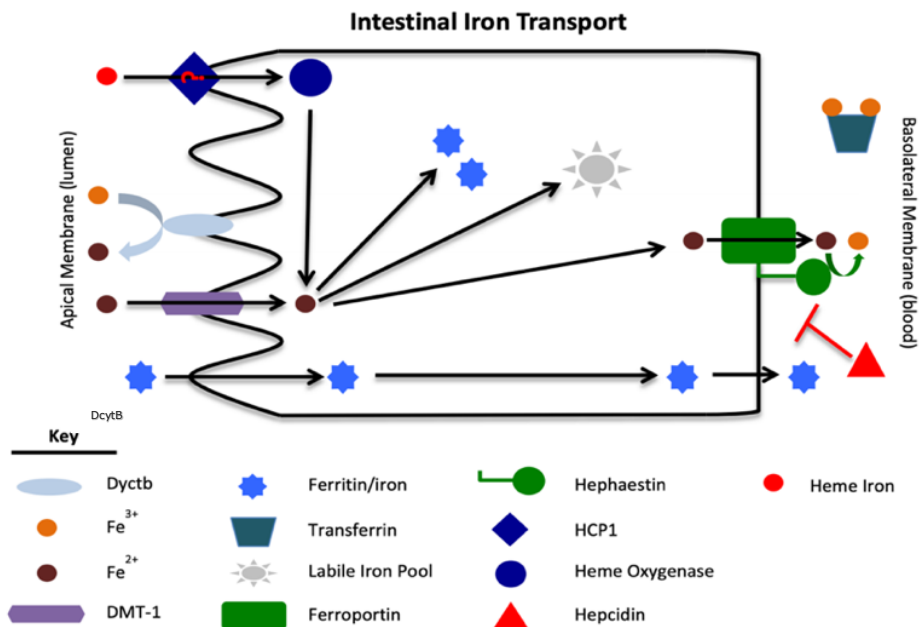
**Supplementary table 4. P- and t-values of regions showing significant differences in iron load between homozygotes and heterozygotes of the  $\epsilon 4$  allele.**

<b>Region</b>	<b>p-value</b>	<b>t-value</b>
left hippocampus	0.05	0.91
left entorhinal	0.04	-1.70
left amygdala	0.05	0.13
left thalamus proper	0.05	0.50
left caudate	0.05	0.57
left putamen	0.05	-0.36
left pallidum	0.05	-0.76
left accumbens area	0.04	1.15
left caudal anterior cingulate	0.05	0.56
left caudal middle frontal	0.03	1.91
left cuneus	0.04	1.38
left fusiform	0.05	0.22
left inferior parietal	0.03	2.11
left inferior temporal	0.04	-1.20
left isthmus cingulate	0.03	2.11
left lateral occipital	0.04	1.05
left lateral orbitofrontal	0.04	-1.33
left lingual	0.04	1.67
left medial orbitofrontal	0.04	-1.62
left middle temporal	0.05	0.18
left parahippocampal	0.05	-0.88
left paracentral	0.04	1.29
left pars opercularis	0.04	1.13
left pars orbitalis	0.05	0.21
left pars triangularis	0.05	0.72
left pericalcarine	0.05	0.61
left postcentral	0.05	1.72
left posterior cingulate	0.04	1.52
left precentral	0.04	1.09
left precuneus	0.03	2.72
left rostral anterior cingulate	0.05	-0.21
left rostral middle frontal	0.04	1.33
left superior frontal	0.05	0.65
left superior parietal	0.03	2.19
left superior temporal	0.04	1.64
left supramarginal	0.02	2.64
left transverse temporal	0.03	2.29
left insula	0.04	1.20
right hippocampus	0.05	0.73
right entorhinal	0.05	-0.06
right amygdala	0.05	-0.14
right thalamus proper	0.05	-0.25
right caudate	0.05	0.38
right putamen	0.05	-0.60
right pallidum	0.04	-1.18
right accumbens area	0.05	0.11
right caudal anterior cingulate	0.05	0.59
right caudal middle frontal	0.05	0.59
right cuneus	0.05	0.47
right fusiform	0.05	-0.82
right inferior parietal	0.05	0.28
right inferior temporal	0.05	-0.35
right isthmus cingulate	0.05	0.51
right lateral occipital	0.05	0.00
right lateral orbitofrontal	0.05	-0.76
right lingual	0.05	0.33
right medial orbitofrontal	0.04	-1.22
right middle temporal	0.04	1.59
right parahippocampal	0.05	-0.39
right paracentral	0.05	0.31
right pars opercularis	0.04	1.00

right pars orbitalis	0.05	0.89
right pars triangularis	0.05	0.14
right pericalcarine	0.05	0.15
right postcentral	0.05	0.73
right posterior cingulate	0.05	0.43
right precentral	0.05	0.85
right precuneus	0.03	1.58
right rostral anterior cingulate	0.05	-0.74
right rostral middle frontal	0.04	0.70
right superior frontal	0.05	0.71
right superior parietal	0.05	0.00
right superior temporal	0.05	-0.07
right supramarginal	0.04	1.29
right transverse temporal	0.05	0.32
right insula	0.04	1.18

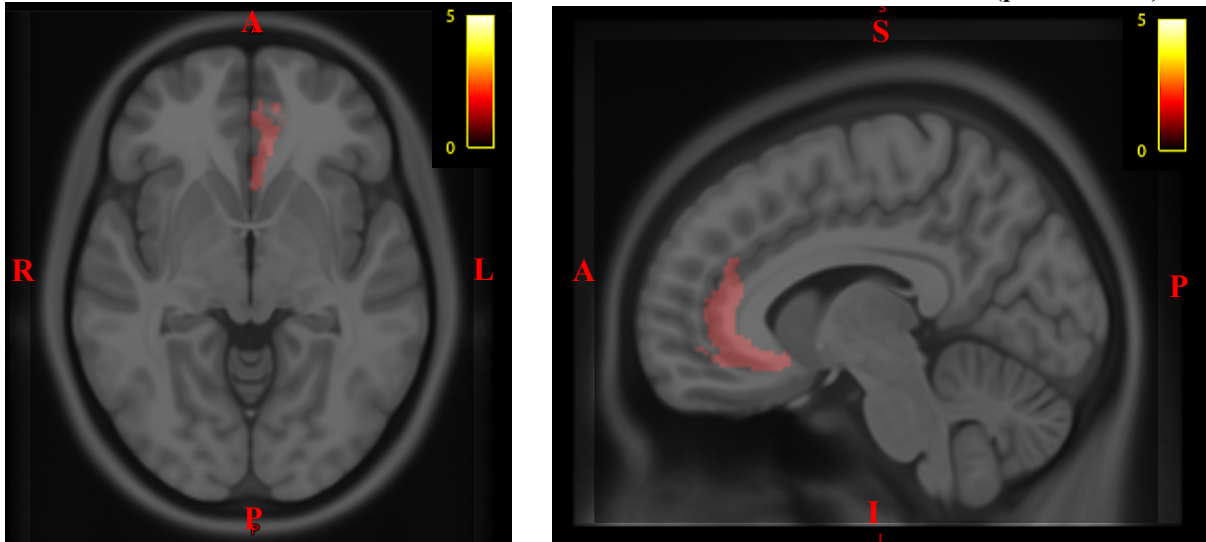
P- and t-values are rounded to two decimal places.

### Supplementary figures



Supplementary Figure 1 Schematic representation of intestinal transport of iron in three main stages. First, DcytB reduces non-heme Fe<sup>3+</sup> into Fe<sup>2+</sup>. Thereafter, Fe<sup>2+</sup> is transported into the enterocyte by DMT-1. For heme iron, HCP1 functions as transporter and heme oxygenase converts heme into Fe<sup>2+</sup>. Second, Fe<sup>2+</sup> is transferred to the basolateral membrane or stored by ferritin. Third, Fe<sup>2+</sup> is transported across the basolateral membrane into the blood circulation by ferroportin. Hephaestin then converts Fe<sup>2+</sup> into Fe<sup>3+</sup>, which can be transported by apo-transferrin [14].

**Brain iron load differences between carriers of one *APOE*  $\epsilon 4$  allele and non-carriers (positive scale)**



*Supplementary Figure 2 Transverse and sagittal images showing increased brain iron values in carriers of one  $\epsilon 4$  *APOE* allele compared to non-carriers in the left rostral anterior cingulate cortex. An intensity scale of zero to five was used.*

